

Electronic Thesis and Dissertation Repository

---

7-28-2016 12:00 AM

## Silicon Anode Materials for Next Generation Lithium-Ion Batteries

Qizheng Li

*The University of Western Ontario*

Supervisor

Xueliang Sun

*The University of Western Ontario*

Graduate Program in Mechanical and Materials Engineering

A thesis submitted in partial fulfillment of the requirements for the degree in Master of  
Engineering Science

© Qizheng Li 2016

Follow this and additional works at: <https://ir.lib.uwo.ca/etd>

 Part of the [Other Materials Science and Engineering Commons](#)

---

### Recommended Citation

Li, Qizheng, "Silicon Anode Materials for Next Generation Lithium-Ion Batteries" (2016). *Electronic Thesis and Dissertation Repository*. 3910.

<https://ir.lib.uwo.ca/etd/3910>

This Dissertation/Thesis is brought to you for free and open access by Scholarship@Western. It has been accepted for inclusion in Electronic Thesis and Dissertation Repository by an authorized administrator of Scholarship@Western. For more information, please contact [wlsadmin@uwo.ca](mailto:wlsadmin@uwo.ca).

## Abstract

Lithium Ion Batteries (LIBs) are a promising green energy storage system with application toward portable electronic devices, electronic vehicles (EVs) and smart grid energy storage. High energy density is one of the most important advantages for LIB, however, improvements toward performance measures, such as energy density, power and rate capability, cycling life, safety and cost, need to meet the different requirements for various applications. It is well known that battery performance is highly dependent on the type of electrode material that is employed. Currently most LIBs are predominantly fabricated using graphite as an anode material. Therefore, finding a qualified candidate of anode material to replace graphite is the key to achieve a higher energy density of LIB. Silicon is a hopeful candidate for use as an anode material due to its super-high specific capacity (4200 mAh/g). However, this material suffers from severe volume change during the lithiation/delithiation process, thereby limiting its practical application in LIB.

In this thesis, three sections of work were made for the practical application of Si anode in LIB. The first section was to develop a novel method to synthesis nanostructured Si anode materials, which is easy to handle, low cost and environmental friendly. The second section is focused on electrode optimization based on an engineering point of view, including electrode mass loading and density, binder selection and optimized cycle mode. The last section pertains to the development of electrolyte, which can further improve battery performance. A better Si-based electrode is presented LIB after this study.

## Keywords

Silicon anode material, etching synthesis, nanomaterial, lithium-ion battery, electrode parameters, binders, electrolyte formula, electrolyte additives.

## Co-Authorship Statement

Book chapter:

**Title:** Advanced Technologies for Li-Ion Rechargeable Batteries

**Author:** Qizheng Li, Xueliang Sun

This chapter was organized by Qizheng under the guidance of Dr. Xueliang Sun. Qizheng Li wrote the entirety of the manuscript to describe the Li-Ion batteries technology in industry. The final version of this manuscript has been published in the book of *Advanced Materials and Technologies for Electrochemical Energy*, CRC Publisher, 2014.

## Acknowledgements

This work was carried out in Dr. Xueliang (Andy) Sun's Nanomaterials and Energy Group at the University of Western Ontario (UWO). Herein, it is my pleasure to express my acknowledgements to Dr. Sun and every individual who contributed to my work during last two years.

First of all, I would like to express my deepest gratitude to my supervisor, Dr. Xueliang Sun, a Professor in Department of Mechanical and Materials Engineering at UWO, and also a Fellow of the Canadian Academy of Engineering. I really appreciated that Dr. Sun provided me with this study opportunity and tremendous support throughout my master's degree in the past two years.

I am also grateful to Mrs. Ruying (Kathy) Li, as our lab manager and research engineer, for tremendous support and help to my project during last two years. Mrs. Li has always been available whenever I needed it. Furthermore, she is always thoughtful to me and all our group members for their lives in Western.

I would also like to thank Dr. Quanming (Harris) Yang, Dr. Yuhai Hu and Springpower International Inc. for their great help and support during the process of my project. The collaboration with SPI helps me to deeply understand the material market which is crucial for cost controlling in Lithium-Ion Battery industry. This experience also helps me to explore the knowledge of the chain of LIB market.

In particularly, I would like to thank my wife, Yanan Luo, my son, Yichen Li, and my daughter, Yihan Li, for their strong support throughout my study. I would also like to express my acknowledgement to my parents and parents-in-law for their unconditional love and support, including my relatives and friends.

I also want to thank all my group members for their great help and support to me in the past two years. I am really lucky that I could work with great people in Western.

Lastly, I am grateful to funding support from Nature Sciences and Engineering Research Council of Canada (NSERC), Springpower International Inc. (SPI), and the University of Western Ontario.

## Table of Contents

Abstract .....	i
Co-Authorship Statement.....	ii
Acknowledgements.....	iii
List of Tables .....	viii
List of Figures .....	ix
List of Abbreviations .....	xv
Chapter 1 .....	1
1 Introduction .....	1
1.1 Introduction of Lithium Ion Batteries .....	1
1.2 Challenges in LIB .....	3
1.3 The solutions for Si anode practical application.....	5
1.3.1 Si anode materials .....	6
1.3.2 Binders .....	21
1.3.3 Electrolyte.....	27
1.4 Thesis objectives.....	29
1.5 Thesis organization .....	32
References .....	33
Chapter 2.....	39
2 Experimental and Characterization .....	39
2.1 Experimental.....	39
2.2 Characterization .....	40
2.2.1 Physical characterizations technique .....	40
2.2.2 Electrochemical characterizations .....	44
References .....	46

Chapter 3.....	47
3 HF free synthesis method for Silicon nanowire.....	47
3.1 Introduction.....	47
3.2 Experimental Section.....	47
3.2.1 Sample preparation and characterization.....	47
3.2.2 Electrochemical Characterization.....	48
3.3 Results and Discussion.....	49
3.3.1 Temperature effect in heating pretreatment.....	49
3.3.2 Storage time effect in 1000°C heating pretreatment.....	51
3.4 Conclusions.....	55
References.....	56
Chapter 4.....	59
4 Electrode optimization: density, loading, binder and cycle mode.....	59
4.1 Introduction.....	59
4.2 Experimental Section.....	59
4.3 Results and Discussion.....	60
4.3.1 Loading and density.....	60
4.3.2 Binder.....	65
4.3.3 Cycle mode.....	67
4.4 Conclusions.....	69
References.....	70
Chapter 5.....	73
5 Synergies Effect of fluoroethylene carbonate (FEC) and vinylene carbonate (VC) on Si Anode for Lithium-Ion Battery.....	73
5.1 Introduction.....	73
5.2 Experimental Section.....	74

5.3 Results and Discussion .....	75
5.4 Conclusions.....	81
References .....	82
Chapter 6.....	87
6 Conclusion and perspective.....	87
6.1 Conclusion .....	87
6.2 Perspective .....	88
Reference.....	89
<b>Curriculum Vitae .....</b>	<b>92</b>



## List of Tables

Table 1.1 Comparison of various anode materials (all the capacity numbers are based on materials in the delithiated state except lithium metal) [16].....	6
Table 1.2 Comparison of energy density and mass loading .....	31
Table 4.1 Work electrodes basic information for density test .....	62
Table 4.2 Work electrodes basic information for loading test.....	63

## List of Figures

Figure 1.1 Comparison of the different battery technologies in terms of volumetric and gravimetric energy density. [9] .....	1
Figure 1.2 Configuration of Lithium Ion Battery work principle. [14] .....	3
Figure 1.3 Potential materials for cathode and anode. [15] .....	4
Figure 1.4 Silicon anode and electrode failure mechanism in Lithium Ion Battery. [20] .....	6
Figure 1.5 SiNP-rGO anode material (a) Schematic illustration of the rGO-Si <sub>NaCl</sub> synthesis. (b) Low and (c) high magnification SEM images of hybrid material. (d) TEM image of SiNP on graphene. (e) HRTEM image of rGO-Si <sub>NaCl</sub> showing the lattice fringes corresponding to crystalline silicon. (f) 1 <sup>st</sup> and 2 <sup>nd</sup> cycle profile of Voltage vs Capacity. (g) Charge and discharge capacities of the rGO-Si <sub>NaCl</sub> electrode after two formation cycles. (h) Discharge capacities of the rGO-Si <sub>NaCl</sub> electrode as a function of C rate. [21].....	7
Figure 1.6 “Metathesis” reaction synthesis SiNPs (a) XRD characterization of SiNPs. (b) Raman characterization of SiNPs. (c) FESEM image and (d) TEM image of SiNPs. (e) EDX spectrum analysis of SiNPs. Cycle performances at (f) 1.2A/g and (g) 3.6A/g current density. [22].....	9
Figure 1.7 SiNWs deposited on carbon paper (a) SEM image of 1.63mg/cm <sup>2</sup> SiNWs 3D anode before cycling, scale bar is 20µm. (b) Low-magnification TEM image. HRTEM image of (c) SiNWs and (d) core-shell structure. (e) Capacity contribution of the carbon matrix only and with SiNWs. (f) 1.06mg Si/cm <sup>2</sup> anode cycle performance. Full cell cycle performance (g) in coin cell format and (h) internal resistance analysis. [28] .....	10
Figure 1.8 (a) and (b) Schematic diagrams of prelithiation. SEM images of SiNWs (c) before and (d) after prelithiation. (e), (f), (g) and (h) are TEM images during prelithiation. (i) Time	

dependence study of prelithiation of SiNWs. (j) Cycling performance of SiNWs prelithiated for 20 and 60 minutes. (k) Voltage vs. Capacity profiles of the first, second and 10<sup>th</sup> cycles of the full cell. (l) Cycling performance of the full cell. [31] ..... 11

Figure 1.9 SiHNTs (a) schematic diagram of synthesis. (b) and (d) SEM images of SiHNTs. (c) TEM image of SiHNTs. SEM images of SiHNTs (e) before cycling, (f) after 2000 cycling with and (g) without SEI. (h) Cycle performance of SiNWs, SiNTs and SiHNTs. (i) Long term cycle performance of SiHNTs. (j) EIS analysis of SiHNTs electrode. [32]..... 12

Figure 1.10 Porous Si@C sphere: (a) Schematic illustration for the synthesis of porous Si@C spheres. (b) Discharge capacities vs. cycle number for bare Si spheres, PVdF-derived carbon and porous Si@C sphere. (c) Discharge-charge curves of Si@C spheres. Morphological, structural and compositional characterizations of porous Si@C spheres: (d, e) SEM images, (f) TEM image, (g, h) HRTEM images, (i) TEM-EDX elemental mapping. Microscopic structural features of porous Si@C spheres in a fully delithiated state after 20 cycles: (j, k) TEM images, (l) HRTEM image, (m) EDX spectrum, and (n) TEM-EDX elemental mapping. [33]..... 13

Figure 1.11 York-Shell Si anode: (a) Schematic of full-lithiated and full-delithiated Si particle. (b) Schematic illustration of Si electrode swelling mode. (c) In-situ TEM technology demonstration. (d) Images of Si particles during lithiation process. (e) Galvanostatic cycling of different silicon nanostructures (PVdF binder). (f) Delithiation capacity of Si@void@C with alginate binder cycled at various rate from 0.1 C to 4C. (g) Delithiation capacity and CE of the first 1000 galvanostatic cycles between 0.01-1V (alginate binder), 0.1C for first cycle, 0.33C for 2<sup>nd</sup> to 10<sup>th</sup> cycles and 1C for the later cycles. [36]..... 14

Figure 1.12 (a) Schematic illustration of the synthesis route of interconnected sub-10nm silicon nanoparticles. (b) SEM image of Si composite. TEM images of (c and d) Si composed of interconnected sub -10nm Si nanoparticles. (e) XRD patterns of silsesquioxane (SiO<sub>1.5</sub>), Si/SiO<sub>2</sub>, and Si. (f) Galvanostatic profiles, (g) Cycle performance and (h) Rate capabilities of Si/C composite. (i) Nyquist plots of Si/C composite anode electrode before and after different cycles. [39]..... 15

Figure 1.13 (a) Synthesis process of G/Si-C. (b) SEM image of G/Si-C. TEM images of (c) low and (d) high magnification. (e) XRD and (f) Raman spectrum of G/Si-C. (g) and (h) Cycling performance of G/Si-C. (i) Impedance spectra of G/Si-C at low and high mass loading. Inserted was the Randles equivalent circuit and enlarged spectra showing difference between G/Si-C@ low and G/Si-C@high, respectively. [40] ..... 16

Figure 1.14 Si@SiO<sub>x</sub>/graphene composite material: (a) Schematic illustration of synthesis route. (b), (c), (d) and (e) TEM images of Si@SiO<sub>x</sub>/graphene. (f) XRD pattern of Si@SiO<sub>x</sub>/graphene. (g) Rate cycle performance of Si@SiO<sub>x</sub>/graphene and (h) galvanostatic charge-discharge profiles of Si@SiO<sub>x</sub>/graphene. [41]..... 18

Figure 1.15 (a) Schematic illustration of the synthetic route. TEM images of (b) bright-field and (c) dark-field of HSQ-derived Si/SiO<sub>x</sub> nanospheres. HRTEM images of (d) a crystalline Si nanodot embedded in a SiO<sub>x</sub> matrix in the HSQ-derived Si/SiO<sub>x</sub> nanospheres and (e) C-coated Si/SiO<sub>x</sub> nanosphere. (f) galvanostatic charge and discharge profiles. (g) Cycle performance and Coulombic efficiencies (insert) of C-coated Si/SiO<sub>x</sub> electrodes. (h) Rate capability of a C-coated Si/SiO<sub>x</sub> electrode at different currents. (i) Cross-sectional FESEM images of C-coated Si/SiO<sub>x</sub> electrode before and after 2 cycles. [42]..... 20

Figure 1.16 (a) Schematic illustration of etching process. SEM images of (b) Bulk Si, (c) etched Si and (d) cross-section of etched Si particles, SEM images of (e) carbon coated porous Si and (f) cross-section of carbon coated porous Si, (g) XRD pattern, (h) Voltage profiles of c-mSi and (i) Charge capacity vs cycle number for the c-mSi at a rate of 0.2C after the first cycle at 0.1C rate. [47]..... 21

Figure 1.17 Schematic illustration of Si-based electrode. [51]..... 21

Figure 1.18 (a) Molecular structure in neutral and charged status. (b) and (c) Schematic illustration of XG binder function on nano-scale. (d) Peeling test results for SiNP electrodes based on five binders. (e) Cycle performance of SiNP electrodes with three binders. SEM surface morphology of electrodes before and after first cycle with (f) native-XG, (g) alginate and (h) Na-CMC binders. [52]..... 23

Figure 1.19 (a) Schematic illustration of Si-SHP/CB electrode. (b) Pure Si electrodes made from Si particles. (c) SHP/CB layer coated on top of Si electrodes with one-time blading. (d) Si electrodes filled with SHP/CB forming a 3D distribution inside electrodes from repeated blading under heating. (e) Cycle performance of thick Si-SHP/CB electrodes. (f) Nyquist plots of the high mass loading 3D Si-SHP/CB electrodes at different cycling status. SEM images of Si-SHP/CB electrodes (g) before and (h) after cycling. Cross-section SEM images of Si-SHP/CB electrodes (i) before and (j) after cycling. (k) Cross-section SEM image of cycled electrode. [53]..... 24

Figure 1.20 (a) Synthetic scheme and the relative molar ratio of four functional blocks of polymer binders. (b) Peeling strength test results for four electrodes. (c) The swelling tests of polymer films in the EC/DEC (1:1) electrolyte. (d) Cycle performance for four electrodes without any conductive agent. SEM images of PEFM31 electrodes (e) before and (f) after cycling. TEM images of PEFM21 electrodes (g) before and (h) after cycling. [56]..... 26

Figure 1.21 (a) Cycle performances and (b) Nyquist plots in with/without FEC electrolyte. (c) F 1s, O 1s, and C 1s spectra of the silicon electrode at different SOC in FEC/LP40 electrolyte. SEM images of (d) before and after cycling in (e) LP40 and (f) LP40/FEC electrolyte. Mechanism of FEC protection in (g) LP40/FEC and (h) LP40 electrolyte. [63]. 28

Figure 1.22 Molecular structure of (a) EC and (b) FEC. (c) Cycle performance in electrolytes with different ratio of FEC. EIS analysis results of (d) Nyquist plots and (e) equivalent circuit. (f) Long-term cycle test. [65]..... 29

Figure 1.23 Development of Silicon based Lithium-Ion Batteries. .... 30

Figure 2.1 A picture of Aerosol-Assisted Chemical Vapour Deposition. .... 39

Figure 2.2 A picture of Hitachi S-4800 high-resolution scanning electron microscope. .... 40

Figure 2.3 A picture of HORIBA Scientific LabRAM research Raman spectroscopy. .... 41

Figure 2.4 A picture of the Nicolet 6700 FTIR spectrometer..... 42

Figure 2.5 A picture of Bruker D8 Advance XRD. .... 43

Figure 2.6 A picture of TriStar II Plus Analyzer. ....	43
Figure 2.7 A picture of Biologic VMP3 Potentiostat/Galvanostat/EIS system. ....	44
Figure 2.8 A picture of Arbin BT-2000 battery test system and temperate box.....	45
Figure 2.9 Schematic diagram of Li/Si 2032 coin cell assembly. [1].....	46
Figure 3.1 SEM images of Al-Si alloy powders. ....	48
Figure 3.2 SEM images of Si particles after etching without heat treatment. ....	49
Figure 3.3 Si anode SEM images of temperature effect in 8 h heating pretreatment: (a, b) 700°C, (c, d) 800°C, (e, f) 900°C and (g, h) 1000°C, the scale of (a), (c), (e) and (g) is 5µm, the scale of (b) is 2µm and the scale of (d), (f) and (h) is 500nm. ....	50
Figure 3.4 Cycling performance and cell efficiency of as-prepared SiNWs in different temperature for 8h. ....	51
Figure 3.5 Si anode SEM images of storing time effect in 1000 °C heating pretreatment: (a, b) 2h, (c, d) 4h, (e, f) 6h and (g, h) 8h, the scale of (a), (c), (e) and (g) is 5µm, the scale of (b) is 2µm, and the scale of (d), (f) and (h) is 500nm. ....	52
Figure 3.6 Cycling performance and cell efficiency of as-prepared SiNWs in different storage time at 1000°C. ....	53
Figure 3.7 High resolution SEM images of as-prepared SiNWs after 1000°C, 8h heating pretreatment at different scale: (a) 10µm, (b) 5µm, (c) 1µm and (d) 500nm. ....	54
Figure 3.8 (a) XRD spectra of Si-Al alloy and SiNWs, (b) EDX spectra of SiNWs, (c) surface area for as-prepared SiNWs. ....	55
Figure 4.1 SEM images of SiNWs at two scales. ....	60
Figure 4.2 Schematic illustration of electrode calendar in LIB industry. ....	61
Figure 4.3 Cycling performance of four electrodes with various density.....	61

Figure 4.4 Cycling performance of three electrodes with various loading at same density. ..	63
Figure 4.5 Nyquist plots of three electrodes after 50 cycles. ....	64
Figure 4.6 SEM images of electrodes before (a, c, e), after 100 cycles (b, d) and after 50 cycles (f), (a, b) 0.825mg/cm <sup>2</sup> , (c, d) 1.375mg/cm <sup>2</sup> and (e, f) 2.036mg/cm <sup>2</sup> .....	64
Figure 4.7 Cycling performance of four electrodes with various binders. ....	65
Figure 4.8 Rate capability of four electrodes with various binders. ....	66
Figure 4.9 Mechanical adhesion property of four electrodes: (a) CMC+SBR binder, (b) XG-binder, (c) PAA binder and (d) SA binder. ....	66
Figure 4.10 Cycling performance of two test modes. ....	67
Figure 4.11 SEM images of electrodes surface: New cycle mode electrodes (a) before and (b) after 300 cycles. Normal cycle mode electrodes (c) before and (d) after 100 cycles. ....	68
Figure 4.12 Cycle performance of modified electrode parameter. ....	69
Figure 5.1 Cycle performance of electrodes at room temperature. ....	75
Figure 5.2 Rate capability of electrodes at room temperature. ....	76
Figure 5.3 Nyquist plots of electrodes (a) after first cycle, (b) after 50 cycles and (c) equivalent circuit. ....	77
Figure 5.4 SEM images of electrodes surface (a) before and (b, c, d, e) after 50 cycles at room temperature, (b) BE37, (c) BE37+VC, (d) BE37+FEC, (e) BE37+FEC+VC. ....	78
Figure 5.5 FTIR spectrum of electrodes before and after 50 cycles at room temperature. ....	79
Figure 5.6 Cycle performance of electrodes at 55°C. ....	80
Figure 5.7 Cycle performance of electrodes at -20°C. ....	81

## List of Abbreviations

BET: Brunauer-Emmett-Teller method

CNTs: carbon nanotubes

CV: cyclic voltammetry

CVD: chemical vapour deposition

EDS: Energy dispersive X-ray spectroscopy

EIS: electrochemical impedance spectroscopy

EVs: electric vehicles

FTIR: fourier transform infrared spectroscopy

GNS: graphene nanosheets

LIBs: lithium-ion batteries

NCNTs: nitrogen-doped carbon nanotubes

SiNP: silicon nanoparticle

SiNW: silicon nanowires

SEI: solid electrolyte interphase

SEM: scanning electron microscope

TEM: transmission electron microscope

XRD: X-ray diffraction



# Chapter 1

## 1 Introduction

\* Parts of this chapter have been published in Book chapter “Advanced Technologies for Li-Ion Rechargeable Batteries” in the book of “*Advanced Materials and Technologies for Electrochemical Energy*”, Co-Edited by Pei-Kang Shen, Chao-Yang Wang, Xueliang Sun, San-ping Jiang, and JiuJun Zhang, Publisher: CRC Publisher. (In book series of *Electrochemical Energy Storage and Conversion*), (2014), in press.

### 1.1 Introduction of Lithium Ion Batteries

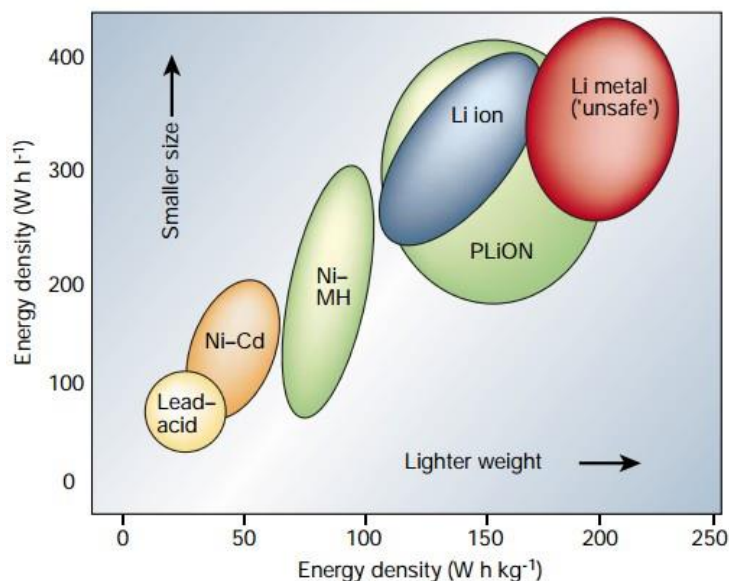
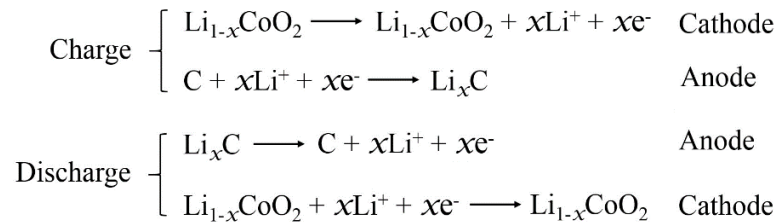


**Figure 1.1 Comparison of the different battery technologies in terms of volumetric and gravimetric energy density. [9]**

Fossil fuels has been rapidly consumed as the main non-renewable resource in last few hundred years. However, it is estimated that the fossil can only last for 50-70 years [1-3] and also leads to many issues, such as greenhouse effect, air pollution [4-5]. It is obvious that the

urgent task has to be taken to find alternative energy sources which are environmental friendly and sustainable. A few clean energy resources such as wind, tide, hydro and solar [6-8] have been studied for decades, and all of these energy are highly dependent with time and location of the operation. Therefore, an effective energy storage system is a must to harvest and store the energy for later usage. Compared with other available batteries in current market, Lithium-ion batteries (LIBs) clearly provide more energy density in the terms of volume or weight (seen Figure 1.1). Therefore, rechargeable LIBs are a fast-growing technology which already widely used in daily life because of their light weight, high voltage, and high-energy density [9-11].

A typical LIB has four key components: cathode, anode, separator, and electrolyte as presented in Figure 1.2. Cathode is the source of  $\text{Li}^+$  and anode is the receptor of  $\text{Li}^+$  during charge process and vice versa in discharge process. Separator is a thin porous polymer film which is immersed by electrolyte. Electrolyte acts as the media which allows the free movement of  $\text{Li}^+$ . Because electrolyte only allows  $\text{Li}^+$  penetrate through, the electron has to go external circuit to transfer between cathode and anode. Most of the battery performance is decided by cathode and anode active materials. During the charging process step,  $\text{Li}^+$  ions are forced to transport from cathode side to anode side under the applied voltage on two electrodes. Meanwhile, the electrons move to anode through external circuit. In this step, the electrical energy will be converted to chemical energy and stored in battery. During discharge, the electron and  $\text{Li}^+$  transports back to cathode. The electrochemical reactions happened on the both electrodes are presented below.



The LIB technology was commercialized by Sony in 1991 and has grown rapidly over the past two decades [12, 13]. After over 20 years development, current commercial LIB has 700Wh/L and 200Wh/kg energy density, 80% capacity retention after 500 cycles. However, these performances are not yet satisfied for certain application, such as EV. For instance,

Tesla Model S (70D) has a 300 Kilometer mileage for each full charge in practical driving which is not enough for a long distance trip. Another problem with LIB for EVs is that its long charging time, which takes over 5 hours to full charge the battery pack. In other words, the energy density and rate performance of the battery packs are still not satisfied. Other applications like the batteries for energy storage system, such as solar and wind energy, have other specific requirements, including rate capability, higher capacity and high/low temperature storage. It is clear that certain designs of LIBs can achieve different battery performances by using different cathode and anode materials, and finally these batteries can meet the requirement for most of the devices and instruments.

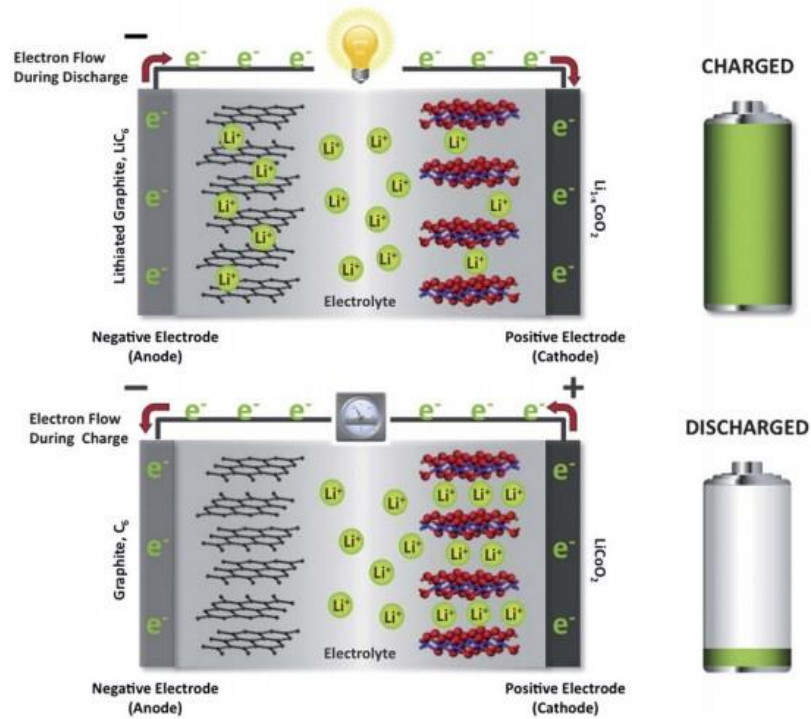


**Figure 1.2 Configuration of Lithium Ion Battery work principle. [14]**

## 1.2 Challenges in LIB

Despite of the development over two decades of LIB industry, the relatively low specific capacity of current commercial cathode (lithium cobalt oxide, 140-170mAh/g) and anode (graphite, 370mAh/g) materials limits the specific energy of LIB. Usually from the point of

view of LIB market, 5-8% capacity increase each year for both LIB manufacturers and customer applications. However, it is difficult to achieve desired capacity due to the limitation of electrode materials availability in the last few years. Some companies are looking for other options to reduce the cost of LIBs, such as longer cycle life and higher cut-off voltage. But LIB researchers and scientists are still facing the problem of improving energy density for next generation LIBs. Changing the active materials for both cathode and anode electrodes is the key to improve the battery performance [14-16]. Great effort had been made for synthesis new materials with higher specific capacities, such as  $\text{Li}_x\text{Ni}_y\text{Co}_{1-y}\text{O}_2$  for cathode and Silicon for anode. Figure 1.3 shows potential electrode materials for LIBs and many works are going on these projects which could lead us to next generation advanced LIBs.

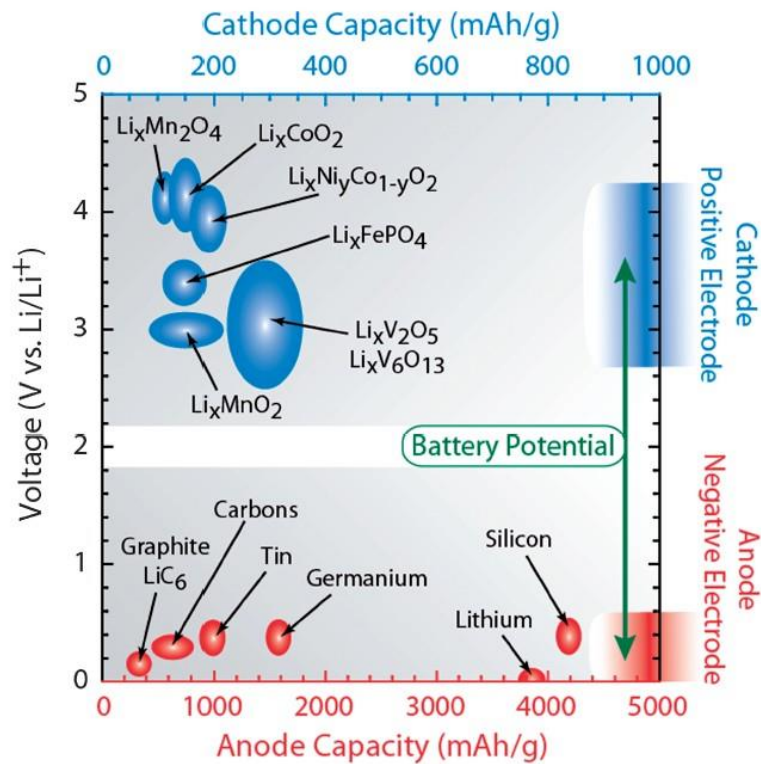


**Figure 1.3 Potential materials for cathode and anode. [15]**

Furthermore, safety of LIB is also a critical issue for large scale applications, especially in EVs and grid energy system, which demand higher capacities by using battery packs. The Battery Management System (BMS) has been invented to reduce the potential of any

accident and minimize the damage before it happens. Several accidents involving LIBs have been reported in elsewhere. In January 2013, the Boeing 787 Dreamliner reported 5 accidents in 7 days, most of them involved their back-up batteries for electric system. The United States Federal Aviation Administration (FAA) ordered a review into the design and manufacture of the Boeing 787 for safety considerations. More airlines have imposed new restrictions on LIBs transportation in the end of 2014 because of its potential safety issues. The Tesla EVs (Model S) also had 4 serious fire accidents in 2013. This was caused by the damage of the battery packs. Therefore, improving safety of LIBs is more important for its further application.

The last challenge for LIBs industry is the manufacturing cost due to its complicated production processes. Basically, current LIBs have three types of format, cylindrical cell, prismatic cell and pouch cell. All of them have mature manufacturing processes, and cylindrical cells (18650 format) have highest production efficiency and lowest cost since full automatic production line is available. Moreover, cylindrical cells provide consistent performance and no swelling which make them more reliable for battery packs. This is part of the reason for Tesla to choose cylindrical battery types for their EV application. Prismatic cells were the main power source for cell phones, but pouch cells have been rapidly seizing market share in the last few years, especially smart phone, tablet and other small portable devices. One of the main advantages is the diversity of cell shape which can provide more freedom for those who design new devices. Furthermore, pouch cell has excellent safety since the battery will not explode in extreme situations. However, compared with cylindrical and prismatic cell, the cost is much expensive due to more processes and production efficiency. It is also difficult to have a full automatic production line as the cell shapes will be changed regularly.

### 1.3 The solutions for Si anode practical application

Based on the requirement of current LIB market, it is quite clear that finding new active materials for next generation LIB is the priority. The development of cathode is mainly focusing on “Li-rich NMC” which combine the beneficial effects of Ni, Co and Mn with

some Li in the transition metal layers and demonstrate a higher capacities exceeding 280 mAh/g [17]. For anode part, according to Table 1.1, Si anode has been considered as one of the most promising anode candidate due to its super high specific capacity (4200mAh/g) [16, 18], which is ten times higher than graphite anode (372mAh/g). Nevertheless, the key problem for Silicon based anode is its huge volume change (420%) during lithiation/delithiation process [16, 19, 20] which leads to rapid pulverization and mechanical integrity damage of Si electrode, resulting loss of electrical contact and rapid capacity fading (Figure 1.4). In addition, binders and electrolyte are also crucial to address the key problem of Si-based electrode during cycling based on mechanical and electrochemical properties.

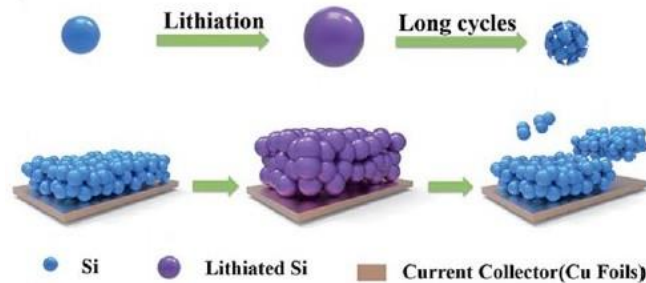


**Figure 1.4 Silicon anode and electrode failure mechanism in Lithium Ion Battery. [20]**

### 1.3.1 Si anode materials

**Table 1.1 Comparison of various anode materials (all the capacity numbers are based on materials in the delithiated state except lithium metal) [16]**

Materials	Li	C	Li <sub>4</sub> Ti <sub>5</sub> O <sub>12</sub>	Si	Sn	Sb	Al	Mg
Density (g/cm <sup>3</sup> )	0.53	2.25	3.5	2.3	7.3	6.7	2.7	1.3
Lithiated phase	Li	LiC <sub>6</sub>	Li <sub>7</sub> Ti <sub>5</sub> O <sub>12</sub>	Li <sub>4.4</sub> Si	Li <sub>4.4</sub> Sn	Li <sub>3</sub> Sb	LiAl	Li <sub>3</sub> Mg
Theoretical specific capacity (mAh/g)	3862	372	175	4200	994	660	993	3350
Volume change (%)	100	12	1	420	260	200	96	100
Potential versus Li (V)	0	0.05	1.6	0.4	0.6	0.9	0.3	0.1

Generally, there are two solutions to overcome huge volume change of silicon anode: (i) preparation of nanoscale materials and (ii) make porous Si anode. Nano-structured Silicon anode can dramatically reduce the volume effect during charging/discharging, which minimizes the electrode swelling thereby improves the cycle stability. Many efforts have been devoted to design various Si nano structures during last 10 years, such as Si nanoparticles (SiNPs) [21-27], Si nanowires (SiNWs) [28-31], Si hollow nanotubes (SiHNTs) [32], Si core-shell [33-37], Si/C composite [38-40] and SiO<sub>x</sub> [41-45].

A new approach of deposition Si nanoparticles on graphene sheet was applied by using graphene oxide and silica nanoparticles [21], then followed by a magnesiothermoic reduction treatment to form Si particles, which is shown in Figure 1.5 (a). This method avoids using chemical vapour deposition (CVD) for the deposition and is also easier to operate. The SEM, TEM and HRTEM techniques confirmed the formation of SiNPs on the graphene sheet.

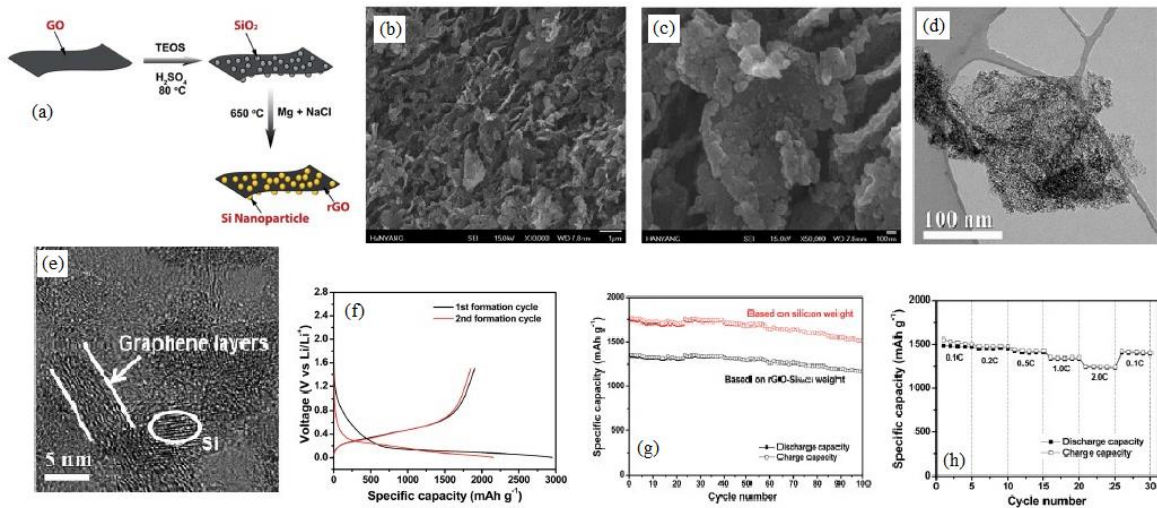
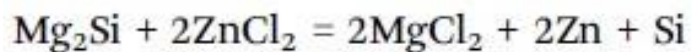


**Figure 1.5 SiNP-rGO anode material (a) Schematic illustration of the rGO-SiNaCl synthesis. (b) Low and (c) high magnification SEM images of hybrid material. (d) TEM image of SiNP on graphene. (e) HRTEM image of rGO-SiNaCl showing the lattice fringes corresponding to crystalline silicon. (f) 1<sup>st</sup> and 2<sup>nd</sup> cycle profile of Voltage vs Capacity. (g) Charge and discharge capacities of the rGO-SiNaCl electrode after two formation cycles. (h) Discharge capacities of the rGO-SiNaCl electrode as a function of C rate. [21]**

According to Figure 1.5 (f – h), the electrochemistry properties are greatly improved. The first two cycles are for the formation treatment, which is the process of forming a stable SEI on anode electrode surface. The profiles were obtained at a current density of 100 mA/g in the potential window of 0.005 to 1.5V. In the first cycle, the charge and discharge capacity were 2949mAh/g and 1902mAh/g, respectively, and the efficiency was about 64.4%. However, the efficiency of 2<sup>nd</sup> cycle was 85.8% and the discharge capacity was 1850mAh/g. The following cycles were conducted at a current density of 2100 mA/g in the voltage window of 0.005 to 1.5V. The retention discharge capacity was 1165mAh/g after 100 cycles, which was about 87 % retention of the discharge capacity obtained at 100mA/g. The C rate test carried out at rates ranging from 0.1 to 2.0C for 5 cycles each. The discharge capacities slightly decreased when higher C rate applied. Compared with other Si anode materials, the C rate performance was greatly improved because of the high conductivity and strength of graphene sheets.

Recently, Metathesis reaction was applied to synthesis SiNPs in one step at low temperature of 300°C [22]. The reaction was very simple which can be described as follow:



The XRD and Raman techniques are used to determine the phases of the samples. Figure 1.6 (a) indicated that the cubic Si (crystalline phase) was synthesized by this method, also confirmed by the result of Raman analysis. The morphology of SiNPs was observed by FESEM and TEM as shown in Figure 1.6 (c) and (d). According to the images, the diameters of SiNPs were in the range from 40 to 100nm. The EDX result also revealed that the formation of SiNPs. After the formation cycles at a current density of 0.2A/g, the Si electrode was activated and exhibited a stable cycle performance both at the current density of 1.2A/g and 3.6A/g, respectively (shown in Figure 1.6 (f) and (g)). After 60 cycles, 1823mAh/g retention capacity was obtained at the current density of 1.2A/g, which equals to the 86 % discharge capacity of the third cycle. As the current density increased to 3.6A/g, discharge capacity of 4<sup>th</sup> cycle was decreased to 950mAh/g, and retained about 795mAh/g after 250 cycles.



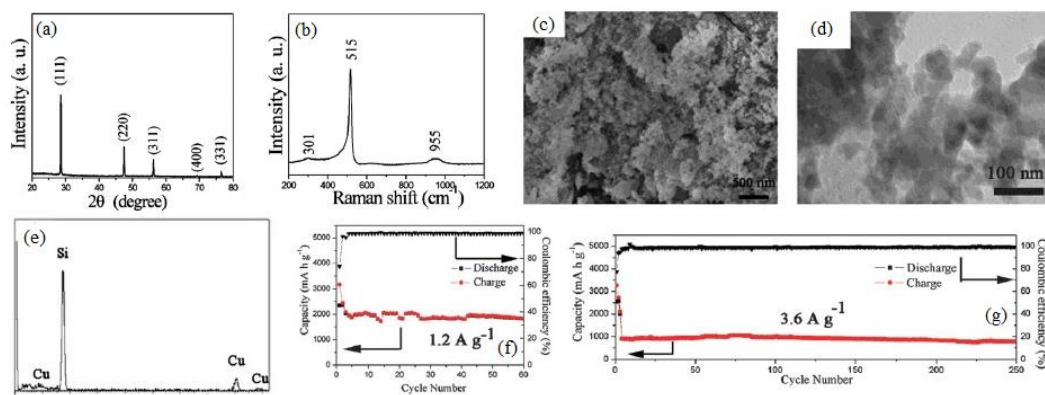


**Figure 1.6 “Metathesis” reaction synthesis SiNPs (a) XRD characterization of SiNPs. (b) Raman characterization of SiNPs. (c) FESEM image and (d) TEM image of SiNPs. (e) EDX spectrum analysis of SiNPs. Cycle performances at (f) 1.2A/g and (g) 3.6A/g current density. [22]**

SiNP is a typical zero dimensional nanomaterial which can achieve the smaller size which facilitate to minimize the volume effect. However, it also has high surface area, decreasing the first charge/discharge efficiency and also affect the slurry condition in water based binder system. One dimensional Si nanowire synthesized using CVD (Vapour-Liquid-Solid mechanism) followed by etching methods. SiNW provides a relative easier structure to blend in slurry, sufficient free space to accommodate volume change and better  $\text{Li}^+$  and electron conductivity in LIBs.

Later, three-dimensional growth of highly dense SiNWs were deposited on carbon paper which shown in Figure 1.7 (a) [28]. TEM image in figure 1.7 confirmed that the SiNW had a core-shell structure. According to HRTEM images, the core shell structure of 34nm crystalline Silicon covered by amorphous shell. The diameter of SiNW was approximately 120nm. The reversible capacity was about  $3\text{mAh}/\text{cm}^2$  achieved with  $1.06\text{mg}/\text{cm}^2$  SiNWs deposition and only  $0.2\text{mAh}/\text{cm}^2$  capacity contributed from carbon matrix. The result of half cell test indicated  $1350\text{mAh}/\text{g}$  reversible capacity retained after 200 cycles, which was 43.5% capacity retention. The full cell consist of SiNW core shell anode are  $\text{LiFePO}_4$  cathode tested at 0.25C exhibited small reversible capacity after 70 cycles without the balance of cathode and anode capacity. Electrochemical impedance spectroscopy (EIS) test shown that internal resistance increased with more cycles, like the normal full cell test.

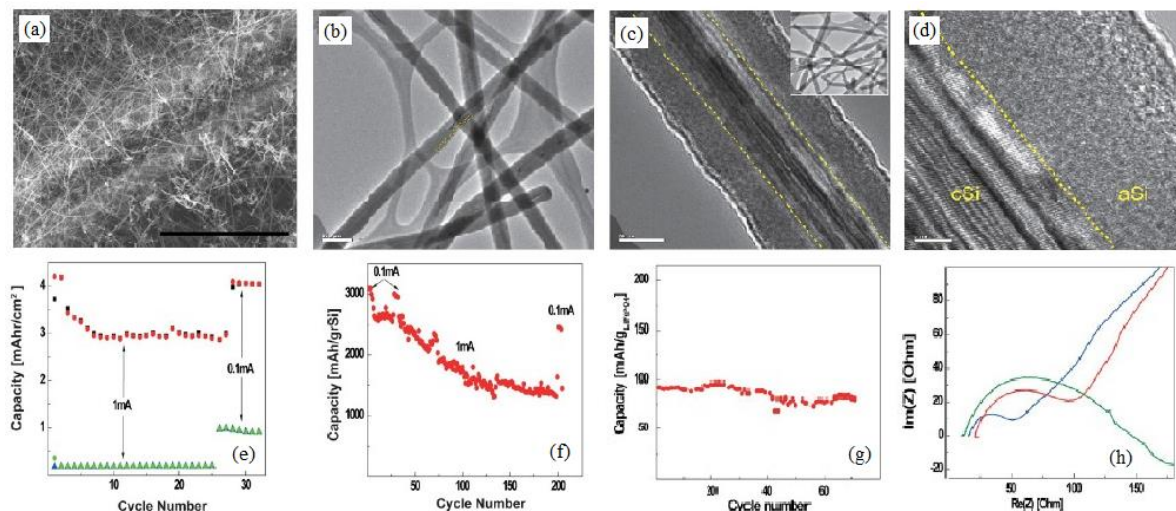


**Figure 1.7 SiNWs deposited on carbon paper (a) SEM image of 1.63mg/cm<sup>2</sup> SiNWs 3D anode before cycling, scale bar is 20μm. (b) Low-magnification TEM image. HRTEM image of (c) SiNWs and (d) core-shell structure. (e) Capacity contribution of the carbon matrix only and with SiNWs. (f) 1.06mg Si/cm<sup>2</sup> anode cycle performance. Full cell cycle performance (g) in coin cell format and (h) internal resistance analysis. [28]**

Of late, SiNWs were grown on stainless steel using CVD method was reported [31] and their performance are shown in Figure 1.8. The SEM images indicated that the morphology of SiNWs were well maintained after prelithiation and diameter of SiNW was slightly increased because of the formation of Si-Li alloy. TEM images also displayed that the structure change during prelithiation process. Initially, the surface of SiNWs was smooth and after prelithiation, the surface of nanowire became rough due to the formation of SEI and Li-Si alloy and the crystalline Si was still existed. The Au catalyst also deformed which revealed that the Au was also lithiated. With longer treatment, less crystalline Si core was observed until fully disappeared. Based on the systematically study of prelithiation time which shown in Figure 1.8 (i), the SiNWs were half lithiated after 20 minutes and full lithiated after 60 minutes. The lithiated electrodes were cycled in half cell configuration and the discharge capacity of full lithiated electrode was much higher than 20 minutes treatment electrode. The cycle stability was also much improved. In addition, full cell test with SiNWs based anode and Sulfur/mesoporous carbon cathode was carried out at 0.2C current density. The full cell

had 80% capacity retention after 10 cycles and the discharge capacity kept decreasing in the following cycles, reaching 52% capacity retention after 20 cycles.

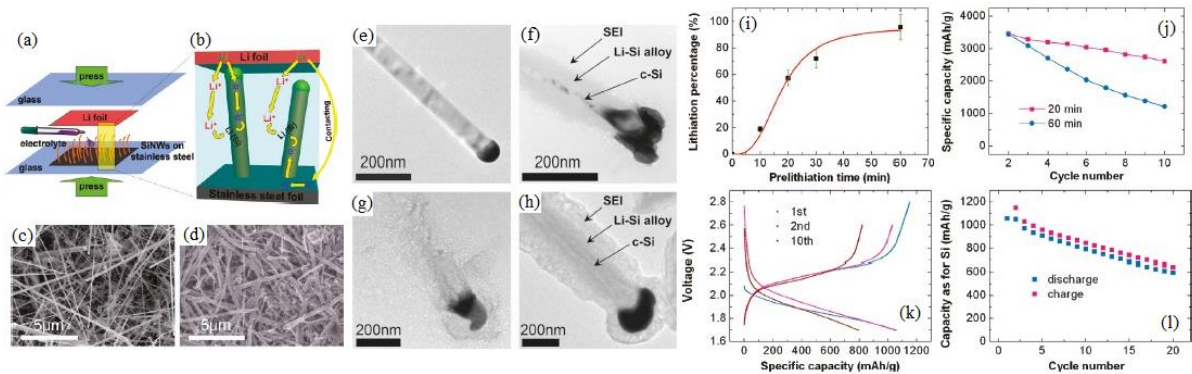


**Figure 1.8 (a) and (b) Schematic diagrams of prelithiation. SEM images of SiNWs (c) before and (d) after prelithiation. (e), (f), (g) and (h) are TEM images during prelithiation. (i) Time dependence study of prelithiation of SiNWs. (j) Cycling performance of SiNWs prelithiated for 20 and 60 minutes. (k) Voltage vs. Capacity profiles of the first, second and 10<sup>th</sup> cycles of the full cell. (l) Cycling performance of the full cell. [31]**

Besides SiNWs, hollow structure Si anode material had the advantage of the inner free space for volume expansion of Si during lithiation process. A novel double walled Si/SiO<sub>x</sub> nanotube anode [32] was designed using polymer template in which the inner layer was active silicon and the outer wall was confining SiO<sub>x</sub>. This unique structure is an excellent structure stabilizer due to the mechanical properties of nanotube. After sealed both tips of nanotubes, the electrolyte only contacted with the outer surface and could not penetrate the inner hollow space (Figure 1.9 (c)). During insertion step, Li<sup>+</sup> penetrated through the outer wall and react with the inner silicon layer. The outer wall was mechanically rigid, so the inner silicon wall expands inward into the hollow space. This inward expansion is probably due to the soft silicon surface. The structure of this anode material was very stable which proved by SEM images (Figure 1.9 (f) and (g)) recorded after 2000<sup>th</sup> cycled electrode. The diameter of SiHNTs almost kept the same and SEI was also stable, confirming by EIS studies presented in figure 1.9 (j). Moreover, the electrochemical performances further indicated that the function of SiO<sub>x</sub> was the key of this structure design which strongly held the SiNT as a

whole. Without the help of  $\text{SiO}_x$  outer layer, SiNTs had 40% capacity retention after 400 cycles and SiNWs only had 20% capacity retention after 150 cycles at 0.2C current density. However, SiHNTs achieved 1350mAh/g capacity after 900 cycles. Long-term cycling test carried out for SiHNTs further confirmed that 88% capacity reserved after 6000<sup>th</sup> cycles at a 10C rate current density.

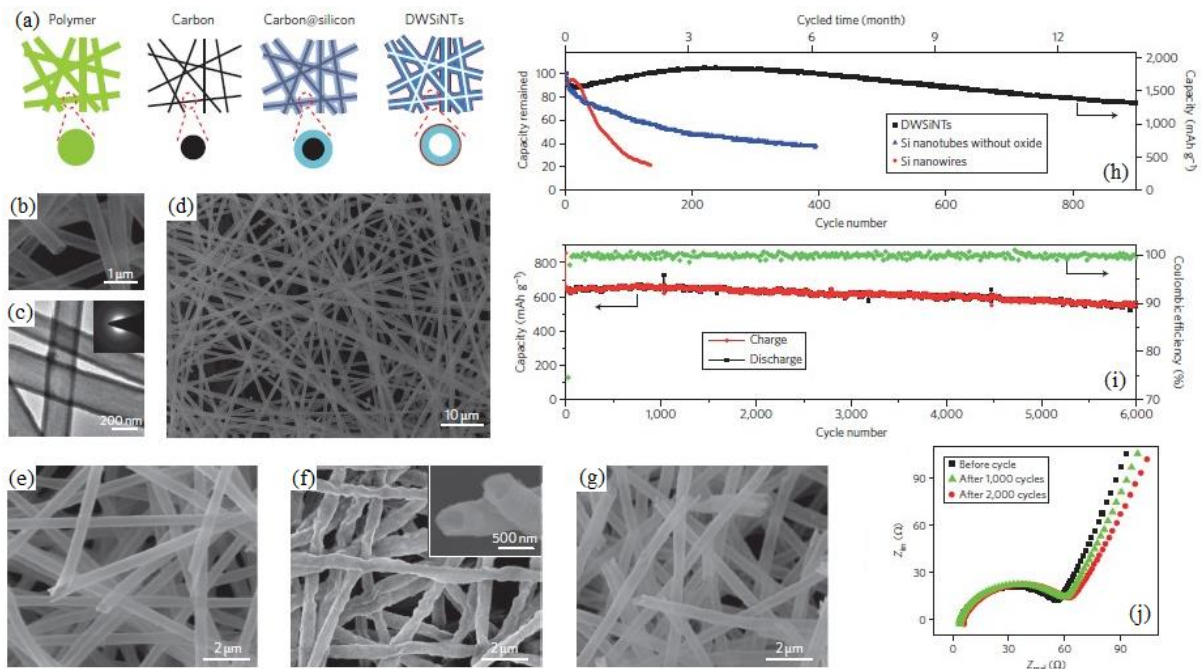


**Figure 1.9 SiHNTs (a) schematic diagram of synthesis. (b) and (d) SEM images of SiHNTs. (c) TEM image of SiHNTs. SEM images of SiHNTs (e) before cycling, (f) after 2000 cycling with and (g) without SEI. (h) Cycle performance of SiNWs, SiNTs and SiHNTs. (i) Long term cycle performance of SiHNTs. (j) EIS analysis of SiHNTs electrode. [32]**

This structure design provides a new concept of void space created inner side of nanoscale material, and  $\text{SiO}_x$  considers as a rigid outer layer which can hold the structure. Although this structure showed enhanced performances, but there are still drawbacks. The first problem is to determine the thickness of  $\text{SiO}_x$  layer that holds the SiNT structure. Further, the control oxidization process of SiNTs surface is also difficult during the formation step. Secondly, sealing the ends of SiNTs is crucial to prevent the inner Si layer from contacting with the electrolyte. The third problem is that the structure is still venerable during the calendar

process. CVD method was applied to deposit Si lay on carbonized polymer fibers, and more similar materials can be explored based on this concept in future with more cost efficiency.

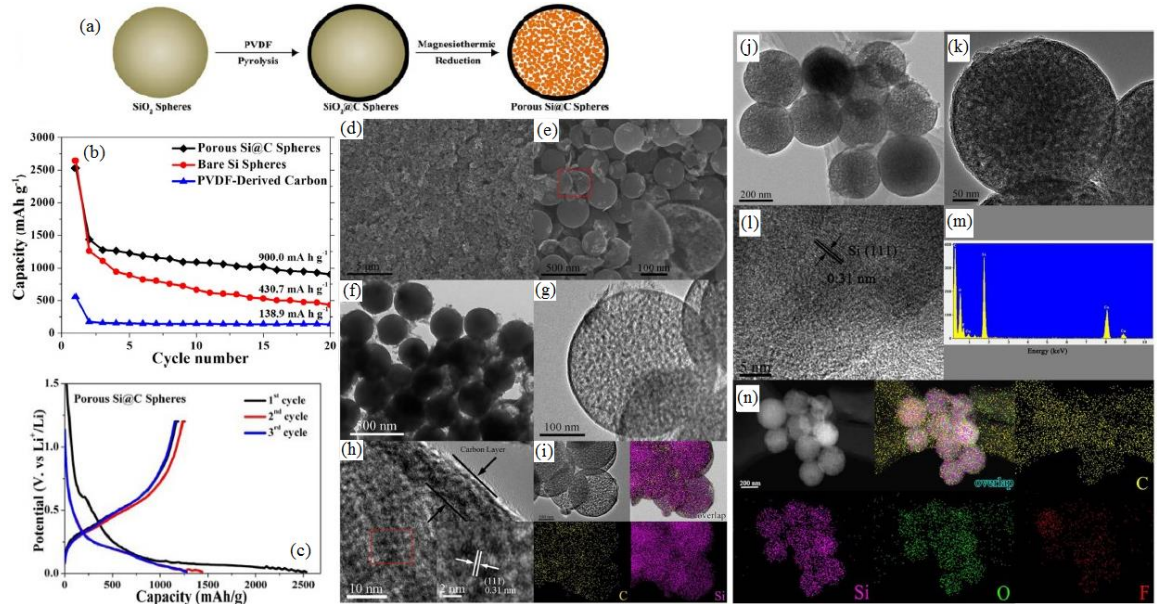


**Figure 1.10 Porous Si@C sphere: (a) Schematic illustration for the synthesis of porous Si@C spheres. (b) Discharge capacities vs. cycle number for bare Si spheres, PVdF-derived carbon and porous Si@C sphere. (c) Discharge-charge curves of Si@C spheres. Morphological, structural and compositional characterizations of porous Si@C spheres: (d, e) SEM images, (f) TEM image, (g, h) HRTEM images, (i) TEM-EDX elemental mapping. Microscopic structural features of porous Si@C spheres in a fully delithiated state after 20 cycles: (j, k) TEM images, (l) HRTEM image, (m) EDX spectrum, and (n) TEM-EDX elemental mapping. [33]**

Core-shell structure is another type of material that could accommodate huge volume change by forming a strong shell layer. Combined with porous structure, core-shell Si anode of porous Si sphere with carbon shell was invented for LIBs [33]. The core-shell structure was developed with SiO<sub>2</sub> sphere and a thin layer of PVdF was formed over SiO<sub>2</sub> sphere and pyrolyzed under the Nitrogen gas atmosphere. As-prepared SiO<sub>2</sub>/C material mixed with Mg powder and calcined at 650°C for 6h under Argon gas. Finally, porous Si@C spheres were obtained by removing excess Mg metal and other Mg by-products in 1M HCl solution. The results of cycling performances shown in Figure 1.10 (b) which clearly revealed that the

porous Si spheres provided over 2 times reversible capacity after 20 cycles in the potential range of 0.01-1.2V at a current density of 0.05C (1C = 4200mA/g). The profiles of voltage vs. capacity of first three cycles revealed that the first efficiency was only 50% and the efficiency was improved over 93% during subsequent cycle. Furthermore, discharge capacities for first three cycles were very close, which indicated that the structure and SEI are stabilized during the initial cycles. The SEM and TEM images before and after cycling test revealed that the porous structure was very stable even after 1000 cycles. EDX analysis results revealed that pristine material only consisted Si and C elements. Two more elements (O and F) were detected after cycling due to the formation of SEI.

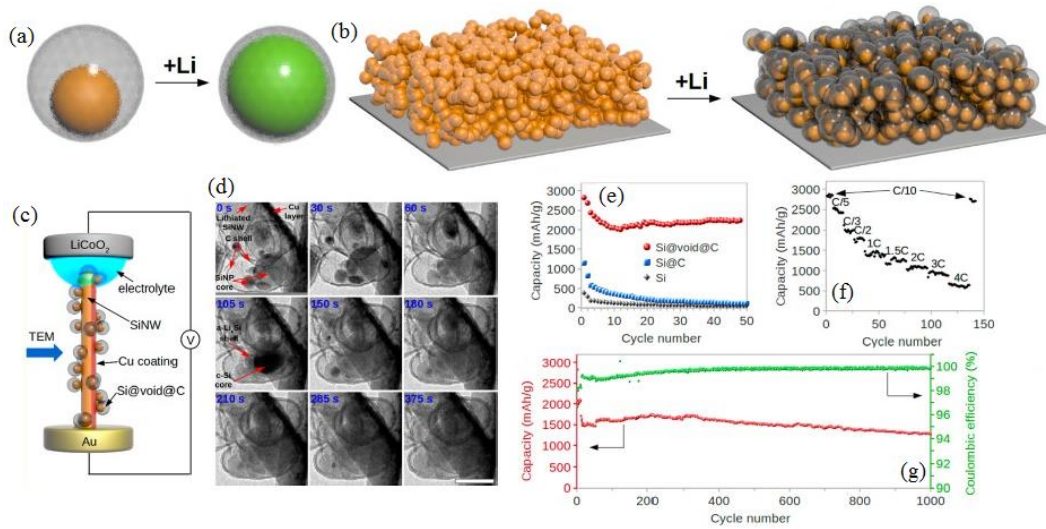


**Figure 1.11 York-Shell Si anode: (a) Schematic of full-lithiated and full-delithiated Si particle. (b) Schematic illustration of Si electrode swelling mode. (c) In-situ TEM technology demonstration. (d) Images of Si particles during lithiation process. (e) Galvanostatic cycling of different silicon nanostructures (PVdF binder). (f) Delithiation capacity of Si@void@C with alginate binder cycled at various rate from 0.1C to 4C. (g) Delithiation capacity and CE of the first 1000 galvanostatic cycles between 0.01-1V (alginate binder), 0.1C for first cycle, 0.33C for 2<sup>nd</sup> to 10<sup>th</sup> cycles and 1C for the later cycles. [36]**

York-shell Si anode material [36] was a kind of modified core-shell structure with void space between Si nano-particles and the outer layer. Figure 1.11 (a) and (b) demonstrated the status of Si particle and electrode between full lithiated and full delithiated. It was clear that the

outer layer could still hold the full lithiated Si particle, which had the maximum volume. In-situ TEM was applied to monitor the SiNP volume expansion to confirm the concept of material structure. According to the TEM images, bigger particles were fully lithiated after 375 seconds and the carbon shell still fully held the Si-Li alloy. Electrochemical tests were also carried out to confirm the performance of the as-prepared materials. It was clear that Si@void@C composite provided a highest specific capacity and good cycle stability during 50 cycles. The C rate result indicated that the anode demonstrated excellent rate capability, exhibiting 600mAh/g at 4C current density and back to 2800mAh/g at 0.1C in following cycles. Long-term cycling test carried out between 0.01 and 1V, the capacity of first cycle was 2833mAh/g at 0.1C current density and increased to 1C for later cycles. The discharge capacity was almost stable around 1500mAh/g, and 1300mAh/g reversible capacity after 1000 cycles.

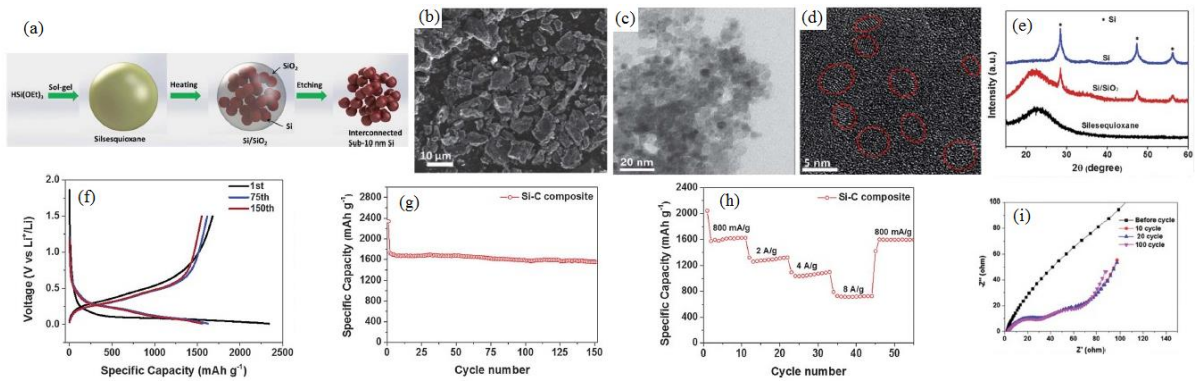


**Figure 1.12 (a) Schematic illustration of the synthesis route of interconnected sub-10 nm silicon nanoparticles. (b) SEM image of Si composite. TEM images of (c and d) Si composed of interconnected sub -10 nm Si nanoparticles. (e) XRD patterns of silsesquioxane ( $\text{SiO}_{1.5}$ ),  $\text{Si/SiO}_2$ , and Si. (f) Galvanostatic profiles, (g) Cycle performance and (h) Rate capabilities of Si/C composite. (i) Nyquist plots of Si/C composite anode electrode before and after different cycles. [39]**

Core-Shell composite Si nanomaterial demonstrated an excellent performance in LIB system. However, micro sized Si anode materials still have its advantage, especially industry application. Generally, the diameters of current active materials are 20-30 $\mu\text{m}$ , and the instruments of slurry making process are ready to blend micro-scale particles. Despite the

excellent performance of nanostructured Si anode, the current techniques are not qualified to apply the nanomaterials due to the smaller size and huge surface area. A micro-sized Si/C composite material synthesized by a two-step process [39]. The synthesis route shown in Figure 1.12 (a), including a sol-gel process and followed by a thermal disproportionation at 1200°C. According to the SEM and TEM spectroscopy observation, Si particles were approximately 10nm and evenly distributed in Si/C composite material. These Si nanoparticles interconnected and formed the micro sized secondary particles. HRTEM technique further indicated that the Si particles were crystalline due to the clear lattice fringe which marked in Figure 1.12 (d). XRD pattern reveals that as-synthesized silicon particles were non-crystalline. The electrochemical performance of secondary Si particles was tested in half cell with a lithium foil counter electrode in CR2016 coin cell format. Galvanostatic profiles demonstrated a stable discharge capacity at 1<sup>st</sup>, 75<sup>th</sup> and 150<sup>th</sup> cycles, respectively. It was obviously that the cell efficiency (CE) of the first cycle was about 60% and the discharge capacities were quite stable for following cycles. Moreover, the rate capability of the secondary Si particles was investigated with increasing current densities from 800mA/g to 8A/g. The discharge capacities decreased with higher current density, however the capacity is retained back to 1600mAh/g after 45 cycles when the current back to 800mA/g. This also confirmed that this structure of Si enables a stable performance in LIB system.

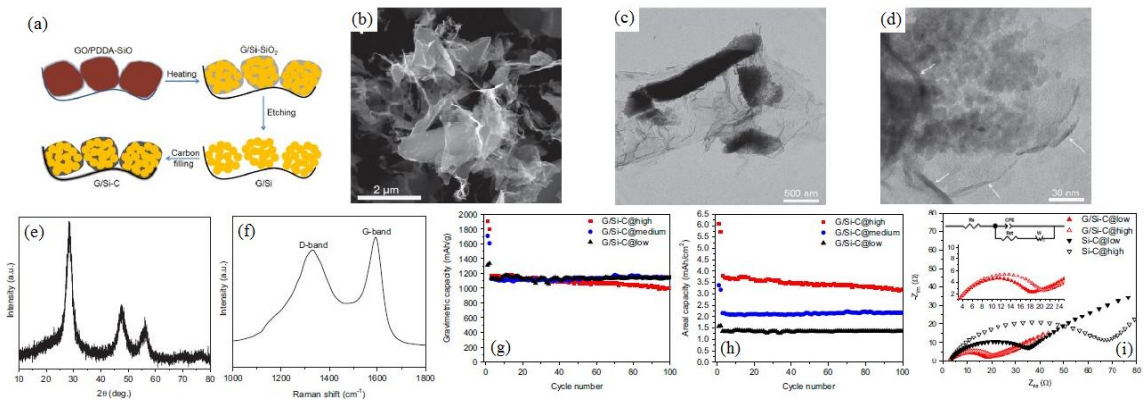


**Figure 1.13 (a) Synthesis process of G/Si-C. (b) SEM image of G/Si-C. TEM images of (c) low and (d) high magnification. (e) XRD and (f) Raman spectrum of G/Si-C. (g) and (h) Cycling performance of G/Si-C. (i) Impedance spectra of G/Si-C at low and high mass loading. Inserted was the Randles equivalent circuit and enlarged spectra showing difference between G/Si-C@ low and G/Si-C@high, respectively. [40]**

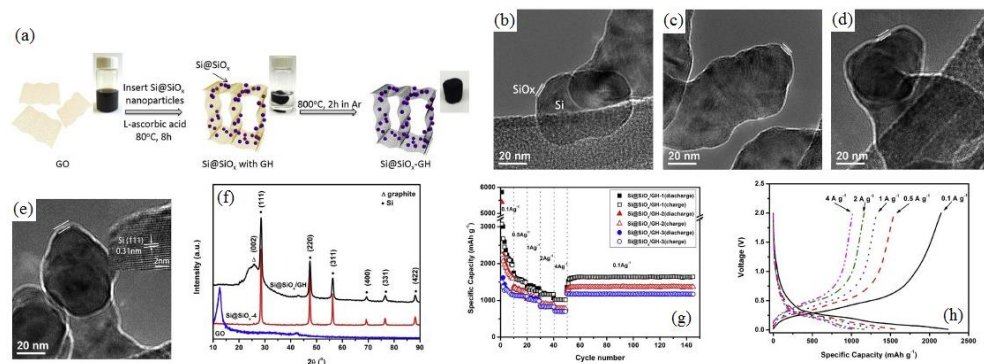


Another secondary micro-sized Si-C composite was proposed by the application of graphene [40], which not only wrapped the Si-C material, also assisted interconnection between Si-C particles. Graphene is a two-dimensional nano-structured material shows extraordinary electronic conductivity and excellent mechanical strength, which greatly improve this Si particles' performances in LIBs. This synthesis method was much complicated (shown in Figure 1.13 (a)), mixing with graphite oxide, PDDA and SiO then heating to form G/Si-SiO<sub>2</sub>, followed an etching treatment and finally filled the material by carbon. SEM and HRTEM images of as-synthesized G/Si-C micro-sized particles revealed that graphene sheets wrapped the Si-C particles. Moreover, Figure 1.13 (d) shown that micro-sized particles were composed of interconnected nanoparticles with 10-15nm size, and the graphene sheet was also clear. XRD pattern indicated that the Si was crystalline. The Raman analysis showed the D (disordered) band and the G (graphite) band of carbon, which further confirmed the presence of carbon in the composite. According to Figure 1.13 (g) and (h), cycle performance demonstrated G/Si-C electrodes with different mass loading in both gravimetric and areal forms. For gravimetric capacity, there was no obvious effect after increasing mass loading, and three mass loading had similar discharge capacities. However, areal capacity dramatically increased with higher mass loading, G/Si-C@high and G/Si-C@low electrodes providing 3.2 and 1.3mAh/cm<sup>2</sup> after 100 cycles, respectively. EIS analysis showed in Figure 1.13 (i) which presented the Nyquist plots of G/Si-C and Si-C electrodes with low and high loadings. It was clear that the internal resistance of Si-C electrode was over 2 times higher than that of G/Si-C, which further confirmed that the introduction of graphene in this structure greatly improved the conductivity.

The concept of SiO<sub>x</sub> matrix is popular in LIB industry mainly because the particle size can be micro sized, which is practical available for current LIB industry capability. SiO<sub>x</sub> materials also provide alternative method to control volume expansion since the oxide silicon is a rigid phase. Compared with other alloy rigid phase (such as Si-Metal alloy), SiO<sub>x</sub> is better because no other elements introduced in LIB system. One of the most important advantages of SiO<sub>x</sub> is low cost which is exactly match the need of LIB industry. Blending with commercial graphite to propose hybrid anode material which deliver higher energy density and practical available in industry as well. The key drawback is low initial efficiency for first cycle

because the existence of oxygen will consume more  $\text{Li}^+$  during cycling. Therefore,  $\text{SiO}_x$  can be considered as an alternative anode material before pure Si material implement.

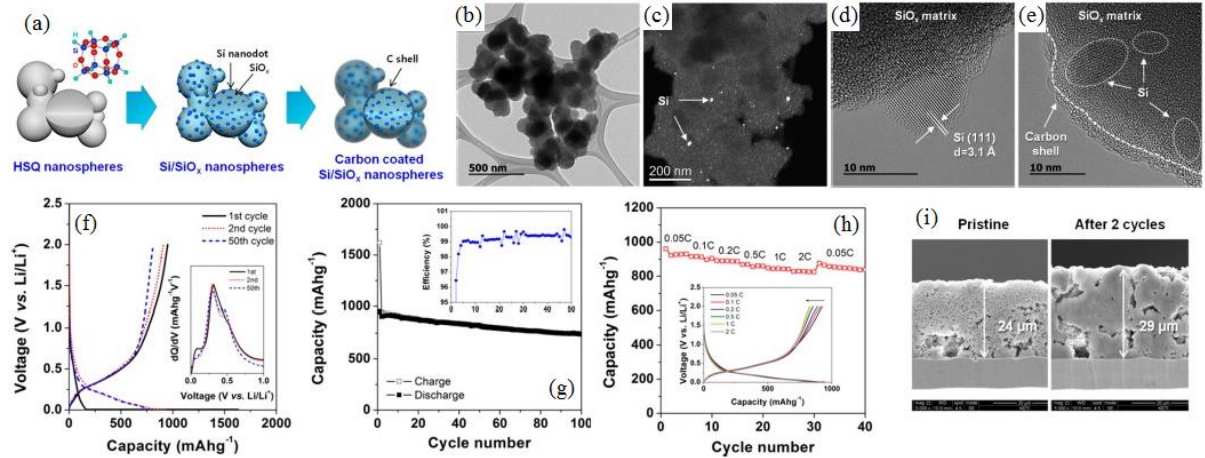
Graphene hydrogel was used as the base of the porous 3D structure, and 50nm SiNPs were introduced in this structure to enhance the performance of the Si anode [41]. Moreover, SiNPs surface covered an ultrathin  $\text{SiO}_x$  layer by an oxidation treatment in an ozone/oxygen flow. The solution based self-assembly process shown in Figure 1.14 (a), containing two steps. This porous structure provided enough active surface to load the  $\text{Si@SiO}_x$  particles and accommodate the huge volume expansion as well. Furthermore, the graphene also improved the electron and lithium ion transportation due to its excellent conductivity. The material morphology and structure were identified by TEM (shown in Figure 1.14 (b), (c), (d) and (e)). SiNPs were coated with a uniform thin layer of amorphous  $\text{SiO}_x$  (thickness of 1.7-4.2nm). A inter planar spacing of 0.313nm was observed at the edge of Si core, which was consistent with the (111) planes of Si [16]. XRD pattern of graphene oxide (GO),  $\text{Si@SiO}_x$ -4,  $\text{Si@SiO}_x/\text{GH}$ -1 were compared in image (f), which indicated successful reduction of GO to reduced GO (rGO). The specific capacities of the  $\text{Si@SiO}_x/\text{GH}$  electrodes were obtained at different C rate which shown in Figure 1.14 (g). It was clear that  $\text{Si@SiO}_x/\text{GH}$ -1 had the best performance in every current density (0.1A/g, 0.5A/g, 1A/g, 2A/g and 4A/g). It had to be noted that all electrodes shown excellent cycle stability after 4A/g test, which indicated that the material and electrode structure were very stable.



**Figure 1.14 Si@SiO<sub>x</sub>/graphene composite material: (a) Schematic illustration of synthesis route. (b), (c), (d) and (e) TEM images of Si@SiO<sub>x</sub>/graphene. (f) XRD pattern of Si@SiO<sub>x</sub>/graphene. (g) Rate cycle performance of Si@SiO<sub>x</sub>/graphene and (h) galvanostatic charge/dishcharge profiles of Si@SiO<sub>x</sub>/graphene. [41]**

Carbon coated Si/SiO<sub>x</sub> composite was reported with a “watermelon” structure [42] by partially reduction in 1200°C under a 4% H<sub>2</sub>/Ar atmosphere. Bright field and dark field of TEM results confirmed that the crystalline Si particles distributed within SiO<sub>x</sub> matrix. Diameter of single Si/SiO<sub>x</sub> particles was about 100-200nm, which related with the size of precursors. HRTEM images further revealed that crystalline Si structure (111) plane was observed and the 5-10nm crystalline Si particles were found on amorphous SiO<sub>x</sub> matrix. The thickness of carbon coating was found to be 2-4nm from TEM images. Figure 1.15 (f) shown the voltage profiles of a carbon coated Si/SiO<sub>x</sub> electrode for 1<sup>st</sup>, 2<sup>nd</sup> and 50<sup>th</sup> cycles. The cell efficiency of the first cycle was about 58% with a discharge capacity of 951mAh/g. The inserted image was the profile of dQ/dV in which a main peak was observed at 0.4V (vs. Li/Li<sup>+</sup>). This indicated that the electrochemical redox reaction between Si and Li<sup>+</sup> happened around this voltage. For long-term cycle test, the result also demonstrated stable performance after the activation cycles. The retention capacity was 740mAh/g after 100 cycles, which equal to 78% of its original capacity. Rate capability test also indicated that the discharge capacities were almost identical as the current density increased from 0.05C to 2C, which further confirmed that this composite material shown excellent conductivity and reversible electrochemistry reaction. Moreover, the SEM image of cross section Si-based electrode before and after 2 cycles proved that the swelling of electrode was only 20% after the activation cycles.

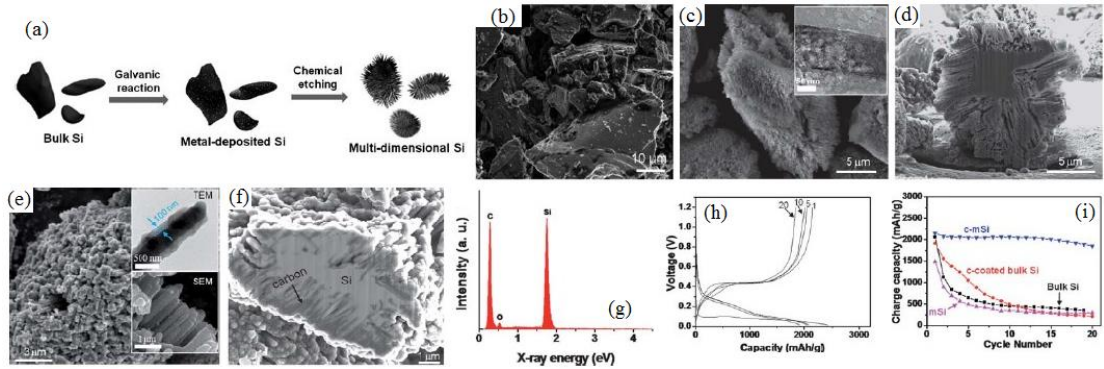
Based on the references above, nano structured Si anode has been greatly improved to achieve stable cycle performance. However, the nanomaterials are not applied in current LIB industry, not only because of the difficulty to produce, but also the cost of the production process is high for LIB application. Therefore, the second solution is to create a porous structure which provides enough void space to accommodate the volume expansion. Another advantage of porous structure Si anode is the particle size can be designed to micro size which is good for practical application in LIB industry.



**Figure 1.15 (a) Schematic illustration of the synthetic route. TEM images of (b) bright-field and (c) dark-field of HSQ-derived Si/SiO<sub>x</sub> nanospheres. HRTEM images of (d) a crystalline Si nanodot embedded in a SiO<sub>x</sub> matrix in the HSQ-derived Si/SiO<sub>x</sub> nanospheres and (e) C-coated Si/SiO<sub>x</sub> nanosphere. (f) galvanostatic charge and discharge profiles. (g) Cycle performance and Coulombic efficiencies (insert) of C-coated Si/SiO<sub>x</sub> electrodes. (h) Rate capability of a carbon coated Si/SiO<sub>x</sub> electrode at different currents. (i) Cross-sectional FESEM images of C-coated Si/SiO<sub>x</sub> electrode before and after 2 cycles. [42]**

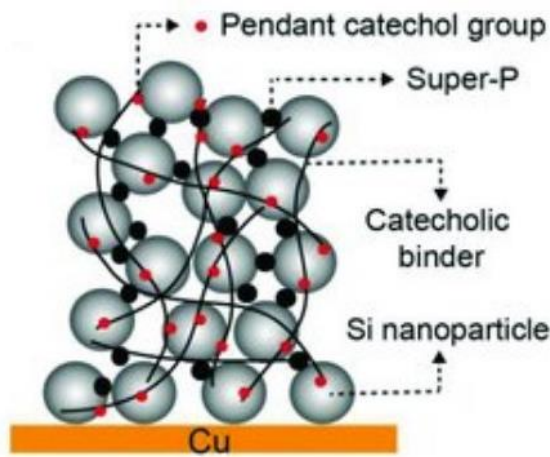
Chemical etching is also a popular method to produce porous Si anode. Figure 1.16 (a) shows a synthesis route of porous Si particle using metal assisted etching method [47]. This method involved depositing silver nanoparticles on micro size Si particle surface. Then, Ag particles embedded on Si spheres dissolved in HF solution to make Si surface porous. The SEM image (Figure 1.16 (d)) of cross section of Si particle confirmed that long holes were created during this etching method. After carbon coating treatment, the holes of porous Si particles were filled up by carbon. The inserted TEM image shown a uniform carbon layer coated on Si nanowire. The XRD pattern indicated that carbon, oxygen and Si elements were detected. Brunauer-Emmett-Teller (BET) result also indicated that the carbon filling greatly reduced the surface area of etched Si particles. Figure 1.16 (h) shown the voltage profiles of c-mSi electrodes with a carbon coating exhibited stable electrochemical reversibility in first 20 cycles. Compared with carbon coated bulk Si, bulk Si and mSi, c-mSi provided enhanced reversible capacity of 1850mAh/g after 20 cycles. The problem for etching methods is the

HF acid which is toxic, corrosive and dangerous. Therefore, safety is the key issue for this method to be applied in practical application.



**Figure 1.16** (a) Schematic illustration of etching process. SEM images of (b) Bulk Si, (c) etched Si and (d) cross-section of etched Si particles, SEM images of (e) carbon coated porous Si and (f) cross-section of carbon coated porous Si, (g) XRD pattern, (h) Voltage profiles of c-mSi and (i) Charge capacity vs cycle number for the c-mSi at a rate of 0.2C after the first cycle at 0.1C rate. [47]

### 1.3.2 Binders



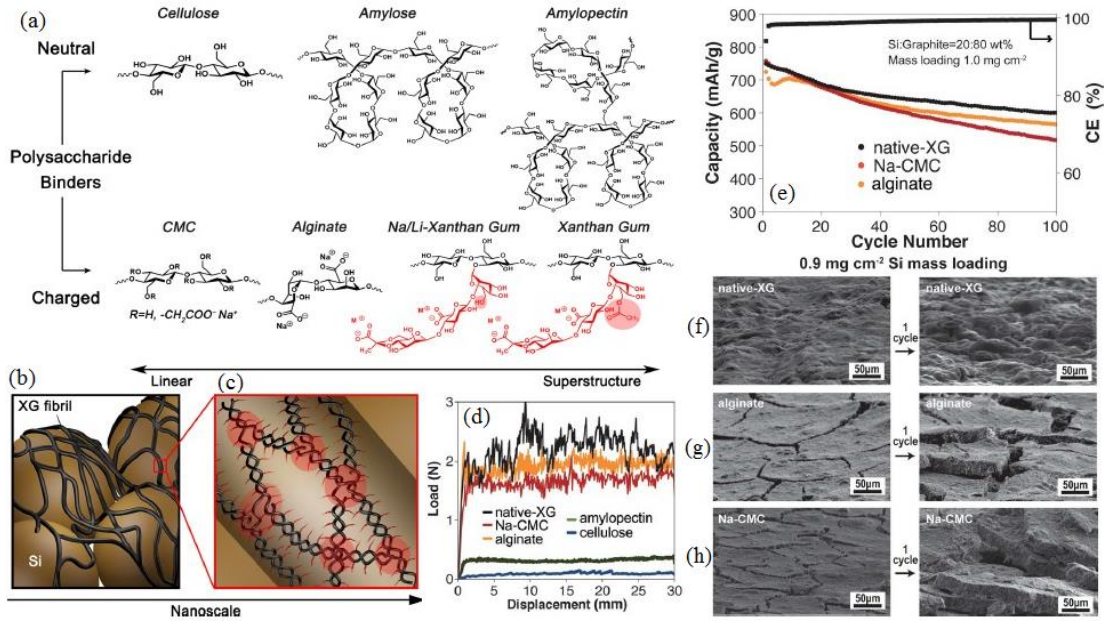
**Figure 1.17** Schematic illustration of Si-based electrode. [51]

Figure 1.17 shows a typical Si-based electrode structure with SiNPs, binder (catecholic binder) and conductive agent (Super-P). It is obviously that the function of conductive agent

is to improve the conductivity of electrode, short the path of electron and lithium ion transportation, reduce the polarization of electrochemical reaction and finally improve the cycle performance [12, 51]. Current conductive agents are carbon materials, such as carbon black and Super-P due to the low cost. Polymer binders are another key component that hold active materials and stick the active particles on the current collector as well. Generally speaking, a good binder material has to possess good mechanical properties and electrochemical stability, such as high ionic conductivity, better adhesion property, less dissolution in electrolyte, proper melting point, high purity, higher tensile strength and narrow molecular weight distribution. Compared with traditional graphite electrode, the binder is more crucial due to the huge volume change of Si-based electrode during cycling. Current commercial polymer binders for graphite are carboxymethyl cellulose (CMC) + styrene butadiene rubber (SBR) or polyvinylidene fluoride (PVdF), are not good enough for Si anode. According to the references, there are two more requirements for Si anode in LIBs. First, the polymerized binder should be a huge net with more cross links which can provide better mechanical properties to accommodate the volume change. Secondly, more functional groups should be synthesized in the end of binder molecular which can form a strong bond with Si anode. More work already have been done [52-61] in last few years in this area.

Compared to CMC and Alginate, XG binder was proposed for SiNP anode which provided more cross links after polymerization as shown in Figure 1.18 (a) and (b) [52]. Moreover, in the end of side chain, acetyl functional groups (shaded in red) were found which was critical in the formation of the double helix superstructure. With the help of this superstructure, a series of inter/intramolecular hydrogen bonding interactions generated the fibrils network which fully covered the surface of SiNPs anode material and provided a self healing effect. This effect was critical for the Si anode to accommodate its huge volume change. It has to be noted that the native-XG binder mainly used as food additives, rheology modifiers, pharmaceutical and cosmetic industries for few decades. Therefore, native-XG has been mass produced for a decades at relatively cheap cost. The result of peeling strength test indicated that the electrode with native-XG binder had higher loading at same displacement, demonstrating the strongest connection with current collector. The binder effect was further proved in cycling test by using Si graphite composite electrode (2:8 mass ratio) at  $1.0\text{mg}/\text{cm}^2$  mass loading. It was clear that the retention capacities of electrode using native-XG, alginate

and CMC binder were 80%, 78% and 68.3%, respectively, after 100 cycles. SEM images of 0.9mg/cm<sup>2</sup> electrode surface prepared with native-XG binder before and after 1<sup>st</sup> cycle further confirmed that there was no obvious crack observed, however more cracks found on other two electrodes constructed with CMC and alginate binder. This result revealed that polymer structure with more cross-link and functional groups facilitated to form a stronger net to hold the Si anode, improving the cycle stability.



**Figure 1.18 (a) Molecular structure in neutral and charged status. (b) and (c) Schematic illustration of XG binder function on nano-scale. (d) Peeling test results for SiNP electrodes based on five binders. (e) Cycle performance of SiNP electrodes with three binders. SEM surface morphology of electrodes before and after first cycle with (f) native-XG, (g) alginate and (h) Na-CMC binders. [52]**

Another approach of self healing polymers (SHPs) as binder for Si electrode was invented [53]. The process was different to traditional electrode preparation as presented in Figure 1.19 (a). Initially, Si slurry was casted on Cu foil followed by drying and pressing treatment. Only Si particles left in this electrode. Then, SHP/CB slurry was coated on the surface of Si electrode by doctor's blade casting method. Blading the electrode surface was critical under heating condition until the SHP/CB infiltrated into the entire thickness of the Si layer. The SEM image Figure 1.19 (d) confirmed that the SHP/CB slurry fully covered the Si particles

and the interface with Cu foil. The size of Si particles was around 800 nm diameter for this electrode. Cycle performance of silicon electrode blended with commercial binders and SHP/CB are shown in Figure 1.19 (e). The result indicated that SHP/CB binder could provide the best cycle stability over 100 cycles based on  $2.0\text{mAh/cm}^2$  and  $3.2\text{mAh/cm}^2$  capacities, and the capacities retention were 90% and 85%, respectively after 120 cycles at a current of  $0.3\text{mA/cm}^2$ . Furthermore, the discharge capacities of electrode with SHP/CB electrodes almost recovered once the current back to  $0.1\text{mA/cm}^2$ . EIS measurement indicated that the internal resistance of half cell was increasing along the cycling test, but the electrodes were much stable after 20<sup>th</sup> cycles. The SEM images of electrodes before and after cycling also confirmed that the structure of electrode was very stable. Despite of the small cracks found in SEM image of cross-section electrode after long-term cycling, the performance was still very stable for over 240 cycles.

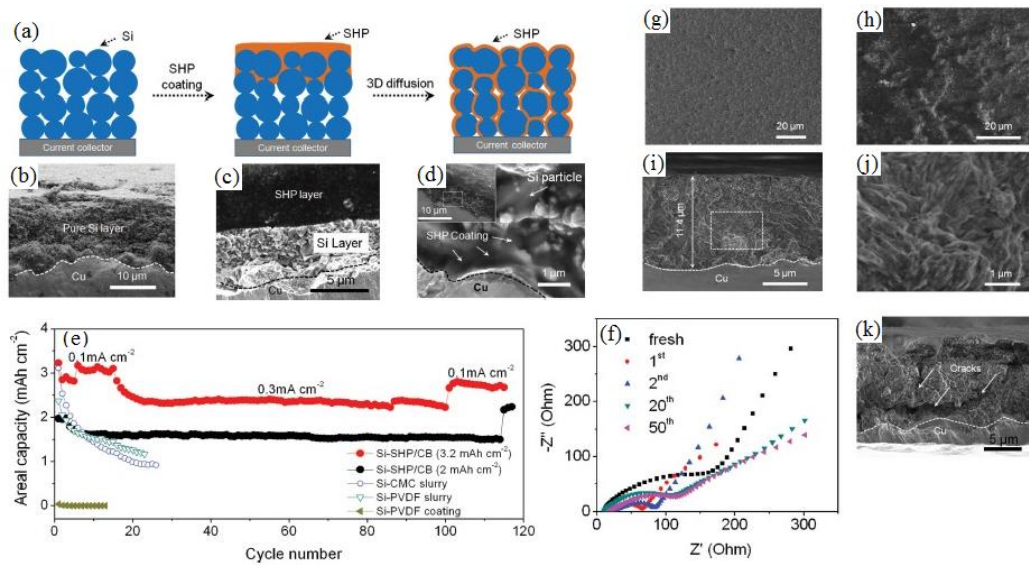


**Figure 1.19 (a) Schematic illustration of Si-SHP/CB electrode. (b) Pure Si electrodes made from Si particles. (c) SHP/CB layer coated on top of Si electrodes with one-time blading. (d) Si electrodes filled with SHP/CB forming a 3D distribution inside electrodes from repeated blading under heating. (e) Cycle performance of thick Si-SHP/CB electrodes. (f) Nyquist plots of the high mass loading 3D Si-SHP/CB electrodes at different cycling status. SEM images of Si-SHP/CB electrodes (g) before and (h) after cycling. Cross-section SEM images of Si-SHP/CB electrodes (i) before and (j) after cycling. (k) Cross section SEM image of cycled electrode. [53]**



Another approach of self-healing polymers (SHPs) on Si electrode was invented [53]. The process was different to traditional electrode preparation as presented in Figure 1.19 (a). Initially, Si slurry was casted on Cu foil followed by drying and pressing treatment. Only Si particles left in this electrode. Then, SHP/CB slurry was coated on the surface of Si electrode by doctor's blade casting method. Blading the electrode surface was critical under heating condition until the SHP/CB infiltrated into the entire thickness of the Si layer. The SEM image Figure 1.19 (d) confirmed that the SHP/CB slurry fully covered the Si particles and the interface with Cu foil. The size of Si particles was around 800nm diameter for this electrode. Cycle performance of silicon electrode blended with commercial binders and SHP/CB are shown in Figure 1.19 (e). The result indicated that SHP/CB binder could provide the best cycle stability over 100 cycles based on 2.0mAh/cm<sup>2</sup> and 3.2mAh/cm<sup>2</sup> capacities, and the capacities retention were 90% and 85%, respectively after 120 cycles at a current of 0.3mA/cm<sup>2</sup>. Furthermore, the discharge capacities of electrode with SHP/CB electrodes almost recovered once the current back to 0.1mA/cm<sup>2</sup>. EIS measurement indicated that the internal resistance of half cell was increasing along the cycling test, but the electrodes were much stable after 20<sup>th</sup> cycles. The SEM images of electrodes before and after cycling also confirmed that the structure of electrode was very stable. Despite of the small cracks found in SEM image of cross section electrode after long-term cycling, the performance was still very stable for over 240 cycles.

Functional binders such as conductive and self healing binders are attracting much more attentions in last few year. Further modified binders formed by introducing different functional groups in binder molecular are created to meet the certain requirements. Alternative method to introduce functional group is using conductive polymer monomer. This could also improve the electrode's conductivity after polymerization. Polyfluorene with octyl side chains, one kind of conductive polymer monomer, was added in a four components binder to make electrode [56]. The total four polymer monomers and their structures and the combinations are compared in figure 1.20 (a). The peeling test indicated that combination of PEFM31 binder exhibited highest mechanical strength at about 1.7lbf load. The swelling test defined as the ratio of the weight of absorbed electrolyte of ethylene carbonate (EC) and diethyl carbonate (DEC) (EC: DEC = 1:1, w/w) to the weight of polymer films in the dry state at room temperature. PFM binder electrode had the lowest electrolyte capability, 10%

after 20h, which indicated that this electrode had the poorest property of electrolyte absorption. On the contrary, the electrodes of PEFM21 and PEFM31 demonstrated better electrolyte absorption of 55% and 28% after 20h. In addition, most of the electrolyte was absorbed in the first hour (about 40% for PEFM21 electrode and 19% for PEFM31 electrode).

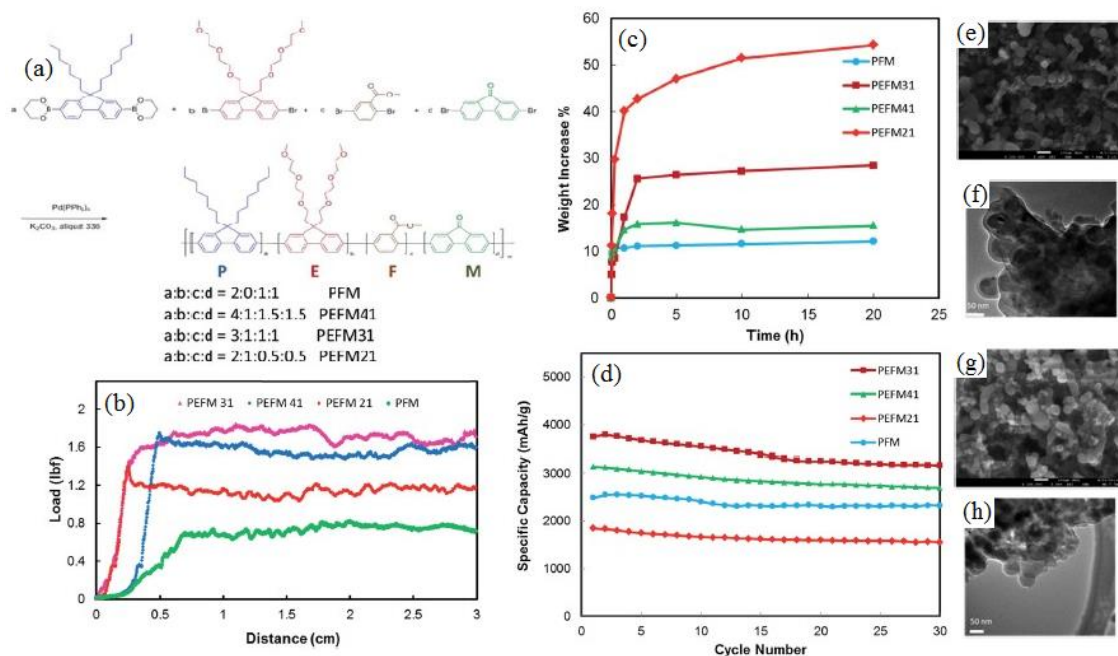


**Figure 1.20 (a) Synthetic scheme and the relative molar ratio of four functional blocks of polymer binders. (b) Peeling strength test results for four electrodes. (c) The swelling tests of polymer films in the EC/DEC (1:1) electrolyte. (d) Cycle performance for four electrodes without any conductive agent. SEM images of PEFM31 electrodes (e) before and (f) after cycling. TEM images of PEFM21 electrodes (g) before and (h) after cycling. [56]**

The electrodes of cycling test were prepared without blending any conductive agent for better comparison. The result clearly distinguished four curves in which the electrode of PEFM31, the polymer binder with medium polarity, had the highest discharge capacities in first 30 cycles. The SEM images before and after cycling shown the distinct difference between PEFM21 and PEFM31 electrodes due to the largest difference in specific capacity. The

surface morphology of electrodes before cycling were similar, and the binder layer also fully covered the Si particles after 1<sup>st</sup> cycle.

In short, for the materials with huge volume change during cycling like Silicon, Germanium and Tin anode, the properties of binder can greatly affect the cycle stability. Therefore, better binder with good mechanical strength and more functional groups are always needed to achieve enhanced electrochemical performances. Furthermore, with the help of more functional groups in polymer molecular, the weight ratio of binder in electrode can also be reduced, which is another way to increase the energy density and reduce the cost as well.

### 1.3.3 Electrolyte

Except cathode and anode active materials, electrolyte is another component which can dramatically affect the LIB performance. Generally speaking, electrolyte is a media to facilitate the movement of Li<sup>+</sup> in battery system. Furthermore, it also involves in electrochemical reactions with active materials, forming a thin layer on both cathode and anode electrodes surface, what is known as solid electrolyte interphase (SEI). SEI is mainly formed in the first few cycles by consuming Li<sup>+</sup>, which is also the reason of low cell efficiency of first cycle. A stable SEI is essential to get stable cyclic performance because it protect the surface of active materials from the degradation of electrochemical reaction. During the process of lithiation/delithiation, SEI film is forming and decomposing at the same time. When the rate of film forming and decomposition are the same, SEI will maintain a balanced thickness to separate active materials and electrolyte. The properties of SEI are determined by the components of SEI formed by electrochemical reaction of solid/liquid interface. Therefore, the proper formulation of electrolyte is required for Si-based electrode in LIB system, including the selection of proper solvents and additives, as well as the combination of these components [62-67].

Fluoroethylene carbonate (FEC) is regarded as one of the most critical additives in Si-based LIBs. However, only few references related with the mechanism of FEC in battery system due to the difficulties of characterization on SEI [68, 69]. Usually, the thickness of SEI layer is only few nanometers which require higher resolution microscopy and higher energy

spectroscopy to analysis it. Si anode material was tested in two electrolytes, LP40 without FEC and LP40/FEC with 10 wt% FEC [63]. The cycle performance demonstrated that more stable cycling can be achieved with FEC/LP40 electrolyte. Nyquist plots were also confirmed that smaller internal resistance detected in FEC/LP40 cell. SEM images indicated that no obvious cracks were found on the surface of cycled Si electrode in FEC/LP40 electrolyte. On the contrary, more cracks were seen on cycled Si electrode without the FEC additive. The most surface sensitive measurement technique like soft X-ray PES was performed to collect the SEI information at different state of charge (SOC). The result revealed that the FEC molecular either de-fluorination or ring opening during the decomposition reaction, finally forming LiF and  $-\text{CHF}-\text{OCO}_2-$  type compounds as the by-products.

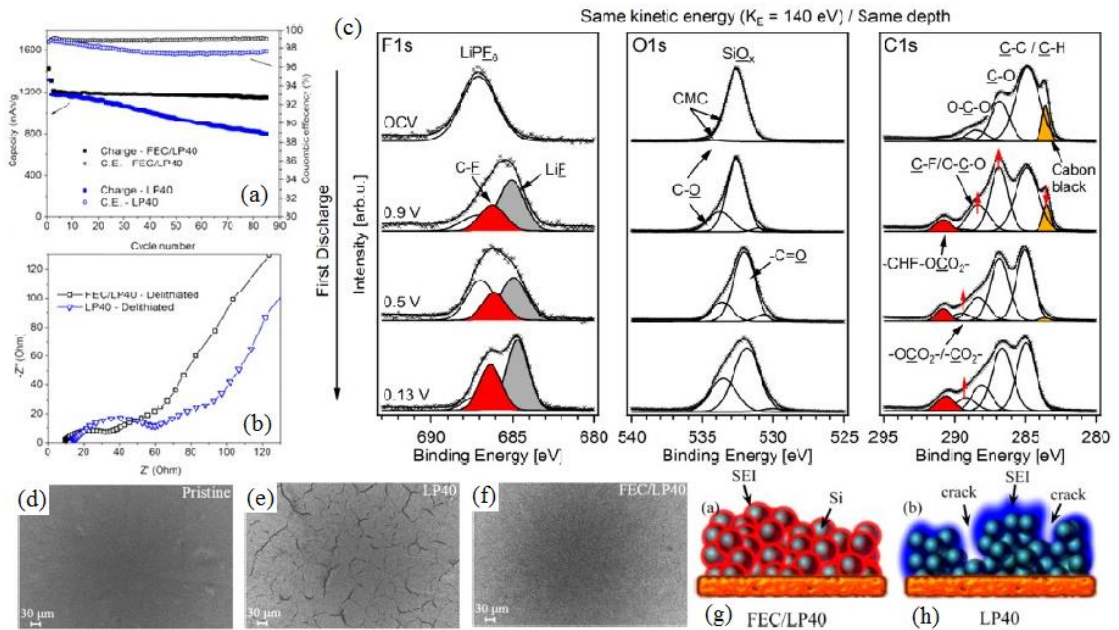


**Figure 1.21 (a) Cycle performances and (b) Nyquist plots in with/without FEC electrolyte. (c) F 1s, O 1s, and C 1s spectra of the silicon electrode at different SOC in FEC/LP40 electrolyte. SEM images of (d) before and after cycling in (e) LP40 and (f) LP40/FEC electrolyte. Mechanism of FEC protection in (g) LP40/FEC and (h) LP40 electrolyte. [63]**

Another approach was carried out to determine the proper ratio of FEC in electrolyte [65]. The cycle performance indicated that the FEC/DMC (50%/50%) electrolyte provided the most stable battery with a 500mAh/g capacity higher than that of FEC/DEC (25%/75%)

electrolyte. EIS analysis revealed that FEC greatly reduced the internal resistance of the battery. The long-term cycling also proved that FEC/DMC electrolyte improved the capacity retention, achieving 2000mAh/g reversible capacity after 250 cycles.

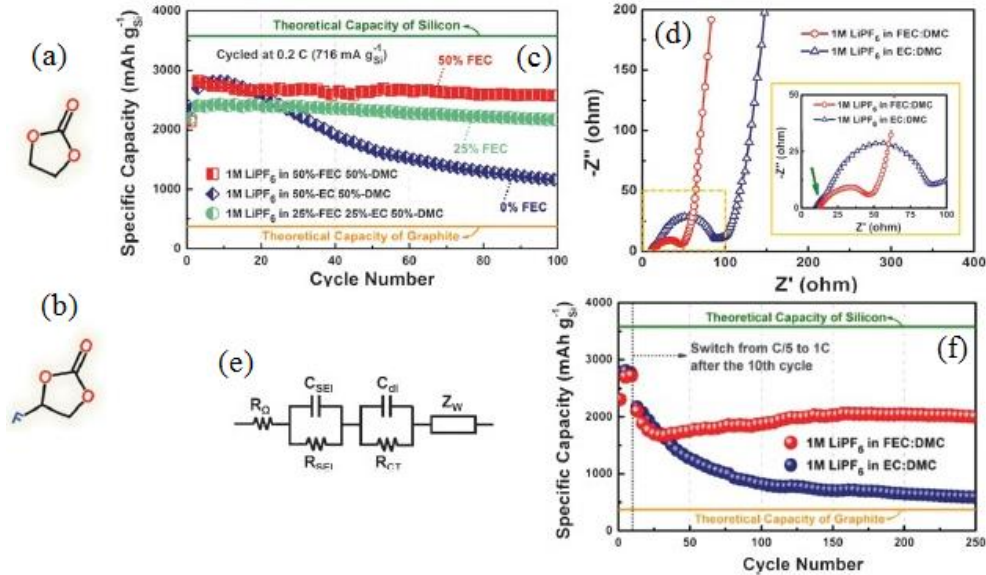


**Figure 1.22 Molecular structure of (a) EC and (b) FEC. (c) Cycle performance in electrolytes with different ratio of FEC. EIS analysis results of (d) Nyquist plots and (e) equivalent circuit. (f) Long-term cycle test. [65]**

All those three aspects are the key issues in Si-based battery system for next generation high energy density LIBs. More work has to be carried out in future to solve these problems step by step.

## 1.4 Thesis objectives

Silicon suffers from the huge volume change during cycling, which limits its practical application in LIBs. Many scientists are working on this hot topic to overcome the challenge of rapid storage capacity degradation and approach a stable cycle performance of Si. However, LIB is a systematic engineering. Active materials are important, but the other components and processes are also crucial. Based on the academic research in university and research institutions, more work is waiting for us when convert the laboratory level silicon

anode material to the industrial product. Therefore, modification on the electrode and optimization on the whole electrochemistry system are also critical parts of practical application in battery. Three parts of tasks were carried out to focus on this target which shows in Figure 1.23.

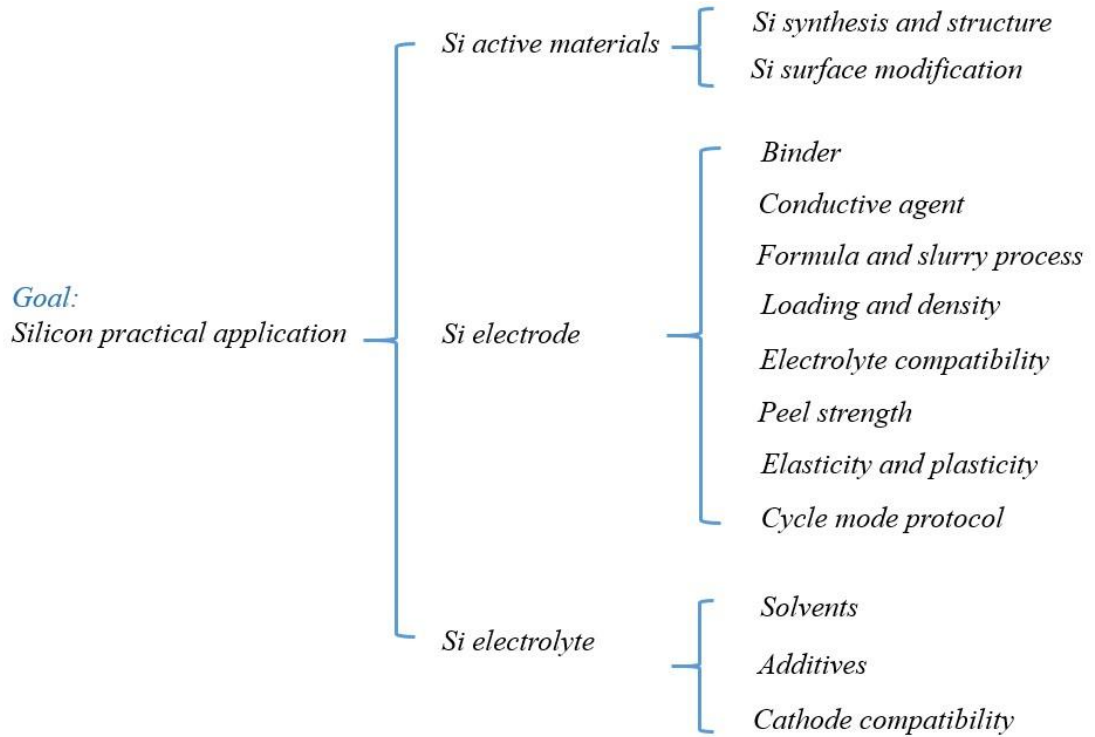


**Figure 1.23 Development of Silicon based Lithium-Ion Batteries.**

#### Part 1. New solution for synthesis Si anode

Silicon element is very stable which only has a higher reaction rate with HF acid etching steps in low temperature. Unfortunately, HF is dangerous and toxic for both human beings and environment. Therefore, metal assist etching synthesis cannot be a good option for mass production of Si anode. Meanwhile, other methods currently using are either expensive or low yield (such as CVD) which is not cost efficiency. In this thesis, a new HF free method to produce SiNW is proposed by using Si-Al alloy.

#### Part 2. Optimization of Si electrode parameters

From the point view of LIB industry, except Si anode materials, a few other factors also have to be solved for Si-based LIBs. One key point is the mass loading of Si electrode. Most references mentioned that better battery performance are obtained from the electrodes with lower mass loading (e.g. 0.2-0.5mg/cm<sup>2</sup>) including the binder and conductive. It's reasonable for initial evaluation the Si anode. However, this low loading is not enough to achieve high energy density in LIBs industry (as seen in Table 1.2). Density of electrode is another parameter which relate with the volumetric energy density of LIBs. Therefore, finding a proper density for specific Si anode is necessary to achieve a stable cycle performance in LIB industry. Binder properties directly affect the stability of Si electrode since the selection of proper binders can greatly improve the connection between active materials and current collector. The last point is to select right components and optimize a proper ratio for a better Si electrode. This part is much related with the proper parameters which facilitate the preparation of practical application of Si anode in LIB industry.

**Table 1.2 Comparison of energy density and mass loading**

	Graphite	SiNW electrode						
Loading - mg/cm <sup>2</sup>	15	0.1	0.5	1.0	1.5	2.0	2.5	3.0
Electrode thickness - μm	83	19.1	23.5	29.0	34.4	40.0	45.5	51.0
Volumetric energy density - Wh/l	672	138.5	562.9	912.4	1153.8	1323.0	1453.8	1556.5
Gravimetric energy density - Wh/kg	223	26.2	126.0	240.5	345.1	441.0	529.2	610.6

*calculation based on: commercial graphite electrode, 18μm Cu foil and one side coating SiNW electrode with formula: 63% SiNW, 22% carbon black, 15% sodium alginate and 0.93g/cm<sup>3</sup> electrode density, 4200mAh/g for SiNW, Average voltage: 1V.*

### Part 3. Electrolyte improvement

The final part of this work will focus on electrolyte, which is not only the medium for the Li<sup>+</sup> transportation, it also involve the electrochemistry reaction during the surface of anode electrode. The solid electrolyte interphase (SEI) is formed in the first few cycles of LIBs and the composition of this thin layer is highly depended on the selection of the electrolyte

components. For silicon anode, a stable SEI is very important for its stable cycle performance. Furthermore, more electrochemical/physical properties of Si electrode can be modified by applying different electrolyte additives, such as flame retardant, high/low temperature cycle performance and storage performance. Moreover, besides cathode and anode materials, electrolyte is the factor left which can adjust the cell performance. A good electrolyte formula with right ratio of these components is also crucial for a stable electrochemistry system of Si based LIBs. The synergies of FEC and VC additives had been proved and discussed to further improve the cycle stability for Si-based LIBs.

## 1.5 Thesis organization

This thesis contains six chapters organized in an integrated article format: an introduction, a summary of the experimental methods, three articles, and a concluding chapter. It is organized in accordance to the Thesis Regulation Guide from the School of Graduate and Postdoctoral Studies at Western University. The outline of each chapter is as follows:

**Chapter 1** is an introduction to the fundamentals of LIBs including the market and work principle, then a brief discussion of anode materials. This is followed by a detailed introduction of synthesis methods, binders and electrolyte for Si-based LIBs. Finally, a proper strategies is proposed for the practical application of Si anode in LIBs.

**Chapter 2** provides a detailed description of the experimental methods for the CVD device to conduct heat treatment process. Most of the characterization techniques are described for testing of the Si anode, electrodes and cycled electrodes. Then detailed assemble process is presented for half cell format LIBs.

**Chapter 3** propose a HF free, simple and low cost method to produce SiNWs and hopefully scale up to industry level. Simple heat-treatment is applied to Al-Si alloy to change the Si phase morphology due to the eutectic effect. Detailed parameters of storage time and treatment temperature were optimized for the better performance of SiNWs.



**Chapter 4** reveals few parameters of Si electrode for industry application. Density and mass loading are crucial because these parameters relate with energy density for full cell design. Higher mass loading and proper density will greatly improve the energy density and mechanical stability. These two parameters were finally optimized for SiNWs electrode. Four binders comparison carried out to determine the best one for Si anode. A new cycle protocol conducted for better controlling electrode swelling.

**Chapter 5** investigates the effect of two carbonate additives (FEC and VC), especially the synergies effect in EC/DEC electrolyte. Detailed performance was examined at 55°C, 25°C and -20°C. Characterization techniques were applied to understand the mechanism of interface modification.

**Chapter 6** discusses the objectives of the thesis and summarizes the results presented in Chapters 3, 4 and 5. Based on the final purpose of industry application, more work has to be done for this conversion and possible future work based on this thesis is suggested.

## References

- [1] S. Shafiee, E. Topal, When will fossil fuel reserves be diminished? *Energy Policy*, **2009**, 37, 181-189.
- [2] C. McGlade, P. Ekins, The geographical distribution of fossil fuels unused when limiting global warming to 2°C, *Nature*, **2015**, 517, 187-202.
- [3] P.D. Frischmann, K. Mahata, F. Würthner, Powering the future of molecular artificial photosynthesis with light-harvesting metallosupramolecular dye assemblies, *Chem. Soc. Rev.*, **2013**, 42, 1847-1870.
- [4] M.E. Mann, R.S. Bradley, M.K. Hughes, Global-scale temperature patterns and climate forcing over the past six centuries, *Nature*, **1998**, 392, 779-787.
- [5] S. Cao, J. Yu, g-C<sub>3</sub>N<sub>4</sub>-based photocatalysts for hydrogen generation, *J. Phys. Chem. Lett.*, **2014**, 5, 2101-2107.
- [6] S. Liu, Z-R. Tang, Y. Sun, J.C. Colmenares, Y-J. Xu, One-dimension-based spatially ordered architectures for solar energy conversion, *Chem. Soc. Rev.*, **2015**, 44, 5053-5075.
- [7] S. Rehman, L.M. Al-Hadhrami, Md. Mahbub Alam, Pumped hydro energy storage system: A technological review, *Renew. Sust. Energy Rev.*, **2015**, 44, 586-598.

- [8] K. Tomabechi, Energy resources in the future, *Energies*, **2010**, 3, 686-695.
- [9] J.M. Tarascon, M. Armand, Issues and challenges facing rechargeable lithium batteries, *Nature*, **2001**, 414, 359-367.
- [10] H. Lbrahim, A. Ilinca, J. Perron, Energy storage systems-characteristics and comparisons, *Renew. Sust. Energy Rev.*, **2008**, 12, 1221-1250.
- [11] C. Liu, F. Li, L. P Ma, H.M. Chen, Advanced materials for energy storage, *Adv. Mater.*, **2010**, 22, E28-E62.
- [12] T. Nagura, K. Tozawa, *Progress in Batteries and Solar Cells*, **1991**, 10, 218.
- [13] M. Winter, J.O. Besenhard, M.E. Spahr, P. Novak, Insertion electrode materials for rechargeable lithium batteries, *Adv. Mater.*, **1998**, 10, 725-763.
- [14] M.M. Thackeray, C. Wolverton, E.D. Isaacs, Electrical energy storage for transportation-approaching the limits of, and going beyond, lithium-ion batteries, *Energy Environ. Sci.*, **2012**, 5, 7854-7863.
- [15] G.M. Ehrlich, *Lithium-Ion Batteries*, in: Linden, D., Reddy, T.B. (eds.) *Handbook of Batteries*, **2002**, 3<sup>rd</sup> ed., 35.1-35.94.
- [16] H. Wu, Y. Cui, Designing nanostructured Si anodes for high energy lithium ion batteries, *Nano Today*, **2012**, 7, 414-429.
- [17] P. Rozier, J.M. Tarascon, Review-Li-rich layered oxide cathodes for next-generation Li-ion batteries: Chances and Challenges, *J. Electrochem. Soc.*, **2015**, 162(14), A2490-2499.
- [18] L. Zhang, R. Rajagopalan, H. Guo, X. Hu, S. Dou, H. Liu, A green and facile way to prepare granadilla-like Silicon-based anode materials for Li-Ion Batteries, *Adv. Funct. Mater.*, **2016**, 26, 440-446.
- [19] W.J. Lee, T.H. Hwang, J.O. Hwang, H.W. Kim, J. Lim, H.Y. Jeong, J. Shim, T.H. Han, J.Y. Kim, J.W. Choi, S.O. Kim, N-doped graphitic self-encapsulation for high performance silicon anodes in lithium-ion batteries, *Energy Environ. Sci.*, **2014**, 7, 621-626.
- [20] Z. Yang, Y. Xia, J. Ji, B. Qiu, K. Zhang, Z. Liu, Superior cycling performance of a sandwich structure Si/C anode for lithium ion batteries, *RSC Adv.*, **2016**, 6, 12107-12114.
- [21] A.G. Kannan, S.H. Kim, H.S. Yang, D-W. Kim, Silicon nanoparticles grown on a reduced graphene oxide surface as high-performance anode materials for lithium-ion batteries, *RSC Adv.*, **2016**, 6, 25159-25166.
- [22] L. Wang, N. Lin, J. Zhou, Y. Zhu, Y. Qian, Silicon nanoparticles obtained via a low temperature chemical “metathesis” synthesis route and their lithium-ion battery properties, *Chem. Commun.*, **2015**, 51, 2345-2348.

- [23] D. Lin, Z. Lu, P-C. Hsu, H.R. Lee, N. Liu, J. Zhao, H. Wang, C. Liu, Y. Cui, A high tap density secondary silicon particle anode fabricated by scalable mechanical pressing for lithium-ion batteries, *Energy Environ. Sci.*, **2015**, 8, 2371-2376.
- [24] D. Tang, R. Yi, M.L. Gordin, M. Melnyk, F. Dai, S. Chen, J. Song, D. Wang, Titanium nitride coating to enhance the performance of silicon nanoparticles as a lithium-ion battery anode, *J. Mater. Chem., A* **2014**, 2, 10375-10378.
- [25] R. Yi, F. Dai, M.L. Gordin, H. Sohn, D. Wang, Influence of Silicon nanoscale building blocks size and carbon coating on the performance of micre-sized Si-C composite Li-Ion anodes, *Adv. Energy Mater.*, **2013**, 3, 1507-1515.
- [26] R. Yi, F. Dai, M.L. Gordin, S. Chen, D. Wang, Micro-sized Si-C composite with interconnected nanoscale building blocks as high-performance anodes for practical application in Lithium-Ion Batteries, *Adv. Energy Mater.*, **2013**, 3, 295-300.
- [27] X. Chen, X. Li, F. Ding, W. Xu, J. Xiao, Y. Cao, P. Meduri, J. Liu, G.L. Graff, J. Zhang, Conductive rigid skeleton supported silicon as high-performance Li-Ion battery anodes, *Nano Letters*, **2012**, 12, 4124-4130.
- [28] E. Peled, F. Patolsky, D. Golodnitsky, K. Freedman, G. Davidi, D. Schneier, Tissue-like silicon nanowires-based three-dimensional anodes for high-capacity Lithium Ion Batteries, *Nano Letters*, **2015**, 15(6), 3907-3916.
- [29] P.P. Prosini, C. Cento, F. Alessandrini, P. Gislou, A. Mancini, A. Ruffoloni, F. Rondino, A. Santoni, Electrochemical characterization of silicon nanowires as an anode for lithium batteries, *Solid State Ionics*, **2014**, 260, 49-54.
- [30] S. Sim, P. Oh, S. Park, J. Cho, Critical thickness of SiO<sub>2</sub> coating layer on core@shell bulk@nanowire Si anode materials for Li-Ion Batteries, *Adv. Mater.*, **2013**, 25, 4498-4503.
- [31] N. Liu, L. Hu, M.T. McDowell, A. Jackson, Y. Cui, Prelithiated Silicon nanowires as an anode for lithium ion batteries, *ACS Nano*, **2011**, 5(8), 6487-6493.
- [32] H. Wu, G. Chan, J.W. Choi, I. Ryu, Y. Yao, M.T. McDowell, S.W. Lee, A. Jackson, Y. Yang, L. Hu, Y. Cui, Stable cycling of double-walled silicon nanotube battery anodes through solid-electrolyte interphase control, *Nature Nanotech.*, **2012**, 7, 310-315.
- [33] H. Wang, P. Wu, H. Shi, F. Lou, Y. Tang, T. Zhou, Y. Zhou, T. Lu, Porous Si spheres encapsulated in carbon shells with enhanced anodic performance in lithium-ion batteries, *Mater. Res. Bull.*, **2014**, 55, 71-77.
- [34] G. Zhao, L. Zhang, Y. Meng, N. Zhang, K. Sun, High storage performance of core-shell Si@C nanoparticles as lithium ion battery anodematerial, *Mater. Lett.*, **2013**, 96, 170-173.
- [35] H-C. Tao, M. Huang, L-Z. Fan, X. Qu, Effect of nitrogen on the electrochemical performance of core-shell structured Si/C nanocomposites as anode materials for Li-ion batteries, *Electrochim. Acta*, **2013**, 89, 394-499.

- [36] N. Liu, H. Wu, M.T. McDowell, Y. Yao, C. Wang, Y. Cui, A Yolk-Shell design for stabilized and scalable Li-Ion battery alloy anodes, *Nano Lett.*, **2012**, 12(6), 3315-3321.
- [37] L-F. Cui, R. Ruffo, C.K. Chan, H. Peng, Y. Cui, Crystalline-amorphous Core-Shell silicon nanowires for high capacity and high current battery electrodes, *Nano Lett.*, **2009**, 9(1), 491-495.
- [38] K. Kierzek, J. Machnikowski, F. Béguin, Toward the realistic silicon/carbon composite for Li-ion secondary battery anode, *J. Appl. Electrochem.*, **2015**, 45, 1-10.
- [39] J. Song, S. Chen, M. Zhou, T. Xu, D. Lv, M.L. Gordin, T. Long, M. Melnyk, D. Wang, Micro-sized silicon-carbon composites composed of carbon-coated sub-10 nm Si primary particles as high-performance anode materials for lithium-ion batteries, *J. Mater. Chem., A* **2014**, 2, 1257-1262.
- [40] R. Yi, J. Zai, F. Dai, M.L. Gordin, D. Wang, Dual conductive network-enabled graphene/Si-C composite anode with high areal capacity for lithium-ion batteries, *Nano Energy*, **2014**, 6, 211-218.
- [41] X. Bai, Y. Yu, H.H. Kung, B. Wang, J. Jiang, Si@SiO<sub>x</sub>/graphene hydrogel composite anode for lithium-ion battery, *J. Power Sources*, **2016**, 306, 42-48.
- [42] M-K. Park, E.Park, J. Lee, G. Jeong, K.J. Kim, J.H. Kim, Y-J. Kim, H. Kim, Hydrogen silsequioxane-derived Si/SiO<sub>x</sub> nanospheres for high-capacity lithium storage materials, *Appl. Mater. Interfaces*, **2014**, 6(12), 9608-9613.
- [43] D. Wang, M. Gao, H. Pan, J. Wang, Y. Liu, High performance amorphous-Si@SiO<sub>x</sub>/C composite anode materials for Li-ion batteries derived from ball-milling and in situ carbonization, *J. Power Sources*, **2014**, 256, 190-199.
- [44] M.A. Al-Maghrabi, J. Suzuki, R.J. Sanderson, V.L. Chevrier, R.A. Dunlap, J.R. Dahn, Combinatorial studies of Si<sub>1-x</sub>O<sub>x</sub> as a potential negative electrode material for Li-Ion battery applications, *J. Electrochem. Soc.*, **2013**, 160(9), A1587-A1593.
- [45] J-I. Lee, K.T. Lee, J. Cho, J. Kim, N-S. Choi, S. Park, Chemical-assisted thermal disproportionation of porous silicon monoxide into silicon-based multicomponent systems, *Angew. Chem.*, **2012**, 51, 2767-2771.
- [46] Z. Lu, N. Liu, H-W. Lee, J. Zhao, W. Li, Y. Li, Y. Cui, Nonfilling carbon coating of porous silicon micrometer-sized particles for high-performance lithium battery anodes, *ACS NANO*, **2015**, 9, 2540-2547.
- [47] B.M. Bang, H. Kim, H.K. Song, J. Cho, S. Park, Scalable approach to multi-dimensional bulk Si anodes via metal-assisted chemical etching, *Energy Environ. Sci.*, **2011**, 4, 5013-5019.

- [48] B.M. Bang, H. Kim, J-P. Lee, J. Cho, S. Park, Mass production of uniform-sized nanoporous silicon nanowire anodes via block copolymer lithography, *Energy Environ. Sci.*, **2011**, 4, 3395-3399.
- [49] J. Cho, Porous Si anode materials for lithium rechargeable batteries, *J. Mater. Chem.* **2010**, 20, 4009-4014.
- [50] H. Kim, B. Han, J. Choo, J. Cho, Three-dimensional porous silicon particles for use in high-performance lithium secondary batteries, *Angew. Chem.*, **2008**, 120, 10305-10308.
- [51] M-H. Ryou, J. Kim, I. Lee, S. Kim, Y.K. Jeong, S. Hong, J.H. Ryu, T-S. Kim, J-K. Park, H. Lee, J.W. Choi, Mussel-inspired adhesive binders for high-performance silicon nanoparticle anodes in Lithium-Ion Batteries, *Adv. Mater.*, **2013**, 25(11), 1571-1576.
- [52] Y.K. Jeong, T-W. Kwon, I. Lee, T-S. Kim, A. Coskun, J.W. Choi, Millipede-inspired structural design principle for high performance polysaccharide binders in silicon anodes, *Energy Environ. Sci.*, **2015**, 8, 1224-1230.
- [53] Z. Chen, C. Wang, J. Lopez, Z. Lu, Y. Cui, Z. Bao, High-areal-capacity silicon electrodes with low-cost silicon particles based on spatial control of self- healing binder, *Adv. Energy Mater.*, **2015**, 5, 1401826.
- [54] S. Klamor, M. Schröder, G. Bruncklaus, P. Niehoff, F. Berkemeier, F.M. Schappacher, M. Winter, On the interaction of water-soluble binders and nano silicon particles: alternative binder towards increased cycling stability at elevated temperatures, *Phys. Chem. Chem. Phys.*, **2015**, 17, 5632-5641.
- [55] S-J. Park, H. Zhao, G. Ai, C. Wang, X. Song, N. Yuca, V.S. Battaglia, W. Yang, G. Liu, Side-chain conducting and phase-separated polymeric binders for high-performance silicon anodes in Lithium-Ion Batteries, *J. Am. Chem. Soc.*, **2015**, 137, 2565-2571.
- [56] M. Wu, X. Song, X. Liu, V. Battaglia, W. Yang, G. Liu, Manipulating the polarity of conductive polymer binders for Si-based anodes in Lithium-Ion Batteries, *J. Mater. Chem., A*. **2015**, 3, 3651-3658.
- [57] J. Song, M. Zhou, R. Yi, T. Xu, M.L. Gordin, D. Tang, Z. Yu, M. Regula, D. Wang, Interpenetrated Gel polymer binder for high-performance silicon anodes in Lithium-Ion Batteries, *Adv. Funct. Mater.*, **2014**, 24, 5904-5910.
- [58] H. Zhao, Z. Wang, P. Lu, M. Jiang, F. Shi, X. Song, Z. Zheng, X. Zhou, Y. Fu, G. Abdelbast, X. Xiao, Z. Liu, V.S. Battaglia, K. Zaghbi, G. Liu, Toward practical application of functional conductive polymer binder for a high-energy Lithium-Ion Battery design, *Nano Lett.*, **2014**, 14, 6704-6710.
- [59] C. Wang, H. Wu, Z. Chen, M.T. McDowell, Y. Cui, Z. Bao, Self-healing chemistry enables the stable operation of silicon microparticle anodes for high-energy Lithium-Ion Batteries, *Nature Chem.*, **2013**, 5, 1042-1048.

- [60] H. Wu, G. Yu, L. Pan, N. Liu, M.T. McDowell, Z. Bao, Y. Cui, Stable Li-Ion Battery anodes by in-situ polymerization of conducting hydrogel to conformally coat silicon nanoparticles, *Nat. Commun.*, **2013**, 4, 1943-1948.
- [61] M. Wu, J.E.C. Sabisch, X. Song, A.M. Minor, V.S. Battaglia, G. Liu, A highly cross-linked polymeric binder for high-performance silicon negative electrodes in Lithium-Ion Batteries, *Angew. Chem. Int. Ed.*, **2012**, 51, 8762-8767.
- [62] K. Schroder, J. Alvarado, T.A. Yersak, J. Li, N. Dudney, L.J. Webb, Y.S. Meng, K.J. Stevenson, The effect of Fluoroethylene Carbonate as an additive on the solid electrolyte interphase on Silicon Lithium-Ion electrodes, *Chem. Mater.*, **2015**, 27, 5531-5542.
- [63] C. Xu, F. Lindgren, B. Philippe, M. Gorgoi, F. Björefors, K. Edström, T. Gustafsson, Improved performance of the silicon anode for Li-Ion Batteries: Understanding the surface modification mechanism of Fluoroethylene Carbonate as an effective electrolyte additive, *Chem. Mater.*, **2015**, 27, 2591-2599.
- [64] M. Nie, D.P. Abraham, Y. Chen, A. Bose, B.L. Lucht, Silicon solid electrolyte interphase (SEI) of Lithium Ion Battery characterized by microscopy and spectroscopy, *J. Phys. Chem. C*, **2013**, 117, 13403-13412.
- [65] Y-M. Lin, K.C. Klavetter, P.R. Abel, N.C. Davy, J.L. Snider, A. Heller, C.B. Mullins, High performance silicon nanoparticle anode in fluoroethylene carbonate-based electrolyte for Li-Ion Batteries, *Chem. Commun.*, **2012**, 48, 7268-7270.
- [66] V. Etacheri, O. Haik, Y. Goffer, G.A. Roberts, I.C. Stefan, R. Fasching, D. Aurbach, Effect of Fluoroethylene Carbonate (FEC) on the performance and surface chemistry of Si-Nanowire Li-Ion Battery anodes, *Langmuir*, **2012**, 28, 965-976.
- [67] H. Nakai, T Kubota, A. Kita, A. Kawashima, Investigation of the solid electrolyte interphase formed by Fluoroethylene Carbonate on Si electrodes, *J. Electrochem. Soc.*, **2011**, 158(7), A798-A801.
- [68] C.C. Nguyen, B.L. Lucht, Comparative study of fluoroethylene carbonate and vinylene carbonate for silicon anodes in lithium ion batteries, *J. Electrochem. Soc.*, **2014**, 161(12), A1933-A1938.
- [69] I.A. Profatilova, C. Stock, A. Schmitz, S. Passerini, M. Winter, Enhanced thermal stability of a lithiated nano-silicon electrode by fluoroethylene carbonate and vinylene carbonate, *J. Power Sources*, **2013**, 222, 140-149.

## Chapter 2

### 2 Experimental and Characterization

#### 2.1 Experimental

The physical and electrochemical parameters of prepared samples were analyzed using various methods including various spectroscopies and impedance analysis. The brief description of the experimental techniques are given in this section.



**Figure 2.1 A picture of Aerosol-Assisted Chemical Vapour Deposition.**

Figure 2.1 shows a typical Chemical Vapour Deposition (CVD) set-up used for the growth of carbon nanotubes (CNTs) and nitrogen doped carbon nanotubes. This device mainly consists of four parts, including the injection part, the ultrasonic part, deposition chamber and post cleaning part. In the injection part, the precursor solution stored in a syringe is controlled injected into the ultrasonic part. The precursor solution is atomized in an ultrasonic processor (VCX 130 PB, Sonics & Materials Inc.), and the treated tiny droplets slowly pass the deposition chamber under argon gas. The catalyst is placed in the middle of furnace which is

the setting temperature area. The deposition reaction happens when the precursor droplets are passing the catalyst particles, and the rest of precursor and other by-products are pumped out. This device also can be used to anneal and reduce Si based anode materials.

## 2.2 Characterization

### 2.2.1 Physical characterizations technique

The characterizations of as prepared materials and after cycling test are crucial to analysis and collect the information about by-products. The SEM, TEM, XRD, Raman, FTIR have been used to analysis the physical properties of samples.



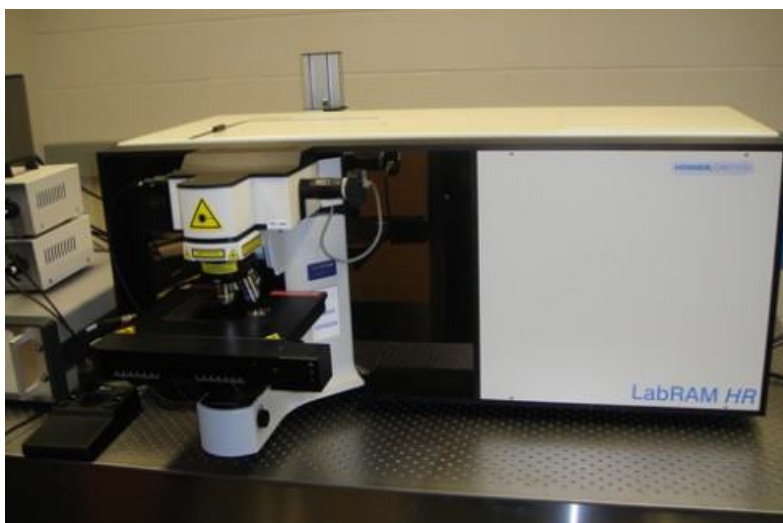
**Figure 2.2 A picture of Hitachi S-4800 high-resolution scanning electron microscope.**

Figure 2.2 shows High-resolution scanning electron microscope (FESEM, Hitachi S-4800) used to observe the morphology of the samples. This technique also equip with energy dispersive X-ray spectroscopy (EDX) to detect the element distribution of the sample. The



SEM produces images by probing the sample with a focused electron beam that is scanned across a rectangular area of the specimen. When the electron beam interacts with the sample surface, it loses energy by different forms such as heat, emission of low energy secondary electrons and high energy backscattered electrons, light emission or X-ray emission. More information can be obtained after analyzing the signals. The magnification of Hitachi S-4800 is in a range of  $\times 20 - \times 800,000$ . The resolution of secondary electron image is 2.0nm at 1kV in a standard mode.

Raman spectroscopy (HORIBA scientific LabRAM) is used to analyze the structure or the phase of the prepared samples, which is shown in Figure 2.3. This instrument is operated with an incident laser beam (green light) at 532.03nm. Raman is commonly used in chemistry to provide a fingerprint by detecting the vibrational rotational, rotation and other low-frequency mode of the material. This technique can analysis the stretch of symmetric molecules or functional groups, especially helpful to identify organic chemicals.



**Figure 2.3 A picture of HORIBA Scientific LabRAM research Raman spectroscopy.**

Fourier transform infrared spectroscopy (FTIR, Nicolet 6700 FTIR spectrometer, Figure 2.4) is used to obtain useful information of functional groups sitting at the surface of the prepared samples. Raman and FTIR techniques are both powerful supplementary tools to further analyze the synthesized Si materials and cycled Si electrodes. Unlike Raman, the main function of FTIR is to analysis the asymmetric stretch of molecules or functional groups,

obtaining different information about Si samples. Therefore, more information about the Si electrode can be collected by employing both of these techniques.



**Figure 2.4 A picture of the Nicolet 6700 FTIR spectrometer.**

X-ray diffraction (XRD) is a versatile, non-destructive technique that reveals detailed information about the crystallographic structure and phase of prepared samples. Figure 2.5 shows Bruker D8 Advance in our laboratory. XRD mainly consists three parts: X-ray tube, sample holder and an X-ray detector. The X-ray generated in X-ray tube bombard the sample, generating X-ray spectra which include the characteristic information of target material. The spectra can be purified by a filter, then collected by X-ray detector, and finally transferred to a curve by operating software. The most popular function of XRD is to analysis the crystalline structure of the materials, even calculate the parameters of cell by measuring scattering intensity at scattering angles.



**Figure 2.5 A picture of Bruker D8 Advance XRD.**

A TriStar II Plus (Micromeritics Instrument Corporation, USA, seen Figure 2.6) is applied to measure the surface area and porosity of as-prepared SiNWs, which is a crucial parameter to evaluate nanostructured materials. This technique bases on the Brunauer-Emmett-Teller theory to explain the physical adsorption of gas molecules on a solid state material surface. Actually, the concept of the theory is an extension of the Langmuir theory, which is a theory for monolayer molecular adsorption. The gas amount for this adsorption can be simply the surface area which fully cover it with a monolayer molecular.



**Figure 2.6 A picture of TriStar II Plus Analyzer.**

## 2.2.2 Electrochemical characterizations

Evaluating the electrochemical performances of the synthesized materials are the key part to optimize the performance of the battery system. Cyclic voltammetry (CV), Electrochemical Impedance Spectroscopy (EIS), room temperature cycle performance, high/low temperature cycle performance, C rate capability are the typical performances to distinguish better battery active materials.

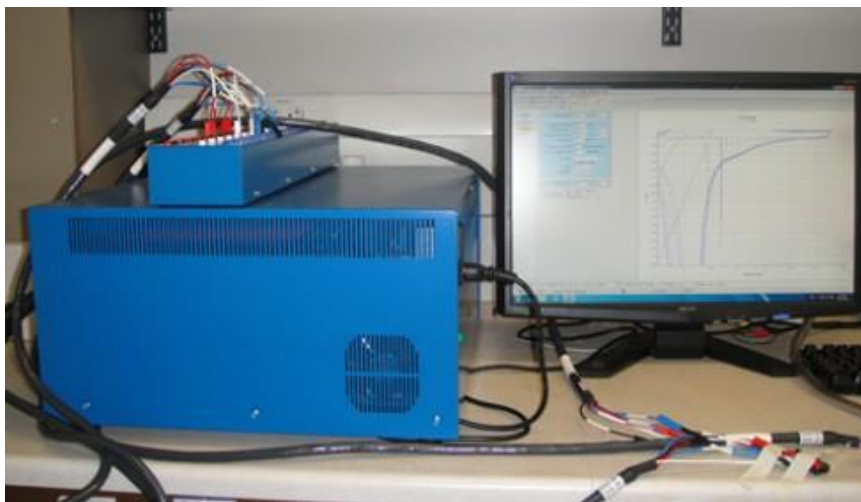


**Figure 2.7** A picture of Biologic VMP3 Potentiostat/Galvanostat/EIS system.

CV and EIS are tested in a VMP3 Potentiostat/Galvanostat/EIS system in our laboratory (seen Figure 2.7). The rate of voltage change over time during test is known as the experiment's scan rate. The potential is applied between the working electrode and the reference electrode while the current is measured between the working electrode and the counter electrode. These data are plotted as current vs applied potential, and more information can be obtained by analyzing the data, such as the oxidize/reduction chemical reaction and electrode impedance.

Cycling stability and C rate capability of Si anodes are evaluated in a Arbin BT-2000 battery test station (seen Figure 2.8). It has to be noted that the coin cell can be tested in a temperature window (-20 °C~ 55°C) with the help of ESPEC temperate box. Generally, the system can control the potential (constant voltage, CV) or current (constant current, CC) which applied on the battery. The machine can record the most information for your sample, such as capacity, voltage, current density, energy, etc.

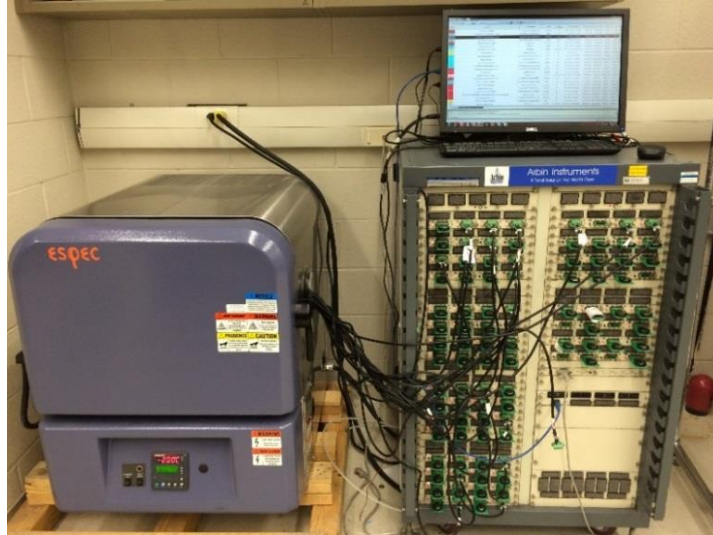


**Figure 2.8 A picture of Arbin BT-2000 battery test system and temperate box.**

Coin type half cells are standard cell format for material and electrolyte evaluation. 2032 coin cell consists a prepared Si electrode, polymer separator (Celgard 2400) and lithium foil as the counter electrode (seen Figure 2.9). The electrolytes include ethylene carbonate (EC), diethyl carbonate (DEC), vinylene carbonate (VC), fluoroethylene carbonate (FEC) and 1.3M  $\text{LiPF}_6$  with different ratio. The coin cells are assembled in a glove box (Vacuum Atmospheres Company) under a dry argon atmosphere (the concentration of  $\text{H}_2\text{O}$  and  $\text{O}_2$  are below 1ppm). For each condition, three cells will be tested to make sure the cycle performance is repeatable.

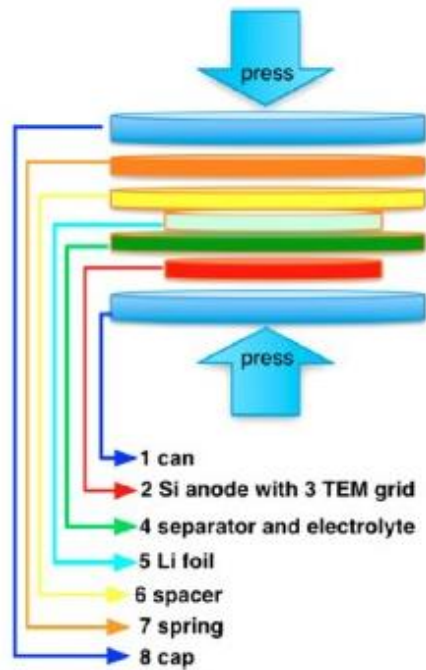


**Figure 2.9 Schematic diagram of Li/Si 2032 coin cell assembly. [1]**

## References

- [1] M. Nie, D.P. Abraham, Y. Chen, A. Bose, B.L. Lucht, Silicon solid electrolyte interphase (SEI) of Lithium Ion Battery characterized by microscopy and spectroscopy, *J. Phys. Chem. C*, **2013**, 117, 13403-13412.

## Chapter 3

### 3 HF free synthesis method for Silicon nanowire

#### 3.1 Introduction

Silicon anode is widely recognized as a promising candidate for next generation LIBs due to its super high theoretical specific capacity of 4,200mAh/g [1, 2], which is ten times higher than that of current commercial graphite anode [3-6]. However, the challenge of Si anode is the huge volume expansion over 400 % on full lithium alloying (lithiation) [2, 7, 8], which degrades the mechanical and electrochemical properties of electrode and leads to rapid capacity fading. In order to overcome this demerit, different nano scale Si anode materials have been studied to overcome the problem of Si anode [30-36]. High performance Si anode materials have been synthesized by CVD method [9-15] and HF etching method [16-18] in previous reports. However, these synthesis methods are not yet acceptable for mass production of Si anode for LIB industry since these methods cannot well control the parameter of Si anodes, and either too expensive or toxic. In this part, a simple method is proposed to prepare high performance SiNWs using Al-Si alloy which is cheap and the Aluminum can be easily removed in acid solution. The process is safe since the HF is not involved and also cost efficient for scaling up production.

#### 3.2 Experimental Section

##### 3.2.1 Sample preparation and characterization

Silicon nanowires (SiNWs) were prepared from a two steps process: heating pretreatment and acid etching process. Commercial aluminum silicon alloy powders contains 12 wt.% Silicon were purchased from VALIMET INC., USA and their morphology is presented in Figure 3.1. Few groups mentioned that the fabric Si phase can be treated after heat treatment

due to the eutectic effect of Si-Al alloy [25, 26]. The alloy powders were annealed under argon gas protection for few hours (2-8h), then cool down to room temperature. Then, etching step was carried out on heat treated alloy powders in 1 M hydrochloric acid (HCl, Sigma, USA, 10 wt.%) until aluminum was completely removed from Al-Si alloy. Finally, the resultant was washed several times using deionized water and the SiNWs were dried in a vacuum at 60°C for 12h. The as-prepared SiNWs was investigated by field emission scanning microscopy (FESEM, Hitachi S4800), energy dispersive X-ray spectroscopy (EDX), X-ray diffraction (Bruker D8 Advance XRD).

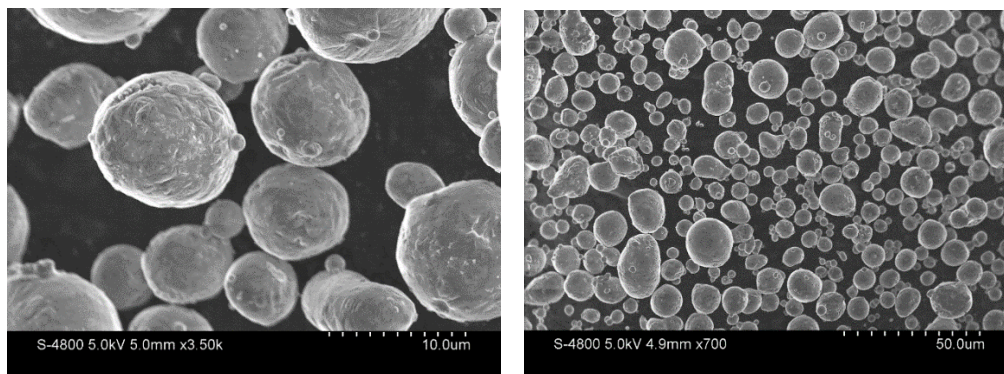


**Figure 3.1 SEM images of Al-Si alloy powders.**

### 3.2.2 Electrochemical Characterization

The SiNWs electrode was prepared by mixing of acetylene black (Gunbai, Denki Kagaku Kogyo, Japan) as conductive agent and sodium alginate (MP Biomedicals, LLC, USA) as binder. The formula of electrode is SiNWs : AB : SA = 63 : 22 : 15 (wt.%). The slurry was casted on 18 $\mu$ m Cu foil and loading of total mass for electrodes was 0.7-0.8mg/cm<sup>2</sup>. After pressed, the electrodes were assembled into 2032 coin cells, while the electrolyte was made by adding 10 v% FEC into 1.3M LiPF<sub>6</sub> in 3:7 v/v EC/DEC electrolyte (BASF, USA). Cycling performance was tested in Arbin BT2000 with activation at a 0.05C current density for a 5 cycles and then cycled at 0.1C for remaining cycles. For activation cycles, only 0.05C current density (constant current) was applied for lithiation and delithiation in a voltage window between 0.01 – 1.5V. The advantage of this method is the low current density facilitates the lithiation of Si material so that the maximum capacity can be fully evaluate.



For subsequent cycles, the cells were tested between 0.01-1V at a 0.1C current density (constant current only). The current and cut-off voltages change is the simulation of the cycle test in LIB industry which will be more reasonable to estimate the performances in full cell. The calculation of C was based on the total mass loading and 4200mAh/g, i.e. 1C = 4200mA/g.

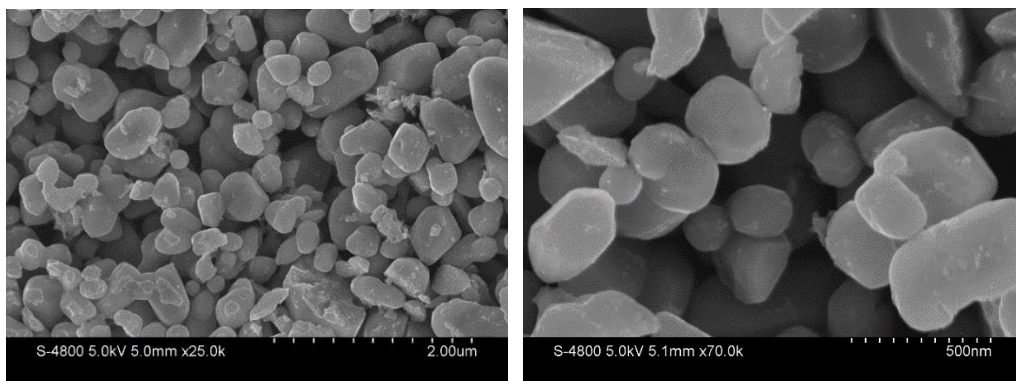


**Figure 3.2 SEM images of Si particles after etching without heat treatment.**

### 3.3 Results and Discussion

The Si particles were obtained by etching treatment of Al-Si alloy in 1M HCl solution for 24 hours. As shown in Figure 3.2, the SEM images revealed that the diameters of Si particles were among about 200nm to 600nm [19-22]. Based on the theory of metallurgy, proper heat treatment can greatly change the shape of Si phase in alloy [23-29], which provide a new concept to produce Si anode. The basic parameters of heat-treatment are temperature, annealing time in a certain temperature and cooling rate. According to the melting point of Si (1414°C) and Al (660.4°C), a series of heating temperature (700-1000°C) and duration time (2-8h) were chosen at a fixed cooling rate in this study.

#### 3.3.1 Temperature effect in heating pretreatment

Initially, the Si-Al powders were calcined at different temperatures ranging from 700°C, 800°C, 900°C and 1000°C for 8h to deform the Si phase in alloy. After etched in HCl solution,

the morphology of four Si samples was shown in Figure 3.3 after etching. It was obvious that the SiNWs did produce after this process, and their morphologies clearly changed at different temperatures. The size of Si particles were approximately 5-15 $\mu\text{m}$ , and the diameter of single SiNW was decreasing after treatment at increasing temperatures, obtaining 600nm (700 $^{\circ}\text{C}$ ), 250nm (800 $^{\circ}\text{C}$ ), 150nm (900 $^{\circ}\text{C}$ ) and 100nm (1000 $^{\circ}\text{C}$ ) SiNWs, respectively.

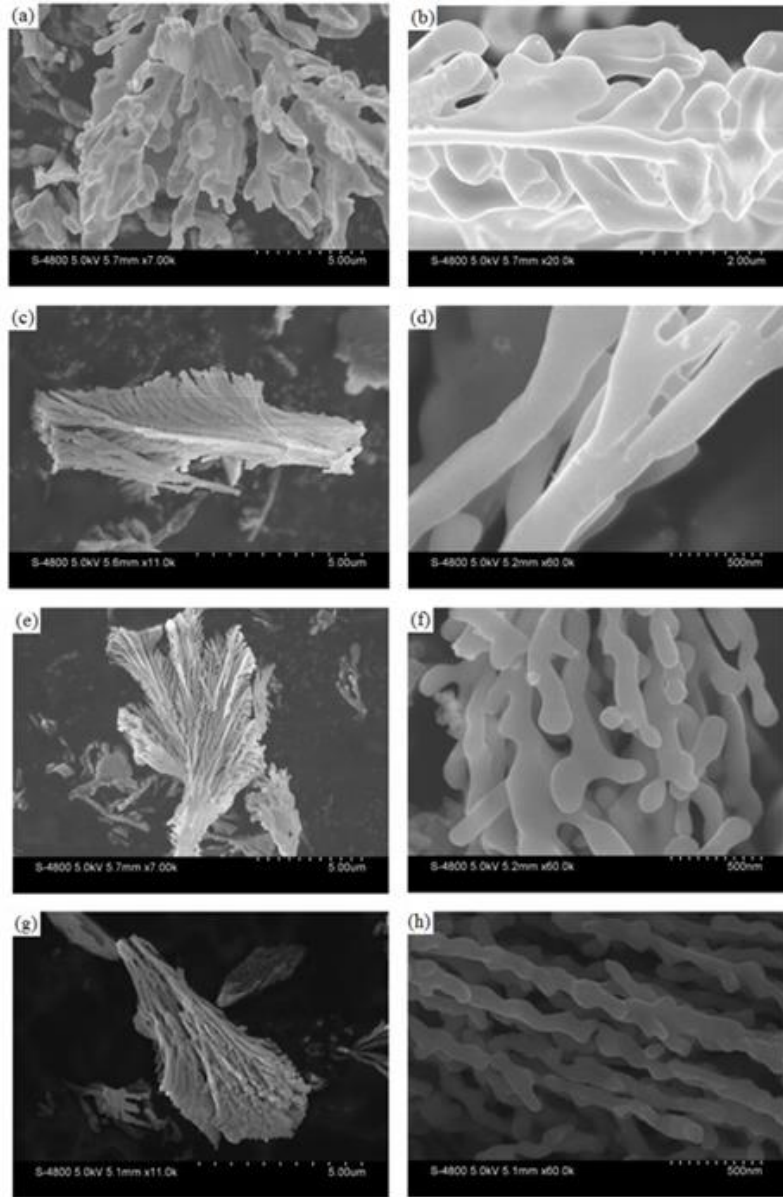


**Figure 3.3 Si anode SEM images of temperature effect in 8h heating pretreatment: (a, b) 700 $^{\circ}\text{C}$ , (c, d) 800 $^{\circ}\text{C}$ , (e, f) 900 $^{\circ}\text{C}$  and (g, h) 1000 $^{\circ}\text{C}$ , the scale of (a), (c), (e) and (g) is 5  $\mu\text{m}$ , the scale of (b) is 2 $\mu\text{m}$  and the scale of (d), (f) and (h) is 500nm.**

According to Figure 3.4, the cycle performances were totally consistent with the SEM studies that the SiNWs produced at 1000°C pretreatment provided the most stable cycling performance and the highest cell efficiency [11, 13]. The reversible discharge capacity was about 1321mAh/g after 50 cycles, corresponding to 78% discharge capacity retention, and the cell efficiency was 97.5% for each single cycle. But, the SiNWs calcined at 700°C only had 422mAh/g reversible capacity after 50 cycles with 23% of capacity retention and 94% cell efficiency. This was mainly because the structure destruction happened during Li<sup>+</sup> insertion/extraction due to huge volume change of bigger SiNWs [7, 8]. It was further confirmed that the nano-scale Si anode material greatly reduced the volume effect and stabilized the material structure, finally improved the cell performance [9, 11].

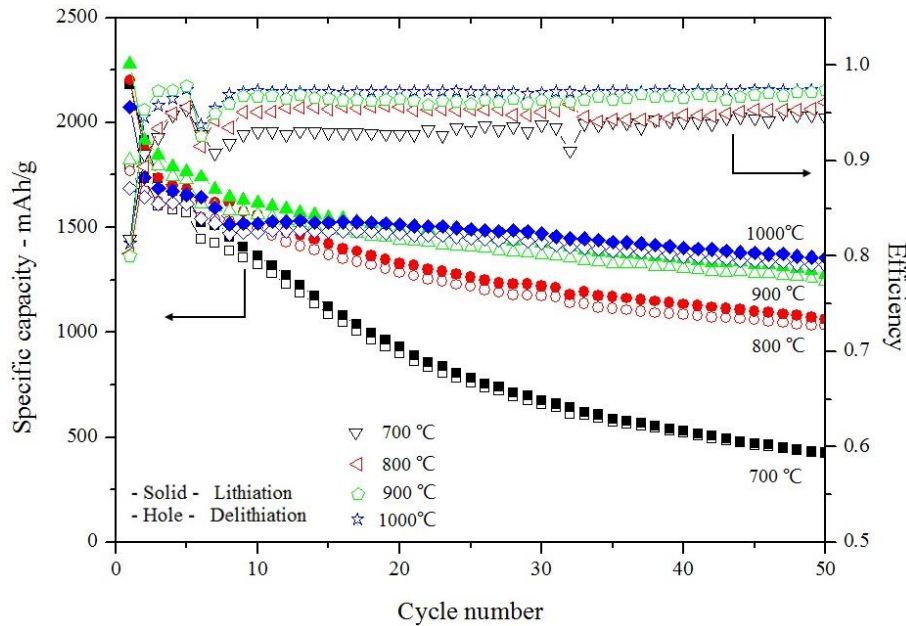


**Figure 3.4 Cycling performance and cell efficiency of as-prepared SiNWs in different temperature for 8h.**

### 3.3.2 Storage time effect in 1000°C heating pretreatment

The effect of calcination time is another key parameter which is critical to affect the morphology of Si phase in alloy. The morphology of SiNW samples calcined at 1000°C with different times (2h, 4h, 6h and 8h) during the was shown in Figure 3.5. The size of Si particles were about 5-15µm and the diameter of each SiNWs was 500nm (2h), 200nm (4h),

150nm (6h) and 100nm (8h), respectively. Therefore, the SiNWs are growing up at an elevated environment in Al-Si alloy. But the deformation of Si phase need relatively longer time due to its high melting point.

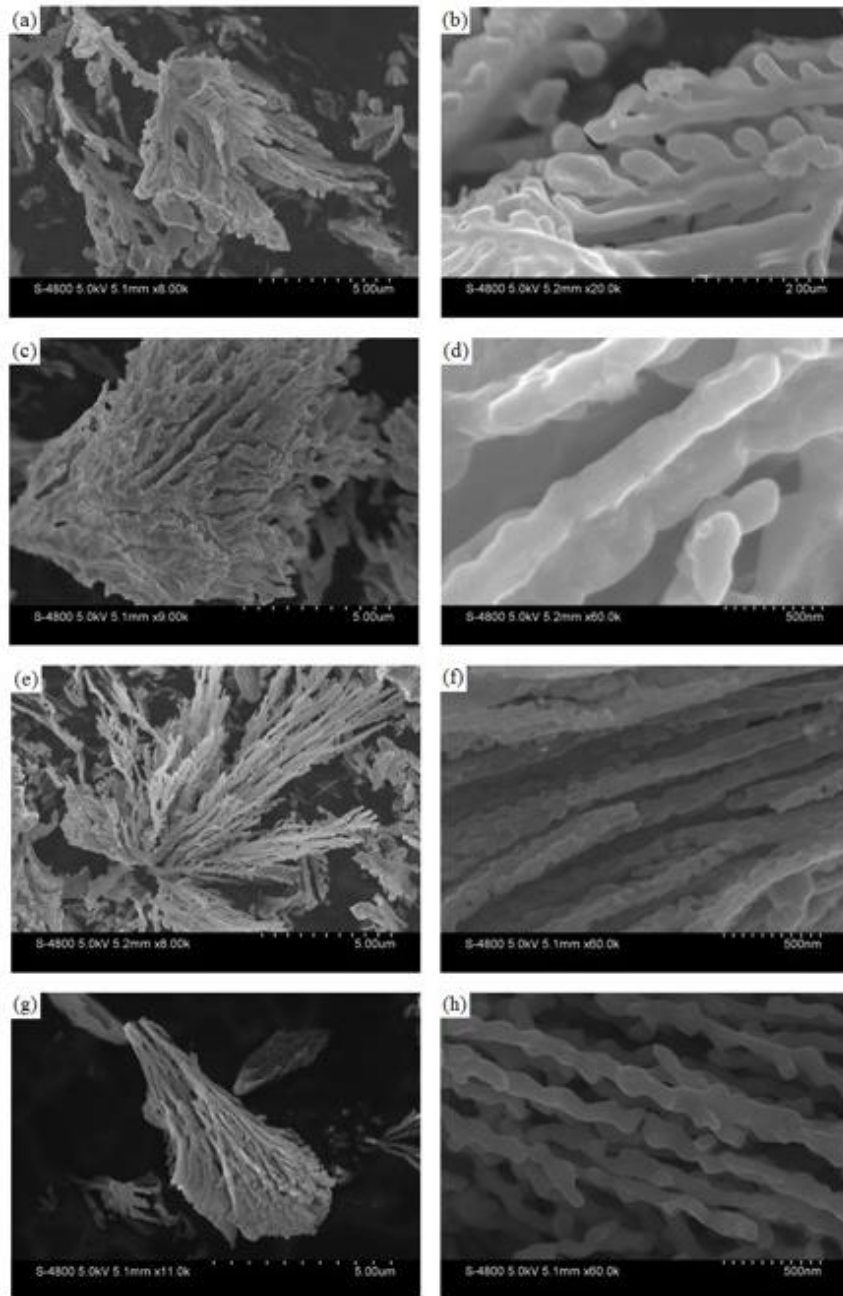


**Figure 3.5 Si anode SEM images of storing time effect in 1000°C heating pretreatment: (a, b) 2h, (c, d) 4h, (e, f) 6h and (g, h) 8h, the scale of (a), (c), (e) and (g) is 5µm, the scale of (b) is 2µm, and the scale of (d), (f) and (h) is 500nm.**

The electrochemical performances also confirmed that the SiNWs sample with smallest diameter provided the best cycle stability (seen Figure 3.6). 8h calcination treatment at 1000°C delivered highest reversible capacity, however, the shorter time of calcination treatment, resulting the poorer of cycle stability.

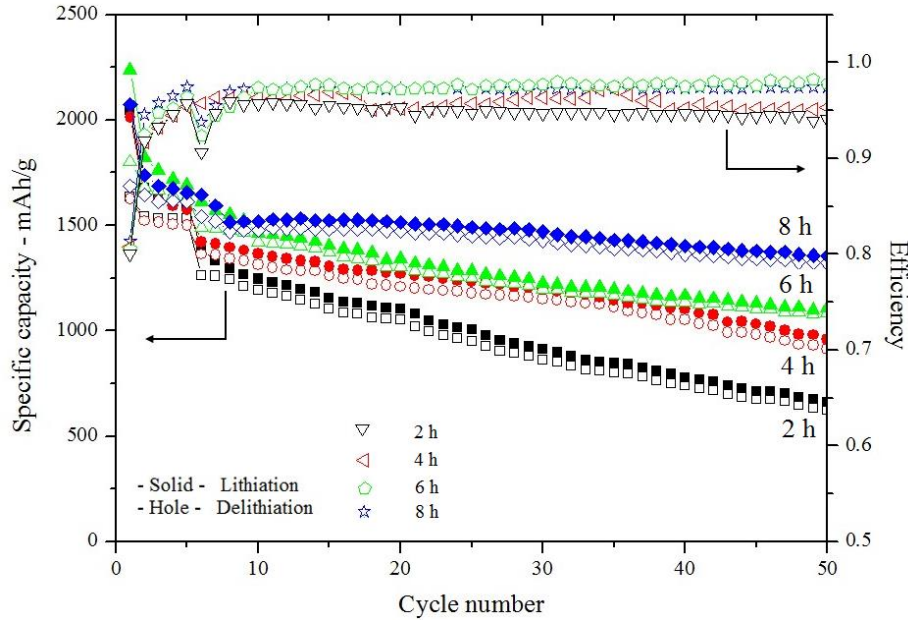


**Figure 3.6 Cycling performance and cell efficiency of as-prepared SiNWs in different storage time at 1000°C.**

According to the results of calcination treatment with different temperature and time, best performance SiNWs can be synthesized at the 1000°C and 8h which has the smallest diameter of each pillar. These results agree with the eutectic effect of Si-Al alloy at elevated temperature [23-29], and fabric Si phase was discovered in alloy. This part of work provides further understanding on the relationship between the Si phase morphology control and heat-treatment. Based on this work, the new Si branches can be generated and grew up from the original Si phase during heat treatment, and nanostructured branches can be achieved at higher temperature and longer time which facilitate the growth of SiNWs (seen Figure 3.7). The Si-Al alloy only exists the Al phase and Si phase which also help us to easily remove the Al from alloy without any usage of HF. This study may be further extending to higher temperature (1000-1414°C) due to the limitation of furnace devices.

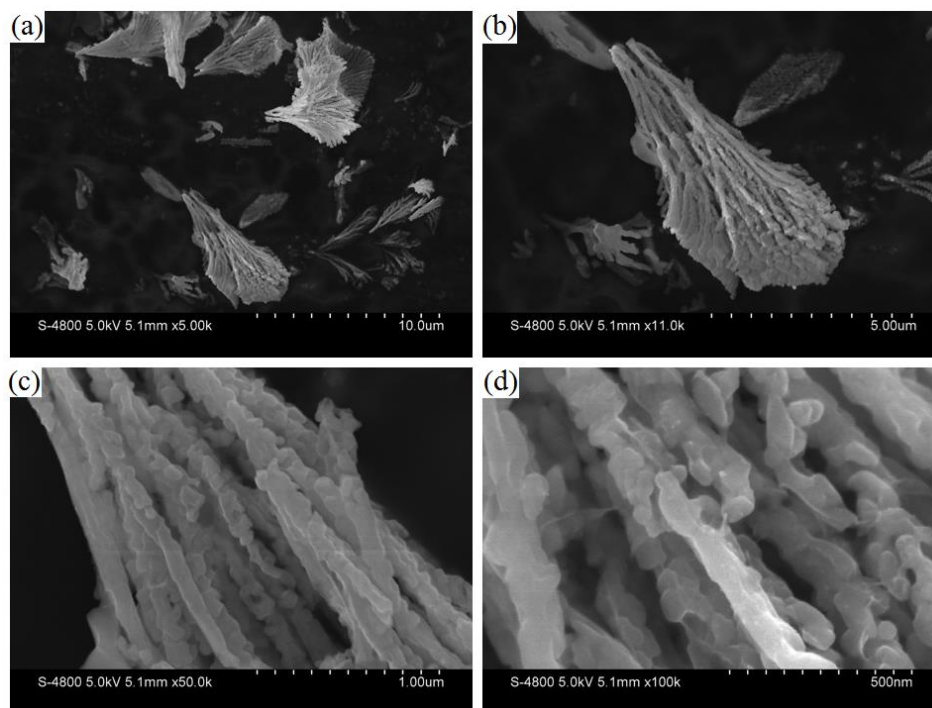


**Figure 3.7 High resolution SEM images of as-prepared SiNWs after 1000°C, 8h heating pretreatment at different scale: (a) 10µm, (b) 5µm, (c) 1µm and (d) 500nm.**

SEM images of detailed SiNWs with best performance shown in Figure 3.7 at different scale. The “coral” micro-scale SiNW particles possessed a length of about 5µm for each particle, with a diameter of 100nm nanowires. It had to be noted that the rough surface of nanowires might be the defects, which could grow smaller Si nanowires [25-27]. XRD spectra (seen Figure 3.8 (a)) revealed the phase change of Al-Si alloy before and after heat treatment and etching. The EDX of Al-Si alloy consisted of crystalline phase of Al and Si while no Al peaks were observed after etching process in fig 3.8 (b) . All Al peaks disappeared after treatment and strong Si peaks left, indicating all Al removed from alloy by HCl etching. The EDX result also confirmed that the as-prepared SiNWs contained Si, Al and O element, while carbon came from the background of conductive tape. It was obvious that most of aluminum was removed in this method, and partial SiNWs may oxidize during the process. The specific surface area of SiNWs was analyzed by TriStar II Plus, and a result of 36.68m<sup>2</sup>/g was obtained from the B.E.T. method (Figure 3.8 (c)).

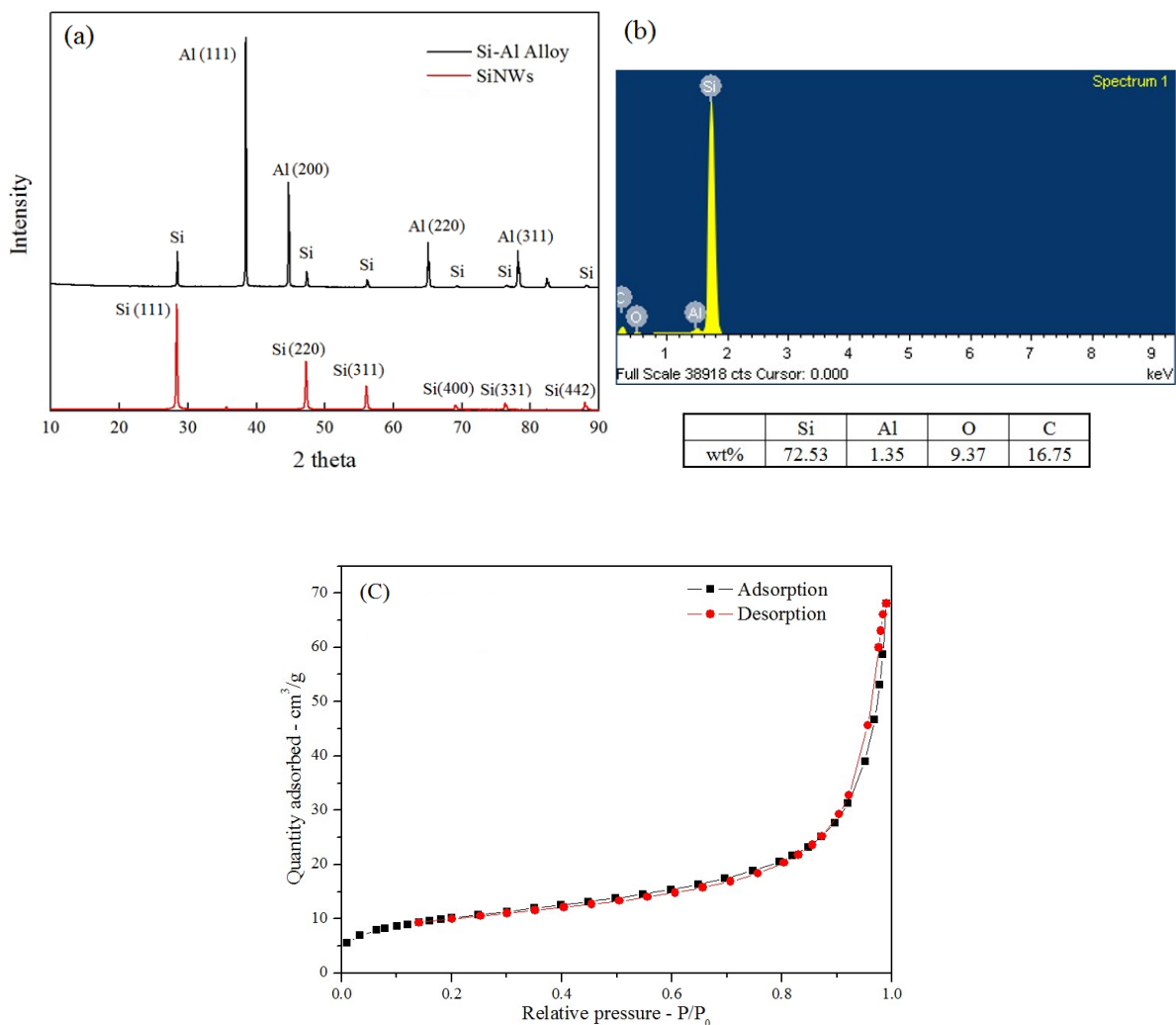


**Figure 3.8 (a) XRD spectra of Si-Al alloy and SiNWs, (b) EDX spectra of SiNWs, (c) surface area for as-prepared SiNWs.**

### 3.4 Conclusions

This part of work reports a new approach of synthesis SiNWs from Si alloy. The morphology of Si phase is manipulated by proper heat-treatment and the acid etching process is totally HF free. Eventually, a simple and safe method was developed to synthesis SiNWs using HCl acid etching heat treated Al-Si alloy. The favored morphology of SiNWs can be achieved by heating at 1000°C for 8 hours and acid etching treatments. The as-prepared SiNWs presented high electrochemical performance in 1.3M LiPF<sub>6</sub>/EC:DEC = 3:7 (v/v)+10 v% FEC

electrolyte in terms of both capacity and stability. This method has a potential commercial value due to its advantages such as safe and HF free processes.

## References

- [1] L. Zhang, R. Rajagopalan, H. Guo, X. Hu, S. Dou, H. Liu, A green and facile way to prepare granadilla-like Silicon-based anode materials for Li-Ion Batteries, *Adv. Funct. Mater.*, **2016**, 26, 440-446.
- [2] A. Magasinski, P. Dixon, B. Hertzberg, A. Kvit, J. Ayala, G. Yushin, High-performance lithium-ion anodes using a hierarchical bottom-up approach, *Nature Mater.*, **2010**, 9, 353-358.
- [3] W-J. Zhang, A review of the electrochemical performance of alloy anodes for lithium-ion batteries, *J. Power Sources*, **2011**, 196, 13-24.
- [4] P.R. Raimann, N.S. Hochgatterer, C. Korepp, K.C. Möller, M. Winter, H. Schröttner, F. Hofer, J.O. Besenhard, Monitoring dynamics of electrode reactions in Li-ion batteries by in situ ESEM, *Ionics*, **2006**, 12, 253-255.
- [5] T.D. Hatchard, J.R. Dahn, In situ XRD and electrochemical study of the reaction of lithium with amorphous silicon, *J. Electrochem. Soc.*, **2004**, 151(6), A838-A842.
- [6] W.J. Weydanz, M. Wohlfahrt-Mehrens, R.A. Huggins, A room temperature study of the binary lithium-silicon and the ternary lithium-chromium-silicon system for use in rechargeable lithium batteries, *J. Power Sources*, **1999**, (81-82), 237-242.
- [7] Z. Yang, Y. Xia, J. Ji, B. Qiu, K. Zhang, Z. Liu, Superior cycling performance of a sandwich structure Si/C anode for lithium ion batteries, *RSC Adv.*, **2016**, 6, 12107-12114.
- [8] L.Y. Beaulieu, K.W. Eberman, R.L. Turner, L.J. Krause, J.R. Dahn, Colossal reversible volume changes in lithium alloys, *Electrochem. Solid-State Lett.*, **2001**, 4(9), A137-A140.
- [9] L.D. Toan, E. Moyon, M.R. Zamfir, J. Joe, Y.W. Kim, D. Pribat, Si nanowires grown by Al-catalyzed plasma-enhanced chemical vapor deposition: synthesis conditions, electrical properties and application to lithium battery anodes, *Mater. Res. Express*, **2016**, 3, 015003.
- [10] E. Peled, F. Patolsky, D. Golodnitsky, K. Freedman, G. Davidi, D. Schneier, Tissue-like silicon nanowires-based three-dimensional anodes for high-capacity lithium ion batteries, *Nano Lett.*, **2015**, 15, 3907-3916.
- [11] W. Wang, Y. Wang, L. Gu, R. Lu, H. Qian, X. Peng, J. Sha, SiC@Si core-shell nanowires on carbon paper as a hybrid anode for lithium-ion batteries, *J. Power Sources*, **2015**, 293, 492-497.



- [12] F. Xia, S. Kwon, W.W. Lee, Z. Liu, S. Kim, T. Song, K.J. Choi, U. Paik, W.I. Park, Graphene as an interfacial layer for improving cycling performance of Si nanowires in lithium-ion batteries, *Nano Lett.*, **2015**, 15, 6658-6664.
- [13] J-H. Cho, S.T. Picraux, Enhanced lithium ion battery cycling of Silicon nanowire anodes by template growth to eliminate silicon underlayer islands, *Nano Lett.*, **2013**, 13, 5740-5747.
- [14] L-F. Cui, Y. Yang, C-M. Hsu, Y. Cui, Carbon-silicon core-shell nanowires as high capacity electrode for lithium ion batteries, *Nano Lett.*, **2009**, 9(9), 3370-3374.
- [15] K. Peng, J. Jie, W. Zhang, S-T. Lee, Silicon nanowires for rechargeable lithium-ion battery anodes, *Appl. Phys. Lett.*, **2008**, 93, 033105.
- [16] Z. Lu, N. Liu, H-W. Lee, J. Zhao, W. Li, Y. Li, Y. Cui, Nonfilling carbon coating of porous silicon micrometer-sized particles for high-performance lithium battery anodes, *ACS NANO*, **2015**, 9, 2540-2547.
- [17] M. Ge, J. Rong, X. Fang, A. Zhang, Y. Lu, C. Zhou, Scalable preparation of porous silicon nanoparticles and their application for lithium-ion battery anodes, *Nano Res.*, **2013**, 6(3), 174-181.
- [18] B.M. Bang, H. Kim, H.K. Song, J. Cho, S. Park, Scalable approach to multi-dimensional bulk Si anodes via metal-assisted chemical etching, *Energy Environ. Sci.*, **2011**, 4, 5013-5019.
- [19] S.W. Lee, H-W. Lee, I. Ryu, W.D. Nix, H. Gao, Y. Cui, Kinetics and fracture resistance of lithiated silicon nanostructure pairs controlled by their mechanical interaction, *Nat. Commun.*, **2015**, 6, 7533.
- [20] M.T. McDowell, S.W. Lee, J.T. Harris, B.A. Korgel, C. Wang, W.D. Nix, Y. Cui, In situ TEM of two-phase lithiation of amorphous silicon nanospheres, *Nano Lett.*, **2013**, 13, 758-764.
- [21] M. Gu, L.R. Parent, B.L. Mehdi, R.R. Unocic, M.T. McDowell, R.L. Sacci, W. Xu, J.G. Connell, P. Xu, P. Abellan, X. Chen, Y. Zhang, D.E. Perea, J.E. Evans, L.J. Lauhon, J-G. Zhang, J. Liu, N.D. Browning, Y. Cui, I. Arslan, C-M. Wang, Demonstration of an electrochemical liquid cell for operando transmission electron microscopy observation of the lithiation/delithiation behavior of Si nanowire battery anodes, *Nano Lett.*, **2013**, 13, 6106-6112.
- [22] K. Zhao, M. Pharr, Q. Wan, W.L. Wang, E. Kaxiras, J.J. Vlassak, Z. Suo, Concurrent reaction and plasticity during initial lithiation of crystalline silicon in lithium-ion batteries, *J. Electrochem. Soc.*, **2012**, 159(3), A238-A243.
- [23] M.C.S. Jr, A.R. Machado, W.F. Sales, M.A.S. Barrozo, E.O. Ezugwu, Machining of aluminum alloys: a review, *Int. J. Adv. Manuf. Technol.*, **2016**, DOI 10.1007/s00170-016-8431-9.

- [24] X. Jian, T.T. Meek, Q. Han, Refinement of eutectic silicon phase of aluminum A356 alloy using high-intensity ultrasonic vibration, *Scripta Mater.*, **2006**, 54, 893-896.
- [25] E. Ogris, A. Wahlen, H. Lüchinger, P.J. Uggowitzer, On the silicon spheroidization in Al-Si alloys, *J. Light Met.*, **2002**, 2, 263-269.
- [26] M.M. Makhlouf, H.V. Guthy, The aluminum-silicon eutectic reaction: mechanisms and crystallography, *J. Light Met.*, **2001**, 1, 199-218.
- [27] J. Chang, I. Moon, C. Choi, Refinement of cast microstructure of hypereutectic Al-Si alloys through the addition of rare earth metals, *J. Mater. Sci.*, **1998**, 33, 5015-5023.
- [28] A.J. Criado, J.A. Martinez, R. Calabrés, Growth of eutectic silicon from primary silicon crystals in aluminum-silicon alloys, *Scripta Mater.*, **1997**, 36(1), 47-54.
- [29] J.I. Lee, H.I. Lee, M.I. Kim, Formation of spherical primary silicon crystals during semi-solid processing of hypereutectic Al-15.5wt%Si alloy, *Scripta Metall. Mater.*, **1995**, 32(12), 1945-1949.
- [30] A.G. Kannan, S.H. Kim, H.S. Yang, D-W. Kim, Silicon nanoparticles grown on a reduced graphene oxide surface as high-performance anode materials for lithium-ion batteries, *RSC Adv.*, **2016**, 6, 25159-25166.
- [31] L. Wang, N. Lin, J. Zhou, Y. Zhu, Y. Qian, Silicon nanoparticles obtained via a low temperature chemical “metathesis” synthesis route and their lithium-ion battery properties, *Chem. Commun.*, **2015**, 51, 2345-2348.
- [32] E. Peled, F. Patolsky, D. Golodnitsky, K. Freedman, G. Davidi, D. Schneier, Tissue-like silicon nanowires-based three-dimensional anodes for high-capacity Lithium Ion Batteries, *Nano Letters*, **2015**, 15(6), 3907-3916.
- [33] P.P. Prosini, C. Cento, F. Alessandrini, P. Gislou, A. Mancini, A. Ruffoloni, F. Rondino, A. Santoni, Electrochemical characterization of silicon nanowires as an anode for lithium batteries, *Solid State Ionics*, **2014**, 260, 49-54.
- [34] H. Wang, P. Wu, H. Shi, F. Lou, Y. Tang, T. Zhou, Y. Zhou, T. Lu, Porous Si spheres encapsulated in carbon shells with enhanced anodic performance in lithium-ion batteries, *Mater. Res. Bull.*, **2014**, 55, 71-77.
- [35] G. Zhao, L. Zhang, Y. Meng, N. Zhang, K. Sun, High storage performance of core-shell Si@C nanoparticles as lithium ion battery anodematerial, *Mater. Lett.*, **2013**, 96, 170-173.
- [36] H. Wu, G. Chan, J.W. Choi, I. Ryu, Y. Yao, M.T. McDowell, S.W. Lee, A. Jackson, Y. Yang, L. Hu, Y. Cui, Stable cycling of double-walled silicon nanotube battery anodes through solid-electrolyte interphase control, *Nature Nanotech.*, **2012**, 7, 310-315.

## Chapter 4

### 4 Electrode optimization: density, loading, binder and cycle mode

#### 4.1 Introduction

The lithium-ion battery performances are not only determined by electrode materials [1-5], but also by other factors like binder, conductive agent, and current collector, etc. Moreover, the battery assembling processes also play crucial roles in achieving stable performance and high efficiency. Compared with electrode materials, less work has been done to investigate these effects, and only few references are available about the effect of process parameters. Noticing these, this chapter will focus on optimizing electrodes to improve the cyclic stability of nano Si materials in half cell format LIB. Few key parameters will be modified in this section including density/loading, binder and cycle mode and their impact on the cycling performance. It has to be noted that all optimizations are based on the SiNWs material which is used in this and following chapter and the test conditions for fabrication of pure silicon electrode.

#### 4.2 Experimental Section

In this work, Silicon nanowires (SiNWs, Springpower International Inc., Canada, seen Figure 4.1), acetylene black (AB, Gunbai, Denki Kagaku Kogyo, Japan) and sodium alginate (SA, MP Biomedicals, LLC, USA) were used for preparing the Si anode electrodes. The control formula of electrode was SiNWs : AB : SA = 63 : 22 : 15 (wt. %). The binder and formula changed and marked for optimization later. The as-prepared slurry was casted on 18 $\mu$ m copper foil and loading of total mass for electrodes was 0.8-2.0mg/cm<sup>2</sup>. The electrodes were cut and assembled into 2032 coin cell after pressing, and the electrolyte was made by adding

10 v % FEC (BASF, USA) into 1.3M LiPF<sub>6</sub> in 3:7 v/v EC/DEC electrolyte (BASF, USA). After ageing for 24 hours at room temperature, the cells were tested on Arbin BT2000. Initially, the cells were cycled at 0.05C current density (constant current) within 0.01-1.5V (vs. Li<sup>+</sup>/Li) to form stable SEI layer and the cells were continuously tested between 0.01-1V (vs. Li<sup>+</sup>/Li) at a 0.1 C current density at constant current (0.1C) and constant voltage (at 0.005C), and only constant current (0.1C) for delithiation. The calculation of C was based on the total mass loading and 4200mAh/g. please see chapter 3 for the same part. EIS spectra was applied to compare the change of internal resistance and the morphology of electrode was observed by FESEM technique.

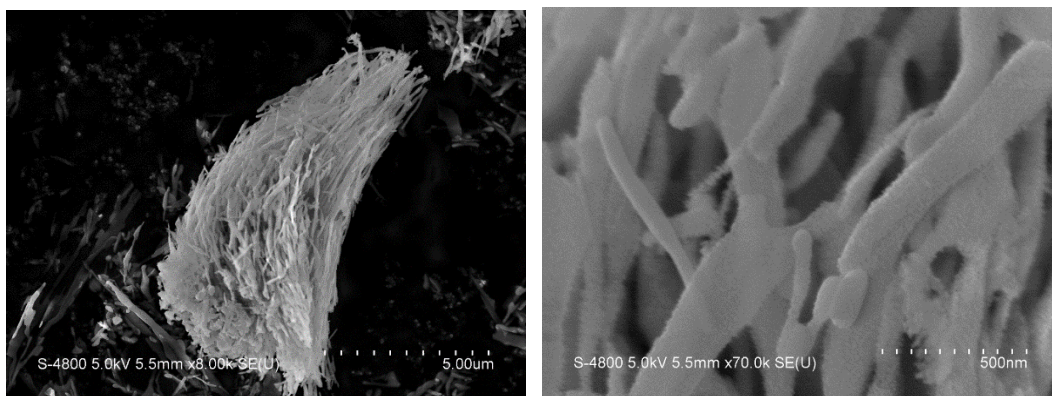


**Figure 4.1** SEM images of SiNWs at two scales.

## 4.3 Results and Discussion

### 4.3.1 Loading and density

Electrode loading is the weight of solid materials within unit area of current collector, including active material, binder and conductive agent. Most of the previous work on Si anode reported the mass loading of electrode was lower than 0.6 mg/cm<sup>2</sup> [6-11], which did not match the energy density of commercial graphite electrode. Generally, the electrode with higher mass loading has higher energy density (seen Table 1.2). In addition, the thickness of electrode greatly affects volumetric energy density of anode and thereby affects the volumetric energy density of LIBs. Figure 4.2 shows a typical calendar process by using roll-to-roll machine in LIB industry. The pressure is applied on both sides of electrode, and the

thickness of electrode is decreased. It is clear that the electrode density increase with increasing same mass loading of the electrode. Moreover, the increased density also improve the electrode conductivity due to better connection of electrode materials. However, excessive calendar can greatly reduce the electrode porosity, limiting the channels for electrolyte. The insufficient electrolyte supply will inevitably lead to electrode “dead area” or abnormal capacity drop, and eventually reduce the cycle stability and battery life. Therefore, it is important to achieve an optimal density which can balance the thickness and performance. This is even more important to silicon based electrodes.

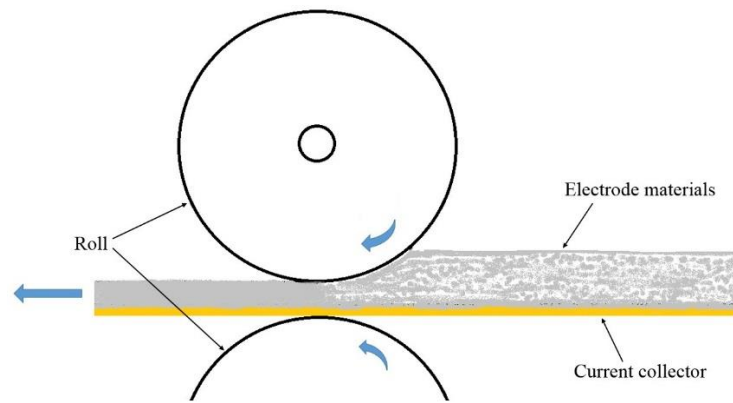


**Figure 4.2** Schematic illustration of electrode calendar in LIB industry.

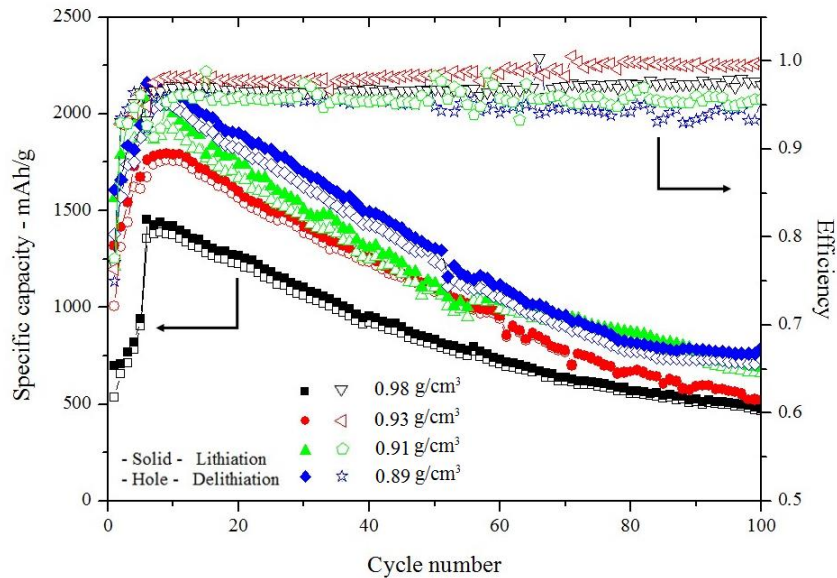


**Figure 4.3** Cycling performance of four electrodes with various density.

Four electrodes were prepared with a mass loading of about 1.4mg/cm<sup>2</sup>, followed by a pressing treatment. The electrode parameters are shown in Table 4.1. After the electrodes assembled in coin cells, the cycle test was carried out with overnight storage (24h) at room temperature. Pretty low charge/discharge capacities were observed for first 5 cycles, especially 0.98g/cm<sup>3</sup> electrode, which was caused by the difficulty of electrolyte uptake in high density electrode. It was obvious that higher density electrodes need more time to fully absorb electrolyte. The specific capacities quickly recovered in first 5 cycles and the cycling performances were much stable after activation cycles, which indicated that more Si anode involved in electrochemical reaction since 6<sup>th</sup> cycle. The trend of cell capacity fade was similar for those four density electrodes, and better capacities were achieved for lower density, such as 0.91 and 0.89g/cm<sup>3</sup>. The reason of this phenomena was the sufficient electrolyte stored in lower density/higher porosity electrodes which finally improved the specific capacity. However, as shown in Table 4.1, the volumetric energy density dropped for those lower density electrodes as well. The highest cell efficiency for 0.93g/cm<sup>3</sup> electrode proved that this cell had a stable electrochemical reaction which was crucial for LIB system. It was clear that this mass loading and electrode density were fit the SiNWs anode material to tolerance the huge material expansion and achieve mechanical stability of electrode. Therefore, this density was chosen for later comparison of different mass loading.

**Table 4.1 Work electrodes basic information for density test**

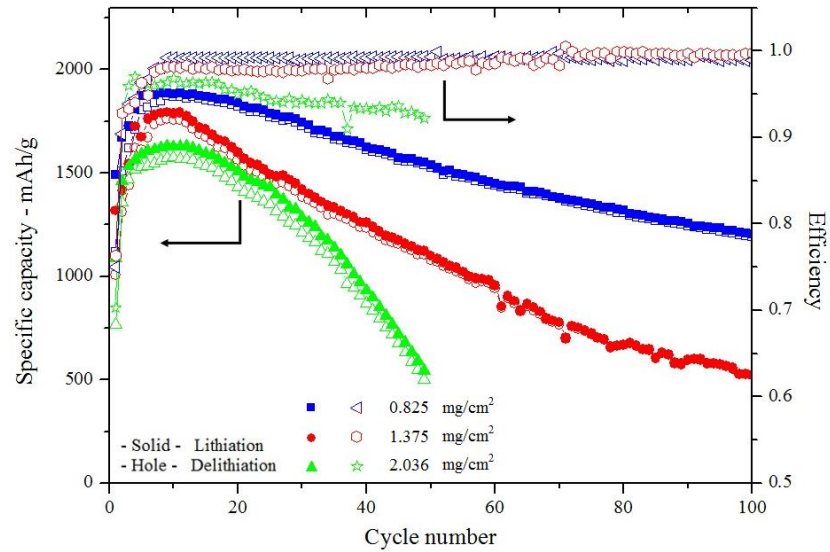
Cell number	Loading - mg/cm <sup>2</sup>	True porosity - %	True density - g/cm <sup>3</sup>	True thickness - μm	Volumetric energy density - Wh/l
1#	1.366	0.55	0.98	13.6	1319.6
2#	1.375	0.57	0.93	14.4	1254.6
3#	1.422	0.58	0.91	15.3	1221.1
4#	1.415	0.59	0.89	15.6	1191.7

Three electrodes with different mass loading were prepared at the density of 0.93g/cm<sup>3</sup> (seen Table 4.2). According to Figure 4.4, the best cell performance was achieved with lowest mass loading electrode, which was about 1250mAh/g reversible capacity after 100 cycles. The cell efficiency and discharge capacity of first cycle were also the highest among cells. On the other hand, the highest mass loading (2.036mg/cm<sup>2</sup>) electrode shown the poorest cycle stability, only 500mAh/g reversible capacity remaining after 50 cycles. This was

reasonable because the polarization of thicker electrode was much aggressive during electrochemical reaction of cycling, leading much fast capacity fading.

**Table 4.2 Work electrodes basic information for loading test**

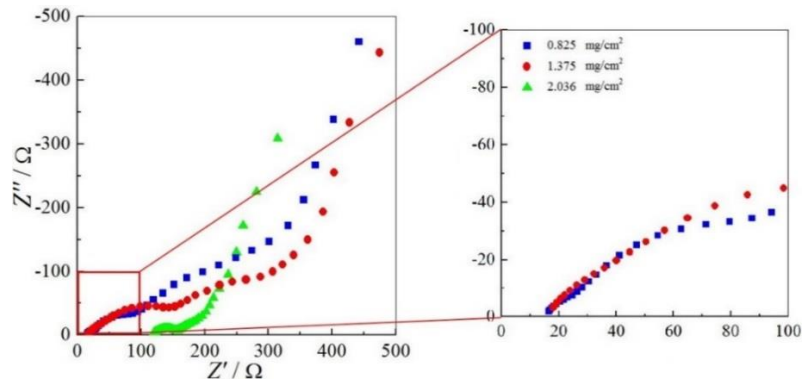
Cell number	Loading - $\text{mg}/\text{cm}^2$	True porosity - %	True density - $\text{g}/\text{cm}^3$	True thickness - $\mu\text{m}$
1#	0.825	0.59	0.89	9.5
2#	1.375	0.57	0.93	14.4
3#	2.036	0.56	0.94	22



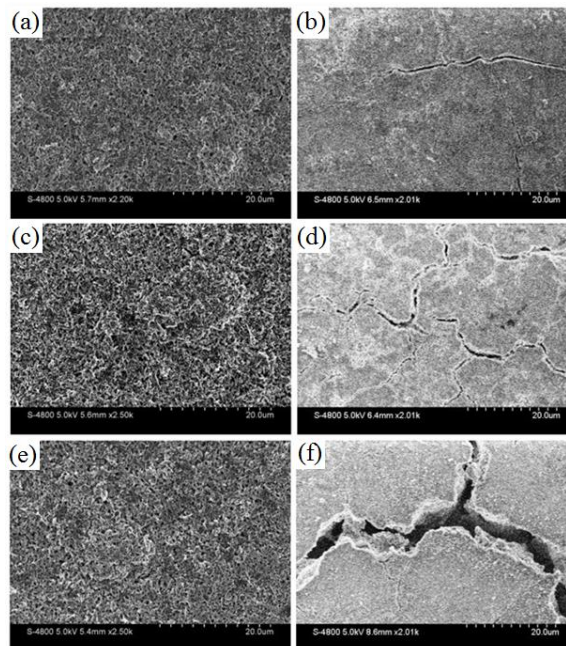
**Figure 4.4 Cycling performance of three electrodes with various loading at same density.**

Figure 4.5 shown Nyquist plots of LIB cells fabricated with electrodes at same density ( $0.93\text{g}/\text{cm}^3$ ) with three mass loading of  $0.825\text{mg}/\text{cm}^2$ ,  $1.375\text{mg}/\text{cm}^2$  and  $2.036\text{mg}/\text{cm}^2$ , respectively. According to the plots, the internal resistance of the cell with  $1.375\text{mg}/\text{cm}^2$  mass loading much higher than that of  $0.825\text{mg}/\text{cm}^2$  electrode, and the  $2.036\text{mg}/\text{cm}^2$  electrode had worst interface condition. It is clear that higher mass loading can cause faster capacity fading due to the longer  $\text{Li}^+$  and electron transportation path which will increase the polarization effect. According to Figure 4.6, the SEM images of cycled electrodes shown that fewer cracks observed on lower mass loading electrode. In addition, about  $5\mu\text{m}$  width cracks

were observed on  $2.036\text{mg}/\text{cm}^2$  cycled electrode which was the reason of capacity fading due to the material loss and detach from current collector [2, 4-6, 11]. The cracks also facilitated the ion and electron transportation because the directly contacted between electrolyte and current collector. This explained that the impedance of highest loading had the low resistance. Therefore, the mass loading of SiNWs electrode is better lower than  $1.375\text{mg}/\text{cm}^2$ . This section clearly point out that the proper mass loading and density for Si anode electrode are crucial for battery design in LIB industry.



**Figure 4.5** Nyquist plots of three electrodes after 50 cycles.



**Figure 4.6** SEM images of electrodes before (a, c, e), after 100 cycles (b, d) and after 50 cycles (f), (a, b)  $0.825\text{mg}/\text{cm}^2$ , (c, d)  $1.375\text{mg}/\text{cm}^2$  and (e, f)  $2.036\text{mg}/\text{cm}^2$ .



### 4.3.2 Binder

Binder plays a crucial role in Si-based electrode. However, current commercial binders, carboxyl methyl cellulose plus styrene butadiene rubber (CMC + SBR) and polyvinylidene fluoride (PVdF), are not satisfied due to low mechanical properties [12-18]. The CMC+SBR binder is a control sample for comparison due to the wide usage in LIB industry. Few binders are compared in this section to evaluate the performance of SiNWs electrode, including native-XG binder (XGB) [19], sodium polyacrylic acid (PAA) and sodium alginate (SA). All the binders are easily available at low cost which is the basic requirement of potential industry application.

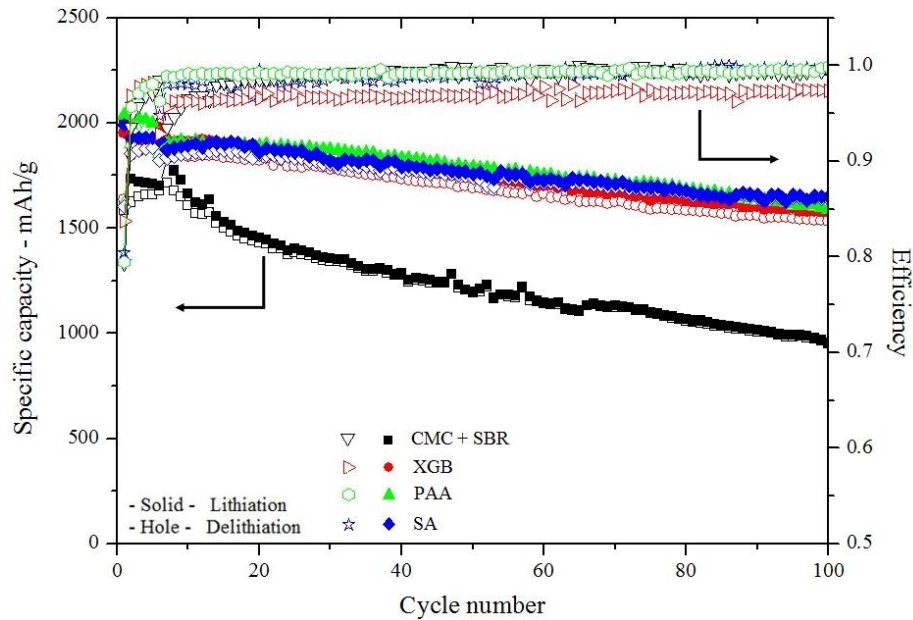


**Figure 4.7 Cycling performance of four electrodes with various binders.**

Using same electrode formula (SiNWs : AB : Binder = 63 : 22 : 15, wt %), SiNWs and conductive agent, four binders were applied to fabricate Si electrodes with  $0.8\text{mg}/\text{cm}^2$  and normal pressure (5000lb for 3 minutes). The cycle performance and rate capability were shown in Figure 4.7 and Figure 4.8, respectively. The result of cycle performance shown that electrode using CMC+SBR binder had the poorest cycle stability, 1000mAh/g reversible capacity after 100 cycles. All other electrodes presented a similar trend of cyclic performance with relatively smaller capacity degradation, and the SA binder showed better performances than PAA and XGB.

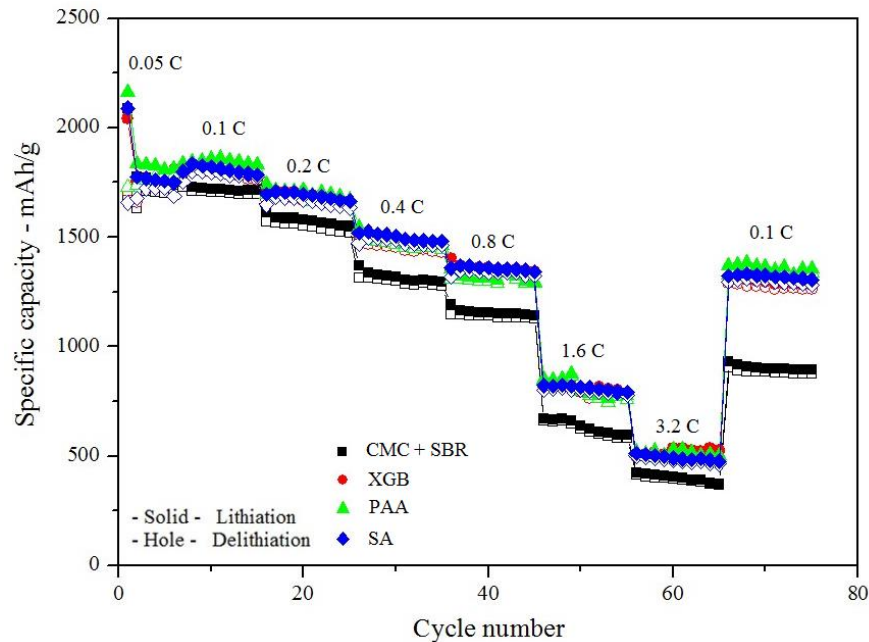


**Figure 4.8 Rate capability of four electrodes with various binders.**

The C rate capability further confirmed that the reversible capacities of CMC+SBR electrode was lower than other three electrodes at each current density. For Si electrode binder, the key note is to form a huge “net” which not only covers the electrode materials, but also creates more crosslinks in the whole electrode, stabilizing the active materials on the electrode. In addition, the better binder is not only holds the electrode materials during cycling, it also improves the adhesion strength between electrode materials and current collector.

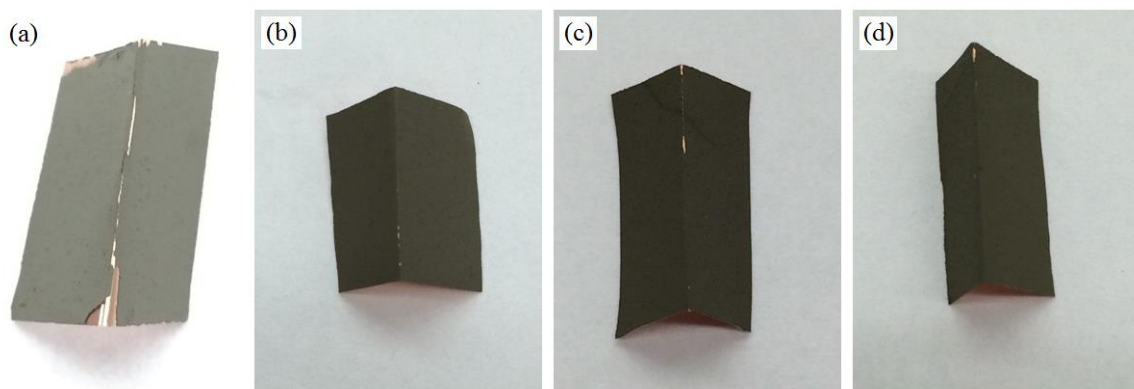


**Figure 4.9 Mechanical adhesion property of four electrodes: (a) CMC+SBR binder, (b) XG-binder, (c) PAA binder and (d) SA binder.**

The fold test is an easy and popular method to test the adhesion property of LIB electrode. The results of fold test for the electrodes with different binders were shown in Figure 4.9, which indicated that electrode prepared with CMC+SBR binder was detached from Cu foil after folding. However, only a little electrode materials detached from foil for other three electrodes. In short, XGB, PAA and SA binders can provide better mechanical properties, improving the cycle stability.

### 4.3.3 Cycle mode

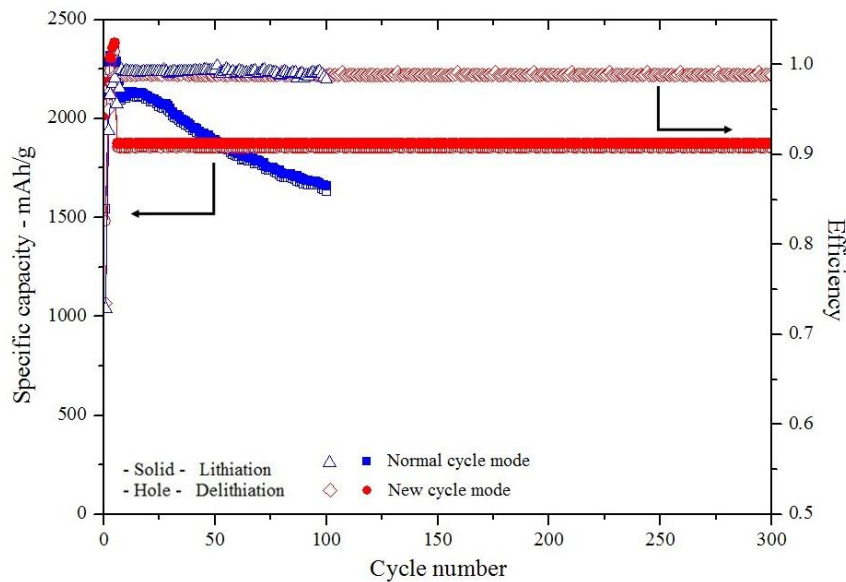


**Figure 4.10** Cycling performance of two test modes.

It is well known that the key problem of Si anode is the 400% volume expansion during  $\text{Li}^+$  insertion/extraction process. According to many references, the expansion of Si material is related to the Li-Si alloy formation [20-27], which could be a new concept for stabilizing cell performance. By controlling the lithiation capacity in Si electrode, the charge/discharge capacity can be greatly improved [15, 28-33]. The electrodes were prepared with mass loading of  $0.8\text{mg}/\text{cm}^2$  and density of  $0.77\text{g}/\text{cm}^3$  which could reduce the polarization effect during test, then assembled 2032 coin cell after normal pressing. Other conditions were the same until finished the first five activation cycles. Another test mode was carried out to show the cycle performance with a lithium insertion capacity limited to 80% of that in formation

step at the same current density (0.1C charge and discharge), and the result was shown in Figure 4.10. Obviously, the new cycle mode was much stable up to 300 cycles. The lithiation capacity of new mode was set to 1872mAh/g, which was the 80% of the 5<sup>th</sup> cycle discharge capacity 2336mAh/g. In the beginning, the discharge capacity of normal cycle mode was much higher than that of new mode. Unfortunately, the capacity of normal mode faded very quickly, and it was lower than new mode after 50 cycles. It also had to be noted that the cell efficiency of new mode was always over 99%.

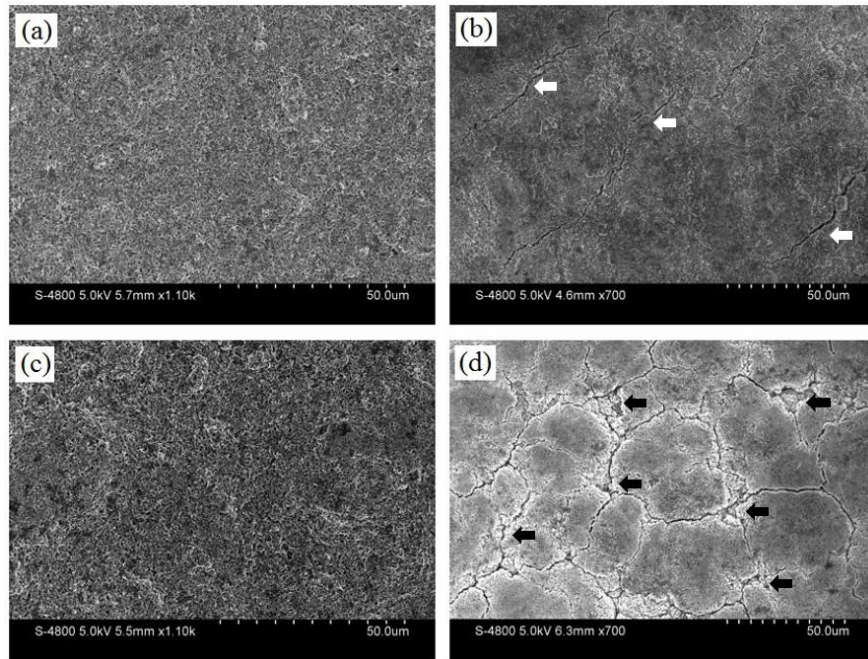


**Figure 4.11 SEM images of electrodes surface: New cycle mode electrodes (a) before and (b) after 300 cycles. Normal cycle mode electrodes (c) before and (d) after 100 cycles.**

The SEM images of electrodes before and after cycling were shown in Figure 4.11. Before cycling, both electrodes were uniform and smooth. However, huge difference was observed after cycling test. For normal cycle mode electrode (Figure 4.11 (d)), more cracks were found and partial active material was lost during cycling due to the aggressive swelling. On the contrary, only few cracks were observed on electrode cycled using for cycle mode even after 300 cycles and the cracks were not linked each other (seen white arrow in Figure 4.11 (b)). Unlike normal cycle test, there was not obviously material loss as well. In general, the

electrode maintained much better by controlling the lithiation of Si anode materials since the deformation of Si material did not reach the maximum volume change, which clearly provided a longer and better cycling performance.

## 4.4 Conclusions

The electrode mass loading, density and binder can greatly affect the cycle stability. Therefore, finding the right combination of these parameters are crucial to achieve cycle stability. Figure 4.12 shown a modified electrode (SA binder,  $0.829\text{mg}/\text{cm}^2$  and  $0.93\text{g}/\text{cm}^3$ ) provide a much stable cycle performance, 78.9% retention capacity after 300 cycles and over 99% cell efficiency. The capacity limitation cycle mode also can improve the cycle stability due to the incomplete lithiation reaction provide a relatively small electrode swelling.

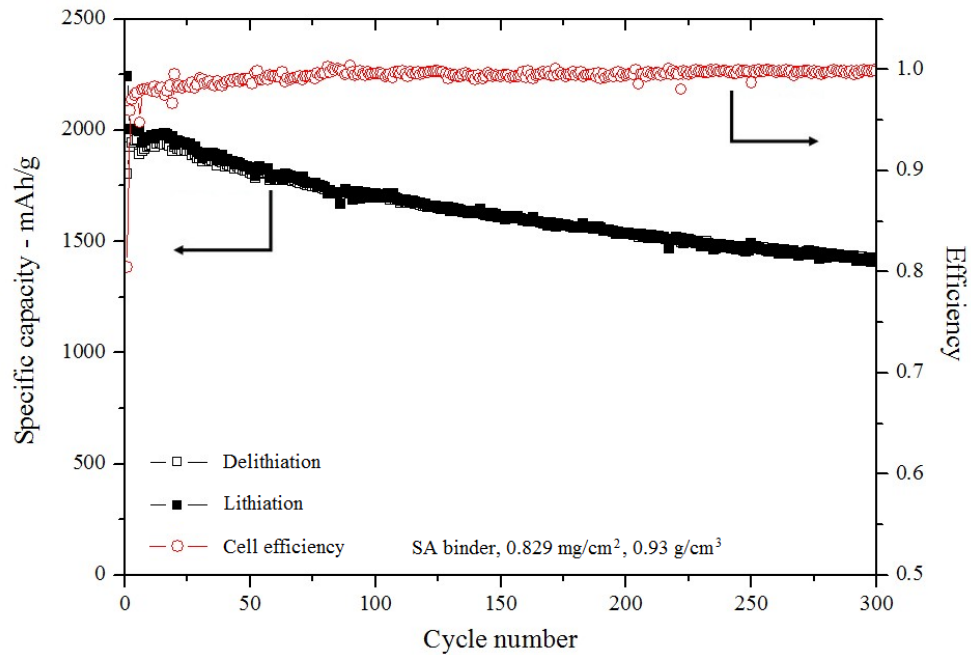


**Figure 4.12 Cycle performance of modified electrode parameter.**

## References

- [1] J. Liang, X. Li, Z. Hou, W. Zhang, Y. Zhu, Y. Qian, A deep reduction and partial oxidation strategy for fabrication of mesoporous Si anode for lithium ion batteries, *ACS NANO*, **2016**, 10, 2295-2304.
- [2] D. Lin, Z. Lu, P-C. Hsu, H.R. Lee, N. Liu, J. Zhao, H. Wang, C. Liu, Y. Cui, A high tap density secondary silicon particle anode fabricated by scalable mechanical pressing for lithium-ion batteries, *Energy Environ. Sci.*, **2015**, 8, 2371-2376.
- [3] W. Li, Y. Tang, W. Kang, Z. Zhang, X. Yang, Y. Zhu, W. Zhang, C-S. Lee, Core-shell Si/C nanospheres embedded in bubble sheet-like carbon film with enhanced performance as lithium ion battery anodes, *Small*, **2015**, 11(11), 1345-1351.
- [4] S. Jing, H. Jiang, Y. Hu, J. Shen, C. Li, Face-to-face contact and open-void coinvolved Si/C nanohybrids Lithium-Ion Battery anodes with extremely long cycle life, *Adv. Funct. Mater.*, **2015**, 25, 5395-5401.
- [5] J. Liu, N. Li, M.D. Goodman, H.G. Zhang, E.S. Epstein, B. Huang, Z. Pan, J. Kim, J.H. Choi, X. Huang, J. Liu, K.J. Hsia, S.J. Dillon, P.V. Braun, Mechanically and chemically robust sandwich-structured C@Si@C nanotube array Li-Ion battery anodes, *ACS NANO*, **2015**, 9(2), 1985-1994.
- [6] L-S. Jiao, J-Y. Liu, H-Y. Li, T-S. Wu, F. Li, H-Y Wang, L. Niu, Facile synthesis of reduced graphene oxide-porous silicon composite as superior anode material for lithium-ion battery anodes, *J. Power Sources*, **2016**, 315, 9-15.
- [7] P. Zhang, L. Huang, Y. Li, X. Ren, L. Deng, Q. Yuan, Si/Ni<sub>3</sub>Si-Encapsulated carbon nanofiber composites as three-dimensional network structured anodes for lithium-ion batteries, *Electrochim. Acta*, **2016**, 192, 385-391.
- [8] Y. Bie, J. Yang, X. Liu, J. Wang, Y. Nuli, W. Lu, Polydopamine wrapping silicon cross-linked with polyacrylic acid as high-performance anode for lithium-ion batteries, *Appl. Mater. Interfaces*, **2016**, 8, 2899-2904.
- [9] Q. Lv, Y. Liu, T. Ma, W. Zhu, X. Qiu, Hollow structured silicon anodes with stabilized solid electrolyte interphase film for lithium-ion batteries, *Appl. Mater. Interfaces*, **2015**, 7, 23501-23506.
- [10] F. Zhang, X. Yang, Y. Xie, N. Yi, Y. Huang, Y. Chen, Pyrolytic carbon-coated Si nanoparticles on elastic graphene framework as anode materials for high-performance lithium ion batteries, *Carbon*, **2015**, 82, 161-167.
- [11] H. Tian, X. Tan, F. Xin, C. Wang, W. Han, Micro-sized nano-porous Si/C anodes for lithium ion batteries, *Nano Energy*, **2015**, 11, 490-499.
- [12] C. Chen, S.H. Lee, M. Cho, J. Kim, Y. Lee, Cross-linked chitosan as an efficient binder for Si anode for Li-Ion batteries, *Appl. Mater. Interface*, **2016**, 8, 2658-2665.

- [13] L. Luo, Y. Xu, H. Zhang, X. Han, H. Dong, X. Xu, C. Chen, Y. Zhang, J. Lin, Comprehensive understanding of high polar polyacrylonitrile as an effective binder for Li-ion battery nano-Si anodes, *Appl. Mater. Interfaces*, **2016**, 8, 8154-8161.
- [14] L. Wei, C. Chen, Z. Hou, H. Wei, Poly (acrylic acid sodium) grafted carboxymethyl cellulose as a high performance polymer binder for silicon anode in lithium ion batteries, *Sci. Rep.*, **2016**, 6, 19583.
- [15] J. Liu, Q. Zhang, T. Zhang, J-T. Li, L. Huang, S-G. Sun, A robust ion-conductive biopolymer as a binder for Si anodes of lithium-ion batteries, *Adv. Funct. Mater.*, **2015**, 25, 3599-3605.
- [16] S-J. Park, H. Zhao, G. Ai, C. Wang, X. Song, N. Yuca, V.S. Battaglia, W. Yang, G. Liu, Side-chain conducting and phase-separated polymeric binders for high-performance silicon anodes in Lithium-Ion batteries, *J. Am. Chem. Soc.*, **2015**, 137, 2565-2571.
- [17] J. Song, M. Zhou, R. Yi, T. Xu, M.L. Gordin, D. Tang, Z. Yu, M. Regula, D. Wang, Interpenetrated Gel polymer binder for high-performance Silicon anodes in Lithium-ion batteries, *Adv. Funct. Mater.*, **2014**, 24, 5904-5910.
- [18] Y.K. Jeong, T-W. Kwon, I. Lee, T-S. Kim, A. Coskun, J.W. Choi, Hyperbranched  $\beta$ -cyclodextrin polymer as an effective multidimensional binder for silicon anodes in lithium rechargeable batteries, *Nano Lett.*, **2014**, 14, 864-870.
- [19] Y.K. Jeong, T-W. Kwon, I. Lee, T-S. Kim, A. Coskun, J.W. Choi, Millipede-inspired structural design principle for high performance polysaccharide binders in silicon anodes, *Energy Environ. Sci.*, **2015**, 8, 1224-1230.
- [20] K. Ogata, E. Salager, C.J. Kerr, A.E. Fraser, C. Ducati, A.J. Morris, S. Hofmann, C.P. Grey, Revealing lithium-silicide phase transformations in nano-structured silicon-based lithium ion batteries via in situ NMR spectroscopy, *Nat. Commun.*, **2014**, 5, 3217.
- [21] S.W. Lee, M.T. McDowell, J.W. Choi, Y. Cui, Anomalous shape changes of silicon nanopillars by electrochemical lithiation, *Nano Lett.*, **2011**, 11, 3034-3039.
- [22] Q. Zhang, Y. Cui, E. Wang, Anisotropic lithium insertion behavior in silicon nanowires: Binding energy, diffusion barrier, and strain effect, *J. Phys. Chem. C*, **2011**, 115, 9376-9381.
- [23] B. Key, R. Bhattacharyya, M. Morcrette, V. Seznéc, J-M. Tarascon, C.P. Grey, Real-time NMR investigations of structural changes in silicon electrodes for lithium-ion batteries, *J. Am. Chem. Soc.*, **2009**, 131, 9239-9249.
- [24] U. Kasavajjula, C. Wang, A.J. Appleby, Nano- and bulk-silicon-based insertion anodes for lithium-ion secondary cells, *J. Power Sources*, **2007**, 163, 1003-1039.
- [25] T.D. Hatchard, J.R. Dahn, In situ XRD and electrochemical study of the reaction of lithium with amorphous silicon, *J. Electrochem. Soc.*, **2004**, 151(6), A838-A842.

- [26] L.Y. Beaulieu, K.W. Eberman, R.L. Turner, L.J. Krause, J.R. Dahn, Colossal reversible volume changes in lithium alloys, *Electrochem. Solid-State Lett.*, **2001**, 4(9), A137-A140.
- [27] H. Li, X. Huang, L. Chen, G. Zhou, Z. Zhang, D. Yu, Y.J. Mo, N. Pei, The crystal structural evolution of nano-Si anode caused by lithium insertion and extraction at room temperature, *Solid State Ionics*, **2000**, 135, 181-191.
- [28] T. Teranishi, Q. Si, F. Mizukoshi, M. Kawakubo, M. Matsui, Y. Takeda, O. Yamamoto, N. Imanishi, Silicon anode for rechargeable aqueous lithium-air batteries, *J. Power Sources*, **2015**, 273, 538-543.
- [29] M. Ling, Y. Xu, H. Zhao, X. Gu, J. Qiu, S. Li, M. Wu, X. Song, C. Yan, G. Liu, S. Zhang, Dual-functional gum Arabic binder for silicon anode in lithium ion batteries, *Nano Energy*, **2015**, 12, 178-185.
- [30] J. Liu, Q. Zhang, T. Zhang, J-T. Li, L. Huang, S-G. Sun, A robust ion-conductive biopolymer as a binder for Si anodes of lithium-ion batteries, *Adv. Funct. Mater.*, **2015**, 25, 3599-3605.
- [31] S. Uchida, M. Mihashi, M. Yamagata, M. Ishikawa, Electrochemical properties of non-nano-silicon negative electrodes prepared with a polyimide binder, *J. Power Sources*, **2015**, 273, 118-122.
- [32] K. Goldshtein, K. Freedman, D. Schneier, L. Burstein, V. Ezersky, E. Peled, D. Golodnitsky, Advanced multiphase Silicon-based anodes for high-energy-density Li-Ion batteries, *J. Electrochem. Soc.*, **2015**, 162(6), A1072-A1079.
- [33] T. Wada, T. Ichitsubo, K. Yubuta, H. Segawa, H. Yoshida, H. Kato, Bulk-nanoporous-silicon negative electrode with extremely high cyclability for lithium-ion batteries prepared using a top-down process, *Nano Lett.*, **2014**, 14, 4505-4510.



## Chapter 5

### 5 Synergies Effect of fluoroethylene carbonate (FEC) and vinylene carbonate (VC) on Si Anode for Lithium-Ion Battery

#### 5.1 Introduction

Rechargeable lithium-ion batteries (LIBs) have been attracted more attention as ideal energy storage device for green energy sources (solar, wind, tide, etc.) because of their high energy density [1-3]. New active materials are highly essential for further improving the energy density of LIBs to meet the ever-growing energy needs and reducing fossil fuel consumption [4-6]. Among the various anode materials, Si is recognized as one of the most promising candidates for next generation LIBs due to its super high theoretical capacity (4200mAh/g), abundance and environmental friendly [7-10]. However, the Si material is still suffering huge volume change during lithiation/delithiation process which finally lead to rapid capacity decay due to stress inducing structure destruction [9, 11-16]. Another consequence of this destruction is solid electrolyte interphase (SEI) [17] which is a very thin film formed on the electrode surface by decomposing of electrolyte components. The SEI formed during the cycles can be broken because of the material cracks in lithiation process and reformed on the fresh Si material surface after each cycle. Moreover, the reforming SEI will consume electrolyte during the electrochemical reaction on the interface of electrolyte/electrode [18-19], and eventually accelerate the capacity fading. Although nanostructured Si anode can greatly minimize the volumetric effect, stable SEI is also important to stabilize cycling performance. It is clear that the properties of SEI are related with the components of electrolyte. Therefore, this thin film can be modified by changing the ratio of components or adding new component in electrolyte. Electrolyte additives, usually less than 5% of total electrolyte, can greatly optimize the battery performance [20-25]. Enormous research efforts have been undertaken to understand the mechanism of additive function on the performance

of LIBs, but more work have to be focused on Si anode. The fluoroethylene carbonate (FEC) [26-34] and vinylene carbonate (VC) [22, 35, 36] are common electrolyte additives for LIB electrolyte, and recently both have found to particularly improve the cycling behavior of Si electrode. But there is no systematic study of synergies effect of FEC and VC in Si-based LIB. In this part, electrochemical performance of SiNWs electrode in four electrolytes (BE37, BE37+VC, BE37+FEC and BE37+VC+FEC) was evaluated, following the surface characterization to reveal the synergies of two additives.

## 5.2 Experimental Section

In this part, Silicon nanowires (SiNWs, Springpower International, Canada), acetylene black (AB, Gunbai, Denki Kagaku Kogyo, Japan) and sodium alginate (SA, MP Biomedicals, LLC, USA) were used for preparing the Si anode electrodes. The formula of electrode was SiNWs : AB : SA = 63 : 22 : 15 (wt.%). The as-prepared slurry was casted on 18 $\mu$ m copper foil and loading of total mass for electrodes was about 0.6mg/cm<sup>2</sup>. The electrodes were cut and assembled into 2032 coin cell after pressing. The control electrolyte was 1.3M LiPF<sub>6</sub> in 3:7 (v/v) EC/DEC electrolyte (BE37) purchased form BASF, USA. Two additives were added in BE37 electrolyte with 3 combinations: FEC (10 v%, BASF, USA), VC (2 v%, J&K Scientific LLC, USA) and FEC+VC (10 v% + 2 v%). Cycle performance was tested in Arbin BT2000 with a 5 formation cycle at a 0.05C current density and charged/discharged at 0.1C for later cycles. The purpose of formation process is to form a stable SEI on the Si electrode surface, and lower current density facilitates this step. Therefore, 0.05C current density was applied for charge and discharge process in a voltage window between 0.01-1.5V (vs. Li<sup>+</sup>/Li) at room temperature. For later cycles, the cycle test was carried out in a voltage window between 0.01-1V (vs. Li<sup>+</sup>/Li) at a 0.1C current density for lithiation, including constant current (CC, 0.1C) and constant voltage (CV, 0.005C), and constant current (CC, 0.1C) for delithiation. The later test mode was similar the full cell test in LIB industry which could get full capacity of Si anode in cell. The calculation of C was based on the total mass loading and 4200mAh/g. The cycle performance also tested at high temperature (55°C) and low temperature (-20°C). EIS spectra was applied to compare the change of internal resistance,

and the morphology of electrode was observed by FESEM technique. FTIR was employed to analysis the electrode surface before and after cycling.

### 5.3 Results and Discussion

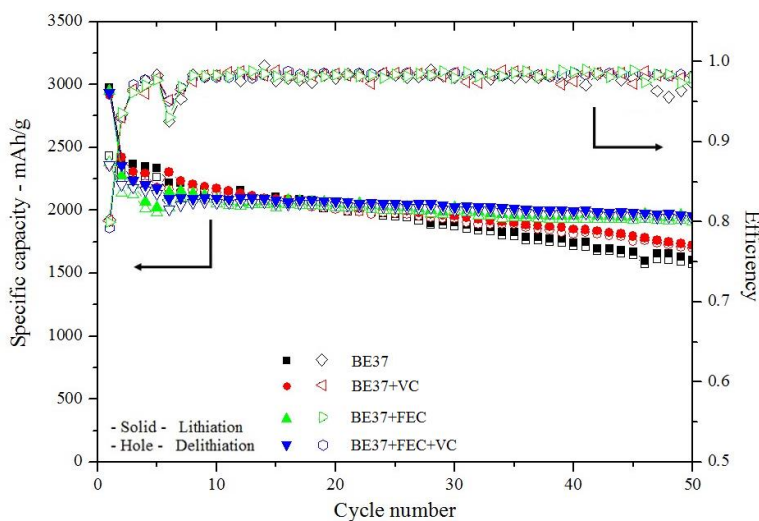


**Figure 5.1 Cycle performance of electrodes at room temperature.**

Electrolyte additives VC and FEC clearly improved the capacity retention and cycle efficiency at room temperature, as shown in Figure 5.1. The electrode of VC+FEC exhibited the highest reversible capacity after 50 cycles, remaining 1931mAh/g and 81.7% capacity retention of the first discharge capacity. The cycle performance of the cell with FEC+VC additive is much stable compared with other three electrodes. The electrode of FEC additive also had similar trend, but the reversible capacity was 1908mAh/g and 80.1% capacity retention after 50 cycles. The electrodes with BE37 and BE37+VC had more capacity loss during the cycles, and the reversible capacity were 1570mAh/g and 1702mAh/g, respectively. It had to be noted that the capacities after formation cycles were dropped more with the existence of FEC in two electrolytes, but less capacity fading after 6<sup>th</sup> cycle. The reason for this was much stable SEI formed on the Si anode surface at the first formation cycles due to the FEC and FEC+VC additives, but for other two electrodes, fragile SEI

broken and reformed during later lithiation/delithiation process which led to more capacity loss [9, 12]. The electrodes of BE37+FEC+VC and BE37+FEC had the higher and stable cell efficiency (around 98-99 %).

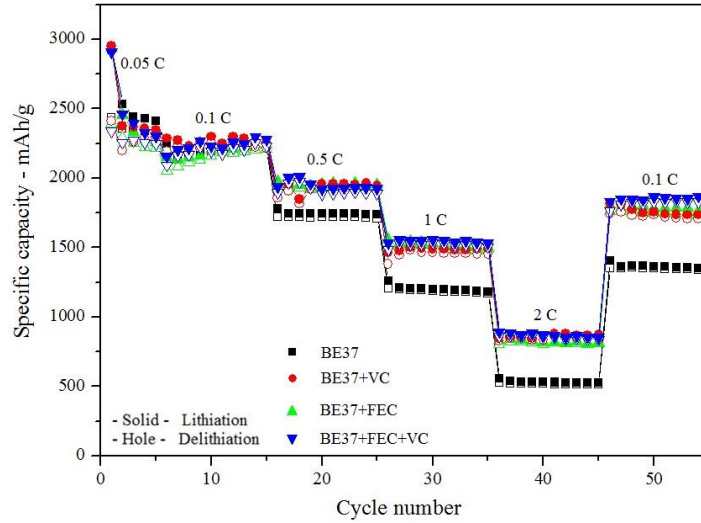


**Figure 5.2 Rate capability of electrodes at room temperature.**

The rate capability of electrodes in four electrolytes was presented in Figure 5.2. After formation process of first five cycles, the electrode of FEC/VC additives delivered a capacity of around 2200mAh/g at 0.1C current density. It was reasonable that the capacity dropped with higher current density, achieving reversible capacity of 850mAh/g at 2C. In addition, the reversible capacity was back to 1830mAh/g after the current density reduced to 0.1C again. It was clear that the rate capability was dramatically improved with the help of additives. The stable SEI, formed in formation cycles, played a crucial role to maintain the mechanical structure of electrode. Enough conductive agent was also important to increase the  $\text{Li}^+$  and electron transportation. However, the electrode without any additives had poorest discharge capacities, around 520mAh/g at 2C and 1330mAh/g at 0.1C, respectively.

Figure 5.3 compared the Nyquist plots of the cells with different electrolytes after 1<sup>st</sup> cycle and 50 cycles. All impedance spectrum were measured after different cycles to confirm the change of electrode surface conditions at the state of full delithiation. The half cell battery can be modeled by an equivalent circuit as shown in Figure 5.3 (c), where  $R_{\Omega}$  is the ohmic

resistance,  $R_{SEI}$  is the charge resistance between the SEI layer and the electrolyte,  $R_{CT}$  is the charge transfer resistance between the SEI and Si,  $C_{SEI}$  is the capacitance of the SEI,  $C_{dl}$  is the double layer capacitance on Si, and  $Z_W$  is the Warburg impedance describing the solid state diffusion of  $Li^+$  in the electrode. A clear difference was observed after first cycle (seen Figure 5. (a)). The initial SEI formed in FEC and FEC/VC electrolytes were better than other two electrodes due to the presence of FEC which dramatically improved the electrode's surface electrochemical property [37-39]. After 50 cycles, another group of spectrum was obtained and presented in Figure 5.3 (b). The  $R_{SEI}$  of BE37 electrolyte was  $116\Omega$  after 1<sup>st</sup> delithiation and  $166\Omega$  after 50 cycles, and the  $R_{SEI}$  of BE37+FEC+VC was  $37\Omega$  after 1<sup>st</sup> delithiation and  $81\Omega$  after 50 cycles. Obviously, according to the comparison, the initial SEI formed on electrode surface in FEC/VC electrolyte had much smaller resistance, which indicated the SEI was quite stable. Furthermore, this stable SEI was still functional after 50 cycles. The resistance of VC and FEC additives were between them, which totally agreed with the cycle performance. It had to be noted that VC optimized the SEI during cycling [40, 41] since it achieved a similar impedance of FEC electrode. The SEM images of electrodes before and after cycling confirmed this phenomenon.

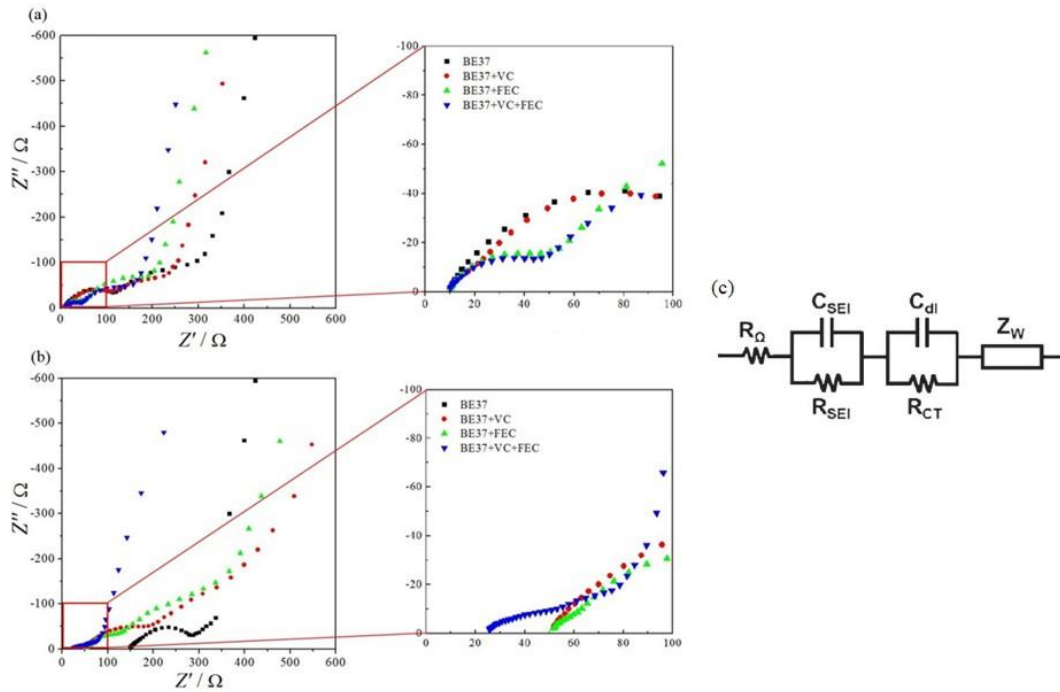


**Figure 5.3 Nyquist plots of electrodes (a) after first cycle, (b) after 50 cycles and (c) equivalent circuit.**

According to Figure 5.4, the SEM image of electrode surface before cycle test was uniform. However, the cracks of 2-3 micros width were observed after 50 cycles on the BE37 electrode surface. With the help of VC or FEC, the cracks were still found on the electrode's surface, but the total length was much less and width of them were less than 1 micro [37, 40, 42]. For the best cycle performance of FEC/VC electrolyte, only few small cracks (the white arrows in Figure 5.4 (e) can be observed and the rest of the electrode surface was still uniform. This was mainly because the stable SEI facilitate to keep the mechanical structure of electrode which held the materials and tightly attached on the current collector.

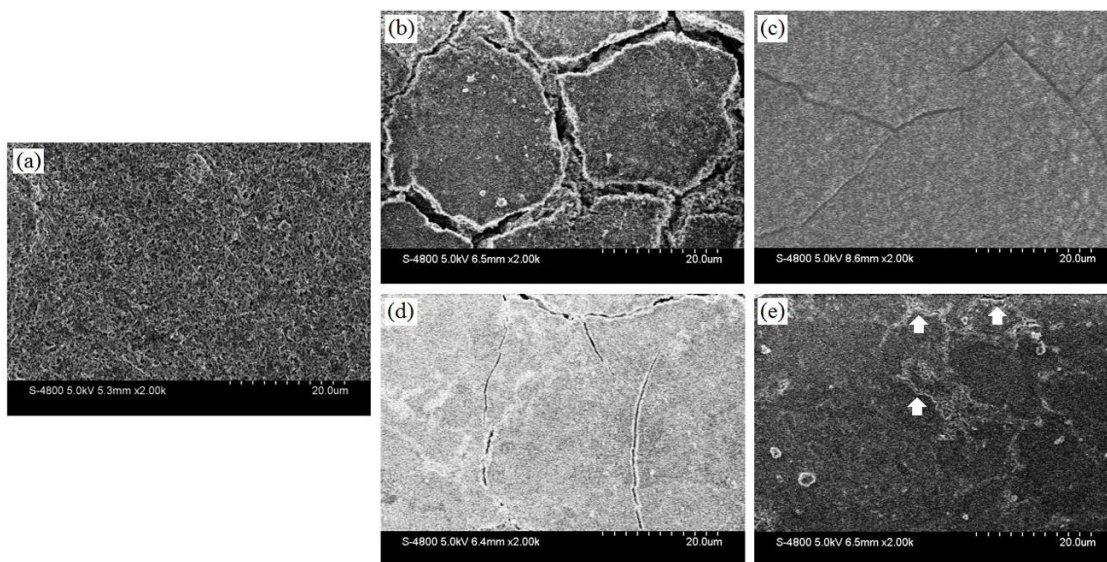


**Figure 5.4 SEM images of electrodes surface (a) before and (b, c, d, e) after 50 cycles at room temperature, (b) BE37, (c) BE37+VC, (d) BE37+FEC, (e) BE37+FEC+VC.**

Figure 5.5 presented the FTIR spectra for the Si electrodes before and after cycling, indicating variations in chemical groups. The pristine electrode was used (electrolyte free) reference to compare all cycled electrodes in electrolyte with different additives. The spectra of BE37 electrode revealed that no intense peak was observed after 50 cycles due to the intensity of peaks decreased gradually as the cycle test increased [42, 43]. The peaks of  $\text{LiPF}_6$  decomposition by-products were observed at  $842\text{cm}^{-1}$  for P-F bond in  $\text{PF}_3$ , and  $905\text{cm}^{-1}$ ,  $730\text{cm}^{-1}$  for P-O-C stretching modes in  $\text{P(OR)}_3$  [44]. The decomposition of EC generated a group of peaks at  $1485$ ,  $1407\text{cm}^{-1}$  for C=O stretching [45] and  $862\text{cm}^{-1}$  for  $\text{OCOO}^-$  bending which came from  $\text{Li}_2\text{CO}_3$  [46]. The peak at  $1309\text{cm}^{-1}$  originated from the

reduction of DEC [44]. For the electrodes with additives, clear peaks were observed at  $1772\text{cm}^{-1}$  and  $1805\text{cm}^{-1}$  after 50 cycles. The peaks around  $1772\text{cm}^{-1}$  corresponded to the C=O stretch mode of DEC and EC decomposition products [44, 45], and the peaks around  $1805\text{cm}^{-1}$  attributed to the formation of poly(VC) [41, 42] and poly(FEC) [38, 42, 43] in the electrochemical interface reaction during cycling. Based on the previous data, it clearly indicated that poly(VC) and poly(FEC) greatly improved the electrode surface cracks due to their better mechanical properties. Furthermore, both these polymer formed in BE37+FEV+VC electrolyte further improved the stability of electrode structure.

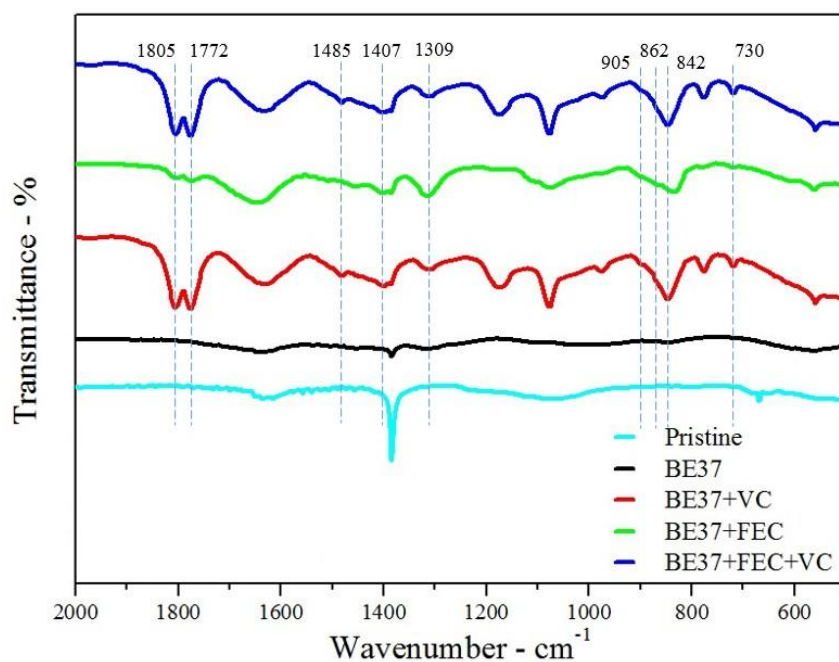


**Figure 5.5 FTIR spectrum of electrodes before and after 50 cycles at room temperature.**

The high temperature cycle performance was carried out in a ESPEC temperate box at the temperature of  $55^{\circ}\text{C}$  (seen Figure 5.6). The formation cycles were conducted at room temperature then transfer to temperate box until the whole cell reached  $55^{\circ}\text{C}$ . Compared with the performance at room temperature, the cycles had more stable with higher discharge capacity and efficiency. The reason was the transportation of  $\text{Li}^{+}$  and electron could be much easier in battery system, which finally facilitated the electrochemical interface reaction. For BE37 electrode, the cycle stability was much improved before 39<sup>th</sup> cycle, then the capacity started to decrease. With the help of additives, the reversible capacities after 50 cycles were

1781mAh/g (VC), 1899mAh/g (FEC) and 2004mAh/g (FEC/VC), respectively. Part of the reason for better performance at high temperature was the additives repaired the cracks which created during cycling [45, 47-51]. The electrolyte solvent and Li salt could immediately form new SEI when in contact with the newly exposed Si anode surface with the help of FEC and VC additives polymerization at elevated temperature.

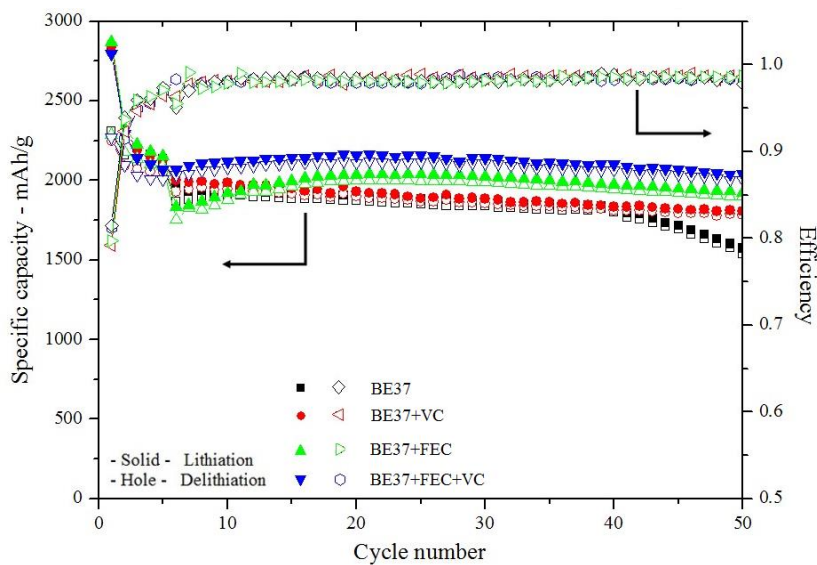


**Figure 5.6 Cycle performance of electrodes at 55°C.**

A similar experiment was conducted to confirm the cycle stability at -20°C. The formation cycles were carried out at room temperature with 0.05C current density then transfer to low temperature box. According to the Figure 5.7, the reversible capacities of 6<sup>th</sup> cycle at -20°C were 162mAh/g (BE37), 768mAh/g (VC), 1067mAh/g (FEC) and 789mAh/g (FEC+VC), respectively. The cell efficiency was also low, around 90-91% for four cells. This was because of the interfacial reaction was suppressed at low temperature and the conductivity of electrolyte was decreased. However, the capacities increased gradually during cycling, reaching 267mAh/g (BE37), 637mAh/g (VC), 949mAh/g (FEC) and 1389mAh/g (FEC+VC). The results revealed that the FEC/VC electrolyte demonstrated the best performance at -20°C, and the FEC additive presented a better performance than that of VC. This probably that new SEI provided a thinner and stable interface which could facilitate the Li<sup>+</sup> and electron transportation, especially important at the low temperature of -20°C.



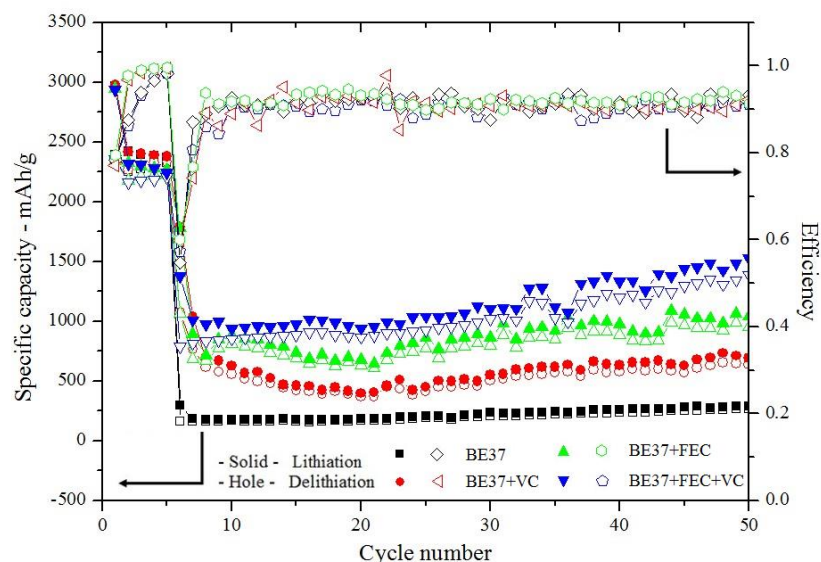


**Figure 5.7 Cycle performance of electrodes at -20°C.**

## 5.4 Conclusions

The effect of additives VC (2 vol%), FEC (10 vol%) and FEC/VC (10/2 vol%) on the cyclic stability of SiNWs electrodes was investigated in BE37 electrolyte. At room and high/low temperatures, the cycle performances revealed that the FEC/VC electrolyte provided the highest cycle stability and reversible capacity and the single usage of FEC and VC additive clearly enhanced the reversible capacity due to the formation of stable SEI with poly(VC) and poly(FEC) on the electrode surface. The impedance results confirmed that the additives dramatically optimized the interface electrochemical condition which also improved the rate capability at room temperature. According to the SEM images of electrode surface, much less cracks were observed after adding additives. Therefore, combined with stable electrochemical interface reaction and stronger poly by-products on the electrode surface, the cycle stability was much improved.

## References

- [1] C. Liu, F. Li, L. P. Ma, H.M. Chen, Advanced materials for energy storage, *Adv. Mater.*, **2010**, 22, E28-E62.
- [2] H. Lbrahim, A. Ilinca, J. Perron, Energy storage systems-characteristics and comparisons, *Renew. Sust. Energy Rev.*, **2008**, 12, 1221-1250.
- [3] J.M. Tarascon, M. Armand, Issues and challenges facing rechargeable lithium batteries, *Nature*, **2001**, 414, 359-367.
- [4] D. Larcher, J-M. Tarascon, Towards greener and more sustainable batteries for electrical energy storage, *Nature Chem.*, **2015**, 7, 19-29.
- [5] S. Cao, J. Yu, g-C<sub>3</sub>N<sub>4</sub>-based photocatalysts for hydrogen generation, *J. Phys. Chem. Lett.*, **2014**, 5, 2101-2107.
- [6] M.E. Mann, R.S. Bradley, M.K. Hughes, Global-scale temperature patterns and climate forcing over the past six centuries, *Nature*, **1998**, 392, 779-787.
- [7] L. Zhang, R. Rajagopalan, H. Guo, X. Hu, S. Dou, H. Liu, A green and facile way to prepare granadilla-like Silicon-based anode materials for Li-Ion Batteries, *Adv. Funct. Mater.*, **2016**, 26, 440-446.
- [8] M.N. Obrovac, V.L. Chevrier, Alloy Negative electrodes for Li-Ion batteries, *Chem. Rev.*, **2014**, 113, 11444-11502.
- [9] H. Wu, Y. Cui, Designing nanostructured Si anodes for high energy lithium ion batteries, *Nano Today*, **2012**, 7, 414-429.
- [10] A. Magasinski, P. Dixon, B. Hertzberg, A. Kvit, J. Ayala, G. Yushin, High-performance lithium-ion anodes using a hierarchical bottom-up approach, *Nature Mater.*, **2010**, 9, 353-358.
- [11] Z. Yang, Y. Xia, J. Ji, B. Qiu, K. Zhang, Z. Liu, Superior cycling performance of a sandwich structure Si/C anode for lithium ion batteries, *RSC Adv.*, **2016**, 6, 12107-12113.
- [12] L. Luo, H. Yang, P. Yan, J.J. Travis, Y. Lee, N. Liu, D.M. Piper, S-H. Lee, P. Zhao, S.M. George, J-G. Zhang, Y. Cui, S. Zhang, C. Ban, C-M. Wang, Surface-Coating regulated lithiation kinetics and degradation in silicon nanowires for lithium ion battery, *ACS NANO*, **2015**, 9(5), 5559-5566.
- [13] W.J. Lee, T.H. Hwang, J.O. Hwang, H.W. Kim, J. Lim, H.Y. Jeong, J. Shim, T.H. Han, J.Y. Kim, J.W. Choi, S.O. Kim, N-doped graphitic self-encapsulation for high performance silicon anodes in lithium-ion batteries, *Energy Environ. Sci.*, **2014**, 7, 621-626.
- [14] N. Liu, H. Wu, M.T. McDowell, Y. Yao, C. Wang, Y. Cui, A Yolk-Shell design for stabilized and scalable Li-Ion battery alloy anodes, *Nano Lett.*, **2012**, 12(6), 3315-3321.

- [15] X.H. Liu, L. Zhong, S. Huang, S.X. Mao, T. Zhu, J.Y. Huang, Size-dependent fracture of silicon nanoparticles during lithiation, *ACS NANO*, **2012**, 6(2), 1522-1531.
- [16] U. Kasavajjula, C. Wang, A.J. Appleby, Nano- and bulk-silicon-based insertion anodes for lithium-ion secondary cells, *J. Power Sources*, **2007**, 163, 1003-1039.
- [17] E. Peled, The electrochemical behavior of Alkali and Alkaline earth metals in nonaqueous battery systems – the solid electrolyte interphase model, *J. Electrochem. Soc.*, **1979**, 126, 2047-2051.
- [18] A. Tokranov, R. Kumar, C. Li, S. Minne, X. Xiao, B.W. Sheldon, Control and optimization of the electrochemical and mechanical properties of the solid electrolyte interphase on silicon electrodes in lithium ion batteries, *Adv. Energy Mater.*, **2016**, 6, 1502302.
- [19] J. Yang, N. Solomatin, A. Kraysberg, Y. Ein-Eli, In-situ spectro-electrochemical insight revealing distinctive silicon anode solid electrolyte interphase formation in a lithium-ion battery, *Chemistry Select*, **2016**, 3, 572-576.
- [20] K. Yamagiva, D. Morita, N. Yabuuchi, T. Tanaka, M. Fukunishi, T. Taki, H. Watanabe, T. Otsuka, T. Yano, J-Y. Son, Y-T. Cui, H. Oji, S. Komaba, Improved high-temperature performance and surface chemistry of Graphite/LiMn<sub>2</sub>O<sub>4</sub> Li-Ion cells by fluorosilane-based electrolyte additive, *Electrochim. Acta*, **2015**, 150, 347-356.
- [21] H.F. Xiang, H.Y. Xu, Z.Z. Wang, C.H. Chen, Dimethyl methylphosphonate (DMMP) as an efficient flame retardant additive for the lithium-ion battery electrolytes, *J. Power Sources*, **2007**, 173, 562-564.
- [22] X.L. Yao, S. Xie, C.H. Chen, Q.S. Wang, J.H. Sun, Y.L. Li, S.X. Lu, Comparative study of trimethyl phosphite and trimethyl phosphate as electrolyte additives in lithium ion batteries, *J. Power Sources*, **2005**, 144, 170-175.
- [23] D. Aurbach, K. Gamolsky, B. Markovsky, Y. Gofer, M. Schmidt, U. Heider, On the use of vinylene carbonate (VC) as an additive to electrolyte solutions for Li-ion batteries, *Electrochim. Acta*, **2002**, 47, 1423-1439.
- [24] G.H. Wrodnigg, J.O. Besenhard, M. Winter, Ethylene sulfite as electrolyte additive for lithium-ion cells with graphitic anodes, *J. Electrochem. Soc.*, **1999**, 146(2), 470-472.
- [25] G.H. Wrodnigg, T.M. Wrodnigg, J.O. Besenhard, M. Winter, Propylene sulfite as film-forming electrolyte additive in lithium ion batteries, *Electrochem. Commun.*, **1999**, 1, 148-150.
- [26] Y. Li, F. Lian, L. Ma, C. Liu, L. Yang, X. Sun, K. Chou, Fluoroethylene carbonate as electrolyte additive for improving the electrochemical performances of high-capacity Li<sub>1.16</sub>[Mn<sub>0.75</sub>Ni<sub>0.25</sub>]<sub>0.84</sub>O<sub>2</sub> material, *Electrochim. Acta*, **2015**, 168, 261-270.

- [27] Y. Horowitz, H-L. Han, P.N. Ross, G.A. Somorjai, In situ potentiodynamic analysis of the electrolyte/silicon electrodes interface reactions – A sum frequency generation vibrational spectroscopy study, *J. Am. Chem. Soc.*, **2016**, 138, 726-729.
- [28] C. Xu, F. Lindgren, B. Philippe, M. Gorgoi, F. Björefors, K. Edström, T. Gustafsson, Improved performance of the silicon anode for Li-Ion batteries: understanding the surface modification mechanism of fluoroethylene carbonate as an effective electrolyte additive, *Chem. Mater.*, **2015**, 27, 2591-2599.
- [29] K. Schroder, J. Alvarado, T.A. Yersak, J. Li, N. Dudney, L.J. Webb, Y.S. Meng, K.J. Stevenson, The effect of fluoroethylene carbonate as an additive on the solid electrolyte interphase on silicon lithium-ion electrodes, *Chem. Mater.*, **2015**, 27, 5531-5542.
- [30] Q. Zhang, X. Xiao, W. Zhou, Y-T. Cheng, M.W. Verbrugge, Toward high cycle efficiency of silicon-based negative electrodes by designing the solid electrolyte interphase, *Adv. Energy Mater.*, **2015**, 5, 1401398.
- [31] B.T. Young, D.R. Heskett, C.C. Nguyen, M. Nie, J.C. Woicik, B.L. Lucht, Hard X-ray photoelectron spectroscopy (HAXPES) investigation of the silicon solid electrolyte interphase (SEI) in lithium-ion batteries, *Appl. Mater. Interfaces*, **2015**, 7, 20004-20011.
- [32] K. Leung, S.B. Rempe, M.E. Foster, Y. Ma, J.M. Martinez del la Hoz, N. Sai, P.B. Balbuena, Modeling electrochemical decomposition of fluoroethylene carbonate on silicon anode surfaces in lithium ion batteries, *J. Electrochem. Soc.*, **2014**, 161(3), A213-A221.
- [33] X. Chen, X. Li, D. Mei, J. Feng, M.Y. Hu, J. Hu, M. Engelhard, J. Zheng, W. Xu, J. Xiao, J. Liu, J-G Zhang, Reduction mechanism of fluoroethylene carbonate for stable solid-electrolyte interphase film on silicon anode, *ChemSusChem.*, **2014**, 7, 549-554.
- [34] Y-M. Lin, K.C. Klavetter, P.R. Abel, N.C. Davy, J.L. Snider, A. Heller, C.B. Mullins, High performance silicon *nanoparticle* anode in fluoroethylene carbonate-based electrolyte for Li-ion batteries, *Chem. Commun.*, **2012**, 48, 7268-7270.
- [35] S. Hy, Y-H. Chen, H-M. Cheng, C-J. Pan, J-H. Cheng, J. Rick, B-J. Hwang, Stabilizing nanosized Si anodes with the synergetic usage of atomic layer deposition and electrolyte additives for Li-ion batteries, *Appl. Mater. Interfaces*, **2015**, 7, 13801-13807.
- [36] L. Martin, H. Martinez, M. Ulldemolins, B. Pecquenard, F. Le Cras, Evolution of the Si electrode/electrolyte interface in lithium batteries characterized by XPS and AFM techniques: the influence of vinylene carbonate additive, *Solid State Ionics*, **2012**, 215, 36-44.
- [37] S.E. Trask, K.Z. Papek, J.A. Gilbert, M Klett, B.J. Polzin, A.N. Jansen, D.P. Abraham, Performance of full cells containing carbonate-based LiFSI electrolyte and Silicon-graphite negative electrodes, *J. Electrochem. Soc.*, **2016**, 163(3), A345-A350.
- [38] V. Etacheri, O. Haik, Y. Goffer, G.A. Roberts, I.C. Stefan, R. Fasching, D. Aurbach, Effect of fluoroethylene carbonate (FEC) on the performance and surface chemistry of Si-nanowire Li-ion battery anode, *Langmuir*, **2011**, 28, 965-976.

- [39] S. Dalavi, P. Guduru, B.L. Lucht, Performance enhancing electrolyte additives for lithium ion batteries with silicon anodes, *J. Electrochem. Soc.*, **2012**, 159(5), A642-A646.
- [40] M. Ulldemolins, F.L. Cras, B. Pecquenard, V.P. Phan, L. Martin, H. Martinez, Investigation on the part played by the solid electrolyte interphase on the electrochemical performances of the silicon electrode for lithium-ion batteries, *J. Power Sources*, **2012**, 206, 245-252.
- [41] H. Ota, Y. Sakata, A. Inoue, S. Yamaguchi, Analysis of vinylene carbonate derived SEI layers on graphite anode, *J. Electrochem. Soc.*, **2004**, 151(10), A1659-A1669.
- [42] C.C. Nguyen, B.L. Lucht, Comparative study of fluoroethylene carbonate and vinylene carbonate for silicon anodes in lithium ion batteries, *J. Electrochem. Soc.*, **2014**, 161(12), A1933-A1938.
- [43] M. Nie, D.P. Abraham, Y. Chen, A. Bose, B.L. Lucht, Silicon solid electrolyte interphase (SEI) of lithium ion battery characterized by microscopy and spectroscopy, *J. Phys. Chem. C*, **2013**, 117, 13403-13412.
- [44] U.S. Vogl, S.F. Lux, E.J. Crumlin, Z. Liu, L. Terborg, M. Winter, R. Kostechi, The mechanism of SEI formation on a single crystal Si(100) electrode, *J. Electrochem. Soc.*, **2015**, 162(4), A603-A607.
- [45] I.A. Profatilova, C. Stock, A. Schmitz, S. Passerini, M. Winter, Enhanced thermal stability of a lithiated nano-silicon electrode by fluoroethylene carbonate and vinylene carbonate, *J. Power Sources*, **2013**, 222, 140-149.
- [46] Y. Ein-Eli, S.F. McDevitt, D. Aurbach, B. Markovsky, A. Schechter, Methyl Propyl Carbonate: A promising single solvent for Li-ion battery electrolytes, *J. Electrochem. Soc.*, **1997**, 144(7), L180-L184.
- [47] I.A. Profatilova, T. Langer, J.P. Badillo, A. Schmitz, H. Orthner, H. Wiggers, S. Passerini, M. Winter, Thermally induced reactions between lithiated nano-silicon electrode and electrolyte for lithium-ion batteries, *J. Electrochem. Soc.*, **2012**, 159(5), A657-A663.
- [48] O. Haik, S. Ganin, G. Gershinsky, E. Zinigrad, B. Markovsky, D. Aurbach, I. Halalay, On the thermal behavior of lithium intercalated graphites, *J. Electrochem. Soc.*, **2011**, 158(8), A913-A923.
- [49] G.V. Zhuang, H. Yang, P.N. Ross, K. Xu, T.R. Jow, Lithium methyl carbonate as a reaction product of metallic lithium and dimethyl carbonate, *Electrochem. Solid-State Lett.*, **2006**, 9(2), A64-A68.
- [50] C.L. Campion, W. Li, B.L. Lucht, Thermal decomposition of LiPF<sub>6</sub>-based electrolytes for lithium-ion batteries, *J. Electrochem. Soc.*, **2005**, 152(12), A2327-A2334.
- [51] J.S. Gnanaraj, E. Zinigrad, L. Asraf, H.E. Gottlieb, M. Sprecher, M. Schmidt, W. Geissler, D. Aurbach, A detailed investigation of the thermal reactions of LiPF<sub>6</sub> solution in

organic carbonates using ARC and DSC, *J. Electrochem. Soc.*, **2003**, 150(11), A1533-A1537.

## Chapter 6

### 6 Conclusion and perspective

#### 6.1 Conclusion

In this thesis, three studies were conducted to enhance the stability of Si anode for practical application in LIBs. These sections included Si anode synthesis, Si electrode optimization and electrolyte improvement. Each part of this thesis plays a crucial role for achieving high performance LIB through the use of Si as an anode material.

The first part of this work presented an HF free chemical etching method to synthesis SiNWs from Si-Al alloy. This method only required a simple heat treatment prior to HCl etching. The process allows for facile handling, while simultaneously imparting low cost and environmental benignity. Optimal conditions for heat treatment was determined to take place at 1000°C for 8 hours under argon gas. As prepared SiNWs had a diameter of 100nm with micro scale particles, including a crystalline Si phase with oxidized Si and small amounts of aluminum. The electrochemical evaluation confirmed a capacity retention of 1321mAh/g after 50 cycles for the prepared SiNWs.

The second part of this work was carried out to optimize the parameter of Si-based electrode, a critical aspect when trying to stable and reproducible cell performance. Electrode mass loading and density, binders and cycle mode protocol were studied. In order to fabricate a high quality Si electrode with appropriate energy density, it was found that having a mass loading of approximately 0.8mg/cm<sup>2</sup> and density of 0.93g/cm<sup>3</sup> was optimal. Compared to the traditional CMC-SBR binder typically used for Si anode electrodes, SA, XGB and PAA binders were found to improve cycle stability due to more robust mechanical properties. The retention capacity of optimized electrode was found to be 78.9% after 300 cycles at room temperature. A new cycle protocol was found to exhibit extremely stable cycle performance

since the Si electrode volume expansion during lithiation process was greatly suppressed by controlled lithiation.

The last part of this work evaluated the synergies of FEC and VC additives for Si anode in half cell LIB. It was determined that FEC and VC could improve cell performance when they were applied in EC/DEC electrolyte. Furthermore, the combined use of these additives in the electrolyte with 10% and 2% (vol %) could further improve the cycle performance in high temperature (55°C), room temperature (25°C), and even low temperature (-20°C) LIB. Nyquist plots confirmed that the internal resistance of FEC/VC electrode was the lowest due preferential SEI formation. It was determined that enhanced mechanical properties attributed to the poly(FEC) and poly(VC) formed on the electrode surface during cycling.

Based on the pure Si anode electrode, most of the work related to the practical application in lithium-ion battery industry.

## 6.2 Perspective

Despite recent efforts made for LIB technology in the last two decades, more work is required for further improving the battery system to achieve greater energy density. According to the work presented in this thesis, the following work can be carried out for future Si anode materials synthesis, Si-based Lithium-ion battery processes, and electrochemical system optimization.

For Si anode materials, further work can be focused on the selection of Si-Al alloy, higher heat treatment temperatures, longer treatment time, and optimization cooling down rate. The different ratio of Si element in Si-Al alloy can greatly affect the yield of SiNWs. The heat pre-treatment process also can dramatically optimize the morphology of the induced Si phase in Si-Al alloy by taking advantage of eutectic effects. Furthermore, an increased annealing temperature (1100-1700°C) can be employed in order to achieve SiNWs with smaller diameter. The research conducted here also suggests that a prolonged calcination storage time may also allow for longer SiNWs. Other methods can be applied to accelerate the eutectic effect, such as ultrasonic vibration the alloy during heat treatment [1]. A proper



cooling down rate helps to frozen the SiNWs structure and avoids the SiNWs to form particles again [2, 3].

The battery assemble process should be further optimized because of the introduction of nanostructured Si anode in LIB system. The slurry making process is crucial step for LIB industry because the quality of electrode directly affect the battery performance, but the huge surface area effect of nanomaterials will greatly change the condition of anode slurry. More detailed work should be done on slurry making process. According to the mutual graphite slurry process, the key point is to improve the capability of Si-based electrode preparation processes since current LIB industry instruments are designed for handing micro scale (usually 25 $\mu$ m) active materials. Selection of binders and optimization of the slurry formula are crucial for accommodating Si volume expansion and electrode swelling during cycling. New binders should be further studied to improve the mechanical properties by more functional groups [4-6], other functions [7-10], as well as reduce the ratio in electrode.

A stable electrochemical system is crucial for LIB, especially Si-based LIB due to the aggressive volume expansion effect. The electrolyte plays a critical role in cycling and performance of LIB. FEC and VC additives have already been shown to greatly optimize cycle stability in half cell test. Additional additives should be studied in carbonate electrolyte for Si-based LIBs to form a stable SEI on electrode surface [11, 12], and more importantly, new electrolyte should be compatible for Si anode material and cathode electrode [13-16]. Therefore, the electrolyte should be further tested and confirmed in full cell evaluation.

Combined all these works together, the practical application of Si anode in LIB industry can dramatically improve the energy density of next generation Lithium-Ion Batteries.

## Reference

[1] X. Jian, T.T. Meek, Q. Han, Refinement of eutectic silicon phase of aluminum A356 alloy using high-intensity ultrasonic vibration, *Scripta Mater.*, **2006**, 54, 893-896.

- [2] M.C.S. Jr, A.R. Machado, W.F. Sales, M.A.S. Barrozo, E.O. Ezugwu, Machining of aluminum alloys: a review, *Int. J. Adv. Manuf. Technol.*, **2016**, DOI 10.1007/s00170-016-8431-9.
- [3] M.M. Makhlof, H.V. Guthy, The aluminum-silicon eutectic reaction: mechanisms and crystallography, *J. Light Met.*, **2001**, 1, 199-218.
- [4] Y.K. Jeong, T-W. Kwon, I. Lee, T-S. Kim, A. Coskun, J.W. Choi, Millipede-inspired structural design principle for high performance polysaccharide binders in silicon anodes, *Energy Environ. Sci.*, **2015**, 8, 1224-1230.
- [5] S-J. Park, H. Zhao, G. Ai, C. Wang, X. Song, N. Yuca, V.S. Battaglia, W. Yang, G. Liu, Side-chain conducting and phase-separated polymeric binders for high-performance silicon anodes in Lithium-Ion Batteries, *J. Am. Chem. Soc.*, **2015**, 137, 2565-2571.
- [6] M. Wu, J.E.C. Sabisch, X. Song, A.M. Minor, V.S. Battaglia, G. Liu, A highly cross-linked polymeric binder for high-performance silicon negative electrodes in Lithium-Ion Batteries, *Angew. Chem. Int. Ed.*, **2012**, 51, 8762-8767.
- [7] Z. Chen, C. Wang, J. Lopez, Z. Lu, Y. Cui, Z. Bao, High-areal-capacity silicon electrodes with low-cost silicon particles based on spatial control of self-healing binder, *Adv. Energy Mater.*, **2015**, 5, 1401826.
- [8] M. Wu, X. Song, X. Liu, V. Battaglia, W. Yang, G. Liu, Manipulating the polarity of conductive polymer binders for Si-based anodes in Lithium-Ion Batteries, *J. Mater. Chem., A*, **2015**, 3, 3651-3658.
- [9] H. Wu, G. Yu, L. Pan, N. Liu, M.T. McDowell, Z. Bao, Y. Cui, Stable Li-ion battery anodes by in-situ polymerization of conducting hydrogel to conformally coat silicon nanoparticles, *Nat. Commun.*, **2013**, 4, 1943-1948.
- [10] D. Mazouzi, Z. Karkar, C.R. Hernandez, P.J. Manero, D. Guyomard, L. Roué, B. Lestriez, Critical roles of binders and formulation at multiscales of silicon-based composite electrodes, *J. Power Sources*, **2015**, 280, 533-549.
- [11] J. Zhao, Z. Lu, H. Wang, W. Liu, H-W. Lee, K. Yan, D. Zhuo, D. Lin, N. Liu, Y. Cui, Artificial solid electrolyte interphase-protected  $\text{Li}_x\text{Si}$  nanoparticles: An efficient and stable prelithiation reagent for lithium-ion batteries, *J. Am. Chem. Soc.*, **2015**, 137, 8372-8375.
- [12] M. Nie, D.P. Abraham, Y. Chen, A. Bose, B.L. Lucht, Silicon solid electrolyte interphase (SEI) of Lithium Ion Battery characterized by microscopy and spectroscopy, *J. Phys. Chem. C*, **2013**, 117, 13403-13412.
- [13] J. Jeong, J-N. Lee, J-K. Park, M-H. Ryou, Y.M. Lee, Stabilizing effect of 2-(triphenylphosphoranylidene) succinic anhydride as electrolyte additive on the lithium metal of lithium metal secondary batteries, *Electrochim. Acta*, **2015**, 170, 353-359.

- [14] D.T. Nguyen, J. Kang, K-M. Nam, Y. Paik, S-W. Song, Understanding interfacial chemistry and stability for performance improvement and fade of high-energy Li-ion battery of  $\text{LiNi}_{0.5}\text{Co}_{0.2}\text{Mn}_{0.3}\text{O}_2$ //Silicon-graphite, *J. Power Sources*, **2016**, 303, 150-158.
- [15] J.H. Lee, C.S. Yoon, J-Y. Hwang, S-J. Kim, F. Maglia, P. Lamp. S-T. Myung, Y-K. Sun, High-energy-density lithium-ion battery using a carbon-nanotube-Si composite anode and a compositionally graded  $\text{Li}[\text{Ni}_{0.85}\text{Co}_{0.05}\text{Mn}_{0.1}]\text{O}_2$  cathode, *Energy Environ. Sci.*, **2016**, 9, 2152-2158.
- [16] C. Chae, H-J. Noh, J.K. Lee, B. Scrosati, Y-K. Sun, A high-energy Li-ion battery using a silicon-based anode and a nano-structured layered composite cathode, *Adv. Funct. Mater.*, **2014**, 24, 3036-3042.

# Curriculum Vitae

**Name:** Qizheng Li

**Post-secondary Education and Degrees:** Department of Mechanical and Materials Engineering  
University of Western Ontario, London, Ontario, Canada  
2014-2016 M.E.Sc.

Department of Materials Science and Engineering  
Beijing University of Chemical Technology, Beijing, P.R. China  
2001-2009 Ph.D.

Department of Materials Science and Engineering  
Beijing University of Chemical Technology, Beijing, P.R. China  
1997-2001 B.Eng.

**Honors and Awards:** Bayer Specialized Scholarship

2003

School-level Eminent Master Degree Candidate  
2003

The Best Poster Presentation  
2003

**Related Work** Research Assistant

**Experience**                      The University of Western Ontario  
  
2014-2016  
  
Project Manager/Senior research engineer  
  
Tianjin Lishen Battery Joint-Stock Co., Ltd., China  
  
2009-2013  
  
Research Assistant  
  
Beijing University of Chemical Technology, China  
  
2001-2009

**Publications:**

***(A) Papers in Journals***

1. Yanan Luo, **Qizheng Li**, Shizhe Song “Corrosion behavior of ZHMn55-3-1 copper alloy in stagnant and flowing seawater with entrained sediment” *Anti-Corrosion Methods and Materials*, **2014**, 61/2, 96-103.
2. **Qizheng Li**, Yu Zuo, Jingmao Zhao, Yuming Tang, Xuhui Zhao, Jinping Xiong “Corrosion behaviors of Ce and Nd modified anodic films on aluminum” *Anti-Corrosion Methods and Materials*, **2010**, 57/5, 238-243.
3. **Qizheng Li**, Yuming Tang, Yu Zuo “The preparation and corrosion resistance of Ce and Nd modified anodic films on aluminum” *Materials Chemistry and Physics*, **2010**, 120, 676-681.
4. **Qizheng Li**, Yu Zuo, Xuhui Zhao, Jinping Xiong “Corrosion resistance of Rare Earth modified anodized films on high purity aluminum” *Journal of The Chinese Rare Earth Society*, **2009**, 27/5, 657-663.
5. **Qizheng Li**, Yu Zuo, Xuhui Zhao, Jingmao Zhao “Study on compound sealing of corrosion resistance on cast aluminum anodic oxide film” *Materials Protection*, **2007**, 40/6, 41-43.

***(B) Conference Papers***

6. **Qizheng Li**, Yu Zuo, Jingmao Zhao, Jinping Xiong, Xuhui Zhao “Rare Earth Modified Anodic Films on Aluminum by a Precursor Method and the Improved Corrosion Resistance” *Proceeding of the 6<sup>th</sup> Cross-Strait Conference on Materials Corrosion and Protection*, Nov. **2008**, Hulien.

7. **Qizheng Li**, Yu Zuo, Xuhui Zhao, Jingmao Zhao “Research On Sealing Processes Of Anodic Film For Cast Aluminum Alloy” *International Symposium on Advanced Materials and their Related Science*, Oct 21~24, **2003**, Beijing, China, 685-689.

**(C) Book chapter**

8. **Qizheng Li** and Xueliang Sun, “Advanced Technologies for Li-Ion Rechargeable Batteries” in the book of “*Advanced Materials and Technologies for Electrochemical Energy*”, Co-Edited by Pei-Kang Shen, Chao-Yang Wang, Xueliang Sun, San-ping Jiang, and Jiujun Zhang, Publisher: CRC Publisher. (In book series of Electrochemical Energy Storage and Conversion), **2014**, in press.

**(D) Patents**

9. Yu Zuo, **Qizheng Li**, and et al. (2009) An aluminum/aluminum alloy anodizing method of oxide precursor. China Patent No.:ZL200910087786.4.

10. Yu Zuo, **Qizheng Li**, and et al. (2004) Rare Earth sealing method for aluminum alloy anodic oxide film. China Patent No.: ZL200410074541.5.

**(E) Project list**

11. Anti-corrosion Material for Supercharger Rotor’s Surface and Technical Research (Project leader, 2004, Beijing University of Chemical Technology)

12. Research of Water-based Antirusting Agent for Heat Sink (2007, Beijing University of Chemical Technology)

13. Study of Alloy Anode Materials for Lithium Ion Battery (Project leader, 2009, Lishen Battery Company)

14. Study of Silicon Anode Battery Electrochemistry System (Project leader, 2010, Lishen Battery Company, National High Technology Research and Development Program of China)

15. Establishment of High Capacity Polymer Lithium Ion Battery (Project leader, 2011, Lishen Battery Company)

16. Research of Alloy Anode Materials for 18650 Lithium Ion Battery (2011, Lishen Battery Company)

17. Research of New Generation Super-high Capacity Lithium Ion Battery (Project leader, 2012, Lishen Battery Company, National Basic Research Program of China)